Faculty of Science and Engineering
Department of Chemical Engineering

Coarse Grid Simulation of Gas-Solid Flows in Riser

Milinkumar T. Shah

This thesis is presented for the Degree of
Doctor of Philosophy
of
Curtin University of Technology

March 2011

Declaration

To the best of my knowledge and belief this thesis contains no material previously published by any other person except where due acknowledgement has been made.

This thesis contains no material which has been accepted for award of any other degree or diploma in any university.

Signature : _____

Date : _____

Biography of the Author

Milinkumar T. Shah was born on 18th June, 1979 in Bharuch, India. After completion of his higher secondary education, he joined the Department of Chemical Engineering, Nirma Institute of Technology to obtain bachelor degree in Chemical Engineering in December, 1996. He completed his engineering degree in June, 2000. Then after, he joined Department of Chemical Engineering, Shri S'ad Vidhya Mandal Institute of Technology as a lecturer. He worked at SVM Institute of Technology for nearly six years before he enrolled as a research student in August, 2007 at Department of Chemical Engineering, Curtin University, Western Australia. During his research, he has extensively worked on computational fluid dynamics modelling of gas-solid flows. His research interests are multiphase flow modelling, computational fluid dynamics and multiphase reactor design. His research has already been acknowledged by journal and conference publications, which includes:

Journal publications:

1. Shah, M.T., Utikar, R.P., Tade, M.O., Pareek, V.K., Evans, G.M., Simulation of gas-solid flows in riser using energy minimization multiscale model: Effect of cluster diameter correlation. Chemical Engineering Science **66**(14), 3291-3300.

2. Shah, M.T., Utikar, R.P., Tade, M.O., Pareek, V.K., 2011. Hydrodynamics of an FCC riser using energy minimization multiscale drag model. Chemical Engineering Journal **168**, 812-821.

3. Shah, M.T., Mayne, J., Utikar, R.P., Tade, M.O., Pareek, V.K., 2010. Gas-solid flow hydrodynamics of an industrial scale catalyst lift engager. Chemical Engineering Journal **159**, 138-148.

4. Shah, M.T., Utikar, R.P., Tade, M.O., Evans, G., Dudukovic, M.P., Pareek, V.K., 2011b. Simulation of gas-solid flows in riser: Effect of boundary conditions. Submitted in Industrial & Engineering Chemistry Research (Manuscrip Number: ie-2011-00940f).

Conference publications:

1. Shah, M.T., Utikar, R.P., Tade, M.O., Pareek, V.K., 2011. Simulation of gas-solid flows in riser using energy minimization multiscale model: Effect of cluster diameter correlation, Presented at GLS - 10, 26-29 June, 2011, Portugal.

2. Shah, M.T., Mayne, J., Utikar, R.P., Tade, M.O., Pareek, V.K., 2009. Hydrodynamics of catalyst lift engager, Presented at CHEMECA, Perth, WA.

3. Shah, M.T., Utikar, R.P., Tade, M.O., Pareek, V.K., 2009. Effect of lift gas velocity on performance of catalyst lift engager, Conveying and Handling of Particulate Solids, Brisbane, Australia.

4. Shah, M.T., Utikar, R.P., Tade, M.O., Pareek, V.K., 2008. Hydrodynamics of solid lift engager using Eulerian granular model, Presented at CHEMCON, Chandigarh, India.

5. M.T. Shah, R.P. Utikar, M.O.Tade and V.K.Pareek, 2008. Hydrodynamics of solid lift engager using Eulerian granular model. Petroleum refining –redefining Upstream & Downstream – Work shop, IIT, Delhi, India.

Abstract

Gas-solid risers have been extensively used as multiphase reactors in circulating fluidized bed (CFB) system such as fluid catalytic cracking (FCC) and Circulating fluidized bed combustion (CFBC). In FCC, a riser facilitates cracking reactions which take place between fluidized catalyst and vaporised vacuum gas oil. Similarly in CFBC, combustion of coal particle occurs in the riser. The gas-solid flow hydrodynamics in riser plays a dominant role in governing the conversion of the chemical process, and in turn the performance of the CFB system. Therefore, several experimental and numerical studies have been conducted on the hydrodynamics of riser. Since experimental studies have been costlier and time consuming, detailed hydrodynamic modelling using computational fluid dynamics (CFD) has emerged as a promising alternative to investigate flows in riser.

Two types of CFD models can be identified i.e. (i) Eulerian-Langrangian (EL) and (ii) Eulerian-Eulerian (EE) models. The Eulerian-Eulerian model considers both phases as interpenetrating continua. As a result, it allows a use of grid size larger than length scales of the flow structures. Therefore, this approach requires less computational power, and can handle large-scale geometry. Due to its computational edge, the Eulerian-Eulerian approach has been widely used to conduct the CFD simulations of gas-solid flows in riser. A literature review on the previous simulation studies revealed several shortcomings, and therefore, investigations on the impact of different modelling parameters were found to be necessary before applying the EE model to industrial-scale simulations. In this study, the EE gas-solid flow model has been used to carry out CFD simulations of risers. The effect of modelling parameters such as boundary conditions, drag models and solid phase closure models have been investigated. Finally, the EE model has been used to carry out industrial scale simulation of the lift engager to study the parametric effect of the lift gas velocity on the catalyst lift rate.

The effect of inlet boundary conditions was investigated by using three different types of inlets for both gas and solid phases. The inlet arrangements had a profound effect on mixing patterns of two phases and energy balances in 2D riser. Furthermore, the effect of wall boundary conditions was also studied by considering

the wall as a partial-slip or no-slip wall for the solid phase. A 3D full-scale riser was also simulated by implementing the boundary conditions similar to the experimental set-up. Although both 2D and 3D simulations could qualitatively predict the radial profiles of solid velocity and volume fraction, they could not predict even qualitative trend of the axial profile of solid volume fractions. Previous studies (Yang et al., 2004, Andrews Iv et al., 2005) showed that the conventional drag model such as that of Gidaspow's could not capture the axial heterogeneity; however a use of the multi-scale drag could remove this draw back. Thus, the drag derived using the energy minimization multi-scale approach was evaluated in another part of the study. The structure-based drag models could capture both axial and radial profiles of voidages, but only qualitatively. Furthermore, the use of different cluster diameter correlations with the EMMS framework gave more accurate predictions with reasonable qualitative agreement with the experimental data. Finally, the EE model was applied to study hydrodynamics of a complex industrial-scale lift engager. In this part, the effect of lift gas velocity on the catalyst lift rate and fluctuations therein were investigated to optimise operating gas velocity. Before conducting the parametric study, the effects of modeling parameters such as drag models and frictional pressure models on the hydrodynamics of the lift engager were also investigated.

In summary, the study has been conducted by performing rigorous CFD simulations of both 2D and 3D risers. The effects of modelling aspects such as boundary conditions and drag models on the hydrodynamics predictions were investigated. The EE model with a structured-based drag from the EMMS model was found to be more effective in capturing an inherent heterogeneity of riser flows. However, the quantitative disagreements between the flow predictions and experimental data still persist.

Acknowledgement

Many people have helped me to carry out this research, and their support has kept me motivated throughout the course of PhD. I express my gratitude towards my supervisor Prof. Vishnu K Pareek for giving me an opportunity to work on this challenging project. I thank him for providing absolute stress less working environment and free access to his time. He allowed me to work on new dimensions of the project, and also nurtured me to be an independent researcher. I also express my gratitude towards Dr. Ranjeet P Utikar for providing new research ideas and teaching CFD technique. I also express my sincere gratitude to Prof. Moses Tade for his support, advice and motivation. I would like to thank my thesis chairman and head of department of chemical engineering, Prof. Ming Ang, for his support and guidance. I also take this opportunity to thank Mr. Jeff Mayne, senior process engineer at BP Kwinana refinery, who gave me the opportunity work on the catalyst lift engager. I would also like to thank my colleagues, particularly Dr. Tejas Bhatelia for his enormous support in learning the CFD tools in early part of the research and Mr. Divyaman Vadnerkar, for his support in using different programming tools. Furthermore, I would also like to thank other colleagues such as Ganesh, Johan and Emmanuel for giving me moral support and pleasant working environment. Here, I also thank secretarial staff, namely Ms. Jann Bolton, Mrs. Naomi Mockford and Mrs. Stephenie Blakiston for their timely help and support.

I express my deepest gratitude towards my wife, Manisha, for allowing me to carry out this study. Without her moral and financial support, I would never think of finishing this doctorate degree. I am also thankful to my parents and family for their support during my good and bad times. Finally, I thank all those who assisted me directly or indirectly in the completion of this research.

Table of Contents

List of figures viii

List of tables xii

Nomenclature xiii

1. Introduction 1

    1.1. Gas-solid flow in the riser 1

    1.2. Modelling of gas –solid flows in CFB 4

    1.3. Objectives of this research 9

    1.4. Contribution of this thesis 10

    1.5. Outline of this thesis 10

2. Hydrodynamics of riser reactors 13

    2.1. Experimental studies 13

    2.2. Numerical studies 26

    2.3 Summary 38

3. Effects of boundary conditions 39

    3.1. Introduction 39

    3.2 Eulerian-Eulerian gas-solid flow model 41

        3.2.1. Averaged balance equations 44

        3.2.2. Interphase drag coefficient 45

        3.2.3. Phase stress tensors 47

        3.3.4. Boundary conditions 49

    3.3. CFD simulations 51

    3.4. Results and discussion 54

        3.4.1. 2D simulations 54

            3.4.1.1. Effects of solid inlet boundary conditions 56

            3.4.1.2 Effects of wall boundary condition 60

        3.4.2. 3D full-scale simulation 63

    3.5. Conclusions 66

4. Application of EMMS drag model 68

    4.1 Introduction 68

    4.2. Energy minimization multi-scale (EMMS) model 71

    4.3. Calculation of EMMS based drag model 78

4.4. CFD simulation 82
4.5. Results and discussion 86
4.5.1. Hydrodynamics of low mass flux FCC riser 86
4.5.2. Hydrodynamics of high mass flux FCC riser 91
4.5.3. Effect of cluster diameter correlation 93
4.6. Conclusions 98
5. Hydrodynamics of an industrial-scale lift engager 100
5.1. Introduction 100
5.2. CFD simulations 103
5.3. Results and discussion 103
5.3.1. Effect of drag models 107
5.3.2. Effect of frictional pressure 110
5.3.3. Effect of lift gas velocity 114
5.4. Conclusions 118
6. Closure 120
6.1. Conclusions 120
6.2. Recommendations for future work 123
Appendix I Drag coefficient using EMMS drag model 125
Appendix II Calibration of Syamlal-O'Brien model 131
References 149

List of figures

Figure 1.1	Riser flows: (a) Schematic of fast fluidization of particles in riser (b) Core-annulus flow structure of radial profiles of solid velocity and volume fraction (Miller and Gidaspow, 1992) (c) S-shape axial profile of voidages (Li and Kwauk, 1994).	3
Figure 1.2	Resolution of gas-solid flows using (a) EE model (b) EL model and (c) DNS.	6
Figure 1.3	Thesis structure.	12
Figure 3.1	Interrelationship between various gas-solid flow models.	42
Figure 3.2	Formulation of the EE model.	43
Figure 3.3	(a) Inlet arrangements in experimental set-up, (b) One solid inlet configuration simulated by Benyahia et al. (2001).	52
Figure 3.4	Inlet arrangements used in 2D simulations (a) BC-A, (b) BC-B, and (c) BC-C.	53
Figure 3.5	Base case simulation results: (a) Mass flow rate at outlet as a function of time; (b) and (c) Time-averaged radial profiles mean solid volume fraction and velocity respectivley.	55
Figure 3.6	Effect of boundary conditions: (a) and (b) Radial profiles of mean solid velocity and volume fraction respectively.	57
Figure 3.7	(a), (c) and (e) solid velocity vector plots for BC-A, BC-B and BC-C respectively and (b), (d) and (f) solid volume fraction contour plots for BC-A, BC-B and BC-C respectively.	58
Figure 3.8	Kinetic energies of gas and solid phases using different inlet boundary conditions.	59
Figure 3.9	Effect of wall boundary conditions: (a) Solid velocity and (b) solid volume fraction profiles using BC-A; (c) Solid velocity and (d) solid volume fraction profiles using BC-B.	62

Figure 3.10	(a) Schematic diagram of 3D riser; (b) and (c) Radial profiles of mean solid volume fraction and velocity respectivley.	64
Figure 3.11	Comparison of results from 2D and 3D simulations along with those from previous study: (a) and (b) Radial profiles of mean solid velocity and velocity respectively; (c) Axial profile of solid volume fraction.	65
Figure 4.1	Flow regimes in gas-solid flows (Li and Kwauk, 1994).	76
Figure 4.2	Schematic of riser flow.	77
Figure 4.3	Drag coefficient calculated using the Gidaspow and EMMS models for (a) low and (b) high mass flux conditions.	80
Figure 4.4	Correction factor of the EMMS drag model for both low and high mass flux conditions.	81
Figure 4.5	Schematic diagram of FCC riser with corresponding dimensions for a low and high mass flux conditions.	85
Figure 4.6	Hydrodynamics of low mass flux riser: (a) Axial profile of voidages along height; and (b) and (c) Radial profiles of voidages at 3.5 and 8.75 m height respectively.	87
Figure 4.7	For low mass flux conditions: (a) Circulating solid flux, and (b) Solid inventory.	88
Figure 4.8	Hydrodynamics of low mass flux riser using a constant solid inventory on a time-averaged basis: (a) Axial profile of voidages along height; (b) and (c) Radial profiles of voidages at 3.5 and 8.75 m height respectively.	89
Figure 4.9	Circulating mass flux for simulations using constant solid inventory boundary conditions.	90
Figure 4.10	Hydrodynamics of high mass flux riser: (a) Axial profile of pressure drop along height; (b) and (c) Radial profiles of voidages at 3.9 and 8.1 m height respectively.	92

Figure 4.11	For high mass flux conditions: (a) Circulating solid flux, and (b) Solid inventory.	93
Figure 4.12	Effect of cluster diameter correlation on values from EMMS model: (a) Cluster diameters, and (b) Drag coefficients.	95
Figure 4.13	Effect of cluster diameter correlations on hydrodynamics of low mass flux riser: (a) Axial profile of voidages along height (b) Radial profiles of voidages at 3.5 and 8.75 m height respectively.	97
Figure 5.1	Schematic diagram of CCR and lift engager.	102
Figure 5.2	(a) Grid design, (b) Initial catalyst accumulation inside the lift engager, and (c) Change in catalyst accumulation as a function of time (Catalyst flow rate = 0.19 kg/s, Primary gas = 5 m/s, Secondary gas velocity = 7 m/s).	105
Figure 5.3	Effect of grid size (Catalyst flow rate = 0.19 kg/s, Primary gas = 5 m/s, Secondary gas velocity = 7 m/s).	106
Figure 5.4	Snap shots: (a) Catalyst volume fraction contour, (b) Catalyst velocity vectors and (c) Path lines of the lift gas entering from primary and secondary gas inlets (Catalyst flow rate = 0.19 kg/s, Primary gas = 5 m/s, Secondary gas velocity = 7 m/s).	107
Figure 5.5	Time-averaged radial profiles: (a), (c) and (e) Catalyst velocity at top of the lift line, middle of the lift line and top of the catalyst bed respectively; and (b), (d) and (e) Catalyst volume fraction at top of the lift line, middle of the lift line and top of the catalyst bed (Catalyst flow rate = 0.19 kg/s, Primary gas = 5 m/s, Secondary gas = 7 m/s).	109
Figure 5.6	Effect of the frictional pressure model on contour of catalyst volume fractions: (a) KTGF based and (b) Johnson and Jackson approach respectively.	111
Figure 5.7	Effect of the frictional pressure model: (a) Catalyst velocity and (b) volume fraction profiles for KTGF based and Johnson and Jackson approach respectively (Catalyst flow rate = 0.19 kg/s, Primary gas = 5 m/s, Secondary gas = 7 m/s).	112

Figure 5.8 Effect of the frictional pressure model: (a) Catalyst velocity and volume fraction profiles for riser simulation with KTGF based model (b) Catalyst velocity and volume fraction profiles for riser simulation with Johnson and Jackson model.

Figure 5.9 Simulated combinations of primary and secondary gas velocities. 115

Figure 5.10 Mass flow rate at outlet as a function of time (Catalyst flow rate = 0.19 kg/s). 116

Figure 5.11 PSDs of solid (a) flow rate and (b) accumulation time series. 117

Figure 5.12 Time averaged profiles along the height of the lift line (a) Catalyst velocity, (b) Catalyst volume fraction (c) Slip velocity (catalyst flow rate = 0.19 kg/s) (d) Comparison between current simulation results with previously published simulation results (Theologos and Markatos, (1994), Particle diameter = 0.503 mm, Particle density = 2643 kg/m3, Riser diameter = 13.5 mm, Riser height = 1.368 m, Superficial velocity of air = 12.3 m/s). 118

Figure A-1 Algorithm to calculate EMMS drag coefficients. 127

Figure A-2 Comparison between calculated values of (a) cluster diameter, (b) cluster fraction and (c) superficial gas velocities and those of Xu and Li, (1998). 128

Figure A-3 Comparison between calculated values of (a) cluster diameter, (b) cluster fraction and (c) superficial gas velocities and those of Yang et al. 2003. 130

Figure B-1 Algorithm for calibration of Syamlal-O'Brien drag model 132

List of tables

Table 1.1	Comparison of gas-solid models.	6
Table 2.1	Summary of experimental studies.	14
Table 2.2	Summary of simulation studies.	27
Table 3.1	Physical properties of gas and solid phases, and simulation parameters.	51
Table 4.1	Contributions to the EMMS model and its applications to the hydrodynamic studies on riser.	72
Table 4.2	EMMS drag equations applied to CFD simulations with corresponding correction factors.	83
Table 4.3	Simulation and model parameters.	84
Table 5.1	Phase properties, modeling and simulation parameters.	104
Table 5.2	Selection of drag model for lift engager	110

Nomenclature

A	Cross sectional area, m^2
a	Average acceleration of particles for a control volume, $m.s^{-2}$
C_D	Drag coefficient of a particle
D_t	Diameter of riser, m
d	Diameter, m
e	Coefficient of restitution
f	Cluster fraction
Fr	empirical material constant, $kg.m^2.s^{-2}$
F	Drag force acting on a single particle
G	Flux, $kg.m^{-2}.s^{-1}$
g	Gravitational acceleration, $m.s^{-2}$
$g_{o,ss}$	Radial distribution function
H	Height of riser, m
I	Unit stress tensor
m	Number of particles per unit volume
n	empirical material constant in frictional pressure model
p	empirical material constant in frictional pressure model
P	Pressure, $kg.m^{-1}.s^{-2}$
Re_s	Particle Reynolds number
u	Velocity, $m.s^{-1}$
U	Superficial velocity, $m.s^{-1}$
U_f	Superficial gas velocity in the cluster phase, $m.s^{-1}$
U_c	Superficial gas velocity in the dilute phase, $m.s^{-1}$
U_{pc}	Superficial particle velocity in the cluster phase, $m.s^{-1}$
U_{pf}	Superficial particle velocity in the dilute phase, $m.s^{-1}$

U_{sc} Superficial slip velocity in the cluster phase, $m.s^{-1}$

U_{sf} Superficial slip velocity in the dilute phase, $m.s^{-1}$

U_{si} Superficial slip velocity at interface between cluster and dilute phases, $m.s^{-1}$

U_s Slip velocity, $m.s^{-1}$

Greek letters

ε Volume fraction

ε_{mf} Minimum fluidizing voidage

β Drag coefficient, $kg.m^3.s^{-1}$

β_0 Standard drag coefficient, $kg.m^3.s^{-1}$

ρ Density, $kg.m^{-3}$

τ Stress tensor, $kg.m^{-1}.s^{-2}$

μ Viscosity, $kg.m^{-1}s^{-1}$

μ_s Solid shear viscosity, $kg.m^{-1}s^{-1}$

λ_s Solid bulk viscosity, $kg.m^{-1}s^{-1}$

Θ_s Granular temperature, $m^2.s^{-2}$

ϕ Angle of internal friction

ϕ Specularity coefficient

ω Correction factor

Subscripts

Col Collisional

c cluster phase

f dilute phase

fri Frictional

g Gas phase

i interface between the cluster and dilute phase

kin Kinetic

max Maximum

min Minimum

p Particle

ss Particle-particle

sw Particle-wall

s Solid phase

slip Slip velocity

Abbreviation

CFD	Computational fluid dynamics
CCR	Continuous catalytic reformer
CFBC	Circulating fluidized bed combustion
DPM	Discrete particle model
DNS	Direct numerical simulation
EE	Eulerian-Eulerian
EL	Eulerian-Langrangian
EGFM	Eulerian granular flow model
EMMS	Energy minimization multiscale modelling
FCC	Fluid catalytic cracking
KTGF	Kinetic theory of granular flows
QUICK	Quadratic Upstream interpolation for convective kinetics
SGS	Sub grid scale
SIMPLE	Semi-implicit method for pressure-linked equations

Circulating fluidized bed (CFB) has been used in various chemical processes such as fluid catalytic cracking (FCC), continuous catalytic reforming (CCR), circulating fluidized bed combustion (CFBC), circulating fluidized bed drying, polymerization etc. The main component of CFB is a riser, where solids are fluidized using gas flowing from the bottom with phases flowing co-currently upward and experiencing a chemical reaction. The gas-solid flow hydrodynamics such as mixing of two phases and formation of flow structures plays a dominant role in determining the extent of conversion, and in turn the performance of the CFB. Currently, designing and scaling-up riser reactors is mostly based on cold-flow pilot scale experiments (Sundaresan, 2000), which are costlier and more time consuming. As a result, the design methods for risers are largely empirical correlations without any in-depth understanding of the gas-solid flow hydrodynamics. Computational fluid dynamics (CFD) modelling can provide a promising alternative for studying the hydrodynamics of gas-solid flows in risers. Such a hydrodynamics study can be helpful in removing errors associated in designing, scaling-up and improving the performance (Dudukovic, 2009). However, currently CFD simulations of risers is a challenging exercise, particularly in modelling boundary conditions, phase interactions and also in capturing both time and length scales of the multiphase flow structures. In this research, CFD has been used to carry out both 2D and 3D simulations of flows in risers. The effects of boundary conditions and drag models on the hydrodynamics predictions have been investigated. After evaluating various modelling aspects, the CFD model has been applied to study the hydrodynamics of an industrial-scale lift engager.

1.1. Gas-solid flows in the riser

The state of gas-solid fluidization in risers can be characterized as a fast fluidization or pneumatic conveying (Grace, 1982). It is evident from various experiments (Miller and Gidaspow, 1992; Li and Kawauk, 1994; Knowlton et al., 1995; Nieuwland et al., 1996a; Bhusarapu et al., 2004) that typical riser flow (Figure 1.1a)

exhibits complex heterogeneity at different length scales. Three scale of heterogeneity namely; macro, meso and micro-scale have been identified by Li and Kwauk, (1994). At macro-scale, a wide variation in the voidage can be seen in both axial and radial direction throughout the equipment (Figure 1.1b and c). At the micro-scale, the heterogeneity is caused by particle-particle collisions and its interaction with the continuous gas phase. In addition to these apparent heterogeneities, the gas-solid flow in risers also shows the formation of particle aggregates called as "clusters" (Figure 1.1a). At the meso-scale, these clusters continuously interact with the surrounding dilute phase.

Miller and Gidaspow (1992) reported a time-averaged solid velocity distribution as a function of radial direction (shown in Figure 1.1b), and observed a higher solid velocity and lower solid volume fraction at the centre. In this region, which the authors referred as the "core" region, the solid particles were carried upward due to the flow of gas. Contrary to this, a downward flow of solids with lower velocity and with higher solid volume fraction was observed near the wall. This region was defined as the "annular" region. The flow with this radial heterogeneity has been generally referred as the "core-annular" flow. The core-annular nature of radial profiles of solid velocity and volume fraction has been widely reported in various experimental studies (Weinstein et al., 1986; Bader et al., 1988; Knowlton et al., 1995). Li et al. (1988) noted two regions in the axial profile of the volume fraction i.e. a dilute top and dense bottom region (Figure 1.1c). Li and Kawauk (1994) denoted such axial profile as an "S-shape" axial profile. Similar axial profile was also observed in the pressure drop data of Knowlton et al. (1995), in which a higher pressure drop was reported in the bottom section with lower value at the top section of the riser. Yerushalmi et al. (1976) observed the formation of clusters and movement of clusters surrounded by a dilute flow. Furthermore, these clusters are dynamic structures, which continuously undergo make-up and break-up processes (Yerushalmi et al., 1976; Subbarao, 1986; Li and Kawauk, 1994). These dynamic flow structures add more complexity to the flows in the riser.

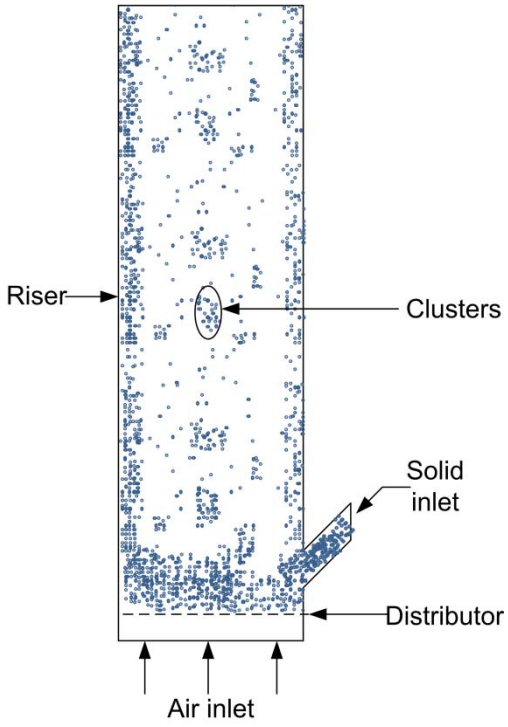

(a)

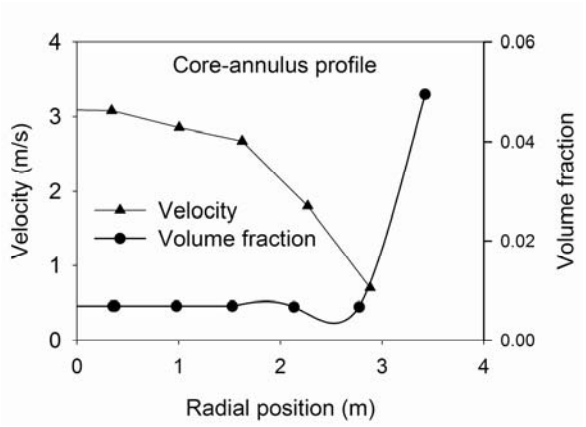

(b)

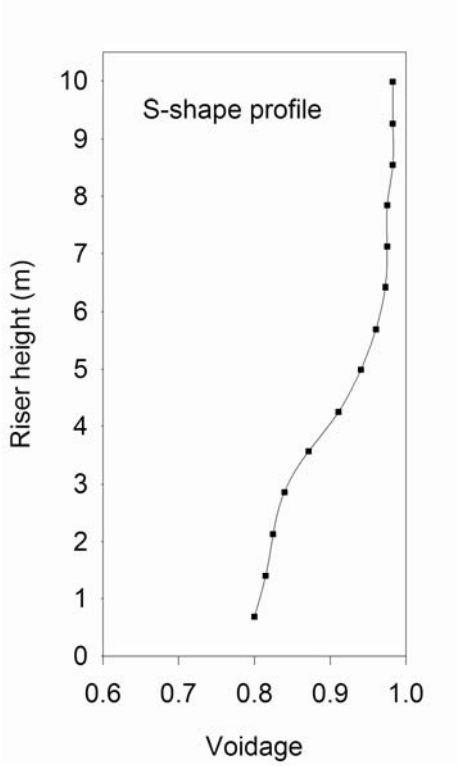

(c)

Figure 1.1: Riser flows: (a) Schematic of fast fluidization of particles in riser (b) Core-annulus flow structure of radial profiles of solid velocity and volume fraction (Miller and Gidaspow, 1992) (c) S-shape axial profile of voidages (Li and Kwauk, 1994).

1.2. Modelling of gas-solid flows in riser

CFD modelling of the gas-solid flows in the riser is rather difficult because of disparate time and length scales of multiphase flow structures (Sundaresan, 2000). The largest flow structures can be of magnitude in meters such as axial and radial heterogeneity, yet these structures can be directly influenced by gas-particle interactions, particle-particle interactions and formation of clusters, which take place below the millimetre scale (Agrawal et al., 2001). As a result, different models have been developed to represent the flow in riser.

The gas-solid flow models can be broadly classified on the basis of description of the solid phase, i.e. (a) by considering a continuum description, which then require a Navier-Stokes equation, this method is then called an Eulerian approach or (b) by considering it as a collection of discrete particles that obey Newton's law, called a Langrangian approach (Van der Hoef et al., 2008). Based on these two options for the solid phase, the models can be categorized in two different categories; namely the Eulerian-Eulerian and Eulerian-Langrangian models.

- Eulerian-Eulerian (EE) model: The EE model (Peirano et al., 2002; Enwald et al., 1996; Ding and Gidaspow, 1990; Sinclair and Jackson, 1989) considers both gas and solid phases to be continuous and fully interpenetrating (Figure 1.2a). The Navier-Stokes equations are then used for mass, momentum and energy conservation in both phases. Due to the continuum description of the discrete particle phase, the EE model requires additional closure laws to describe the rheology of particle phase. These closure laws are derived using the kinetic theory of granular flow (KTGF), which is basically an extension of the classical kinetic theory of gases for the dense particle flow (Lun et al., 1984). The KTGF then provides explicit closures for the solid phase such as the granular temperature, shear viscosity, coefficient of restitution that take into account for energy dissipation due to non-ideal particle–particle collisions. The interactions between the gas and solid phases are accounted for by using an interphase exchange coefficient.

- Eulerian-Langrangian (EL) model: The EL model (Tsuji et al., 1993; Hoomans et al., 1996; van Sint Annaland et al., 2005; Deen et al., 2007), also known as the discrete particle model (DPM), represents the solid phase as a collection of discrete particles (Figure 1.2b). The motion for each individual particle is solved by Newton's law by accounting for the effect of particle collisions and forces acting on the particle by gas. The solution of the equations updates the velocity and position of each particle. The particle-particle collisions are modelled by means of the empirical coefficient of restitution and friction (hard sphere approach) or empirical spring stiffness and a friction coefficient (soft-sphere approach) (Deen et al., 2007). However, the interactions between two phases are modelled using the drag correlation similar to those required in the EE model.

Another approach is direct numerical simulations (DNS) in which both solid and gas phase are resolved at micro-scale (Tsuji, 2007). In DNS, the particle trajectories and flow around individual particles are computed without using empirical constants for particle-particle and gas-particle interactions. It includes direct solution of the Navier-Stokes equations without averaging the parameters for either the solid or gas phase. This method uses the grid size of an order smaller than the size of the particles (Figure 1.2c), and thus, it is computationally very intensive even for small number of particles in laboratory-scale equipment. The Lattice-Boltzmann method has also been used to resolve miro-scale gas-solid flows in which the gas-particle interaction is now handled by boundary conditions at the surface of the solid spheres. Due to its computational intensity, the DNS approach is limited to obtain the interaction parameters between the two phases which are then used in the EE/EL model (Beetstra et al., 2006).

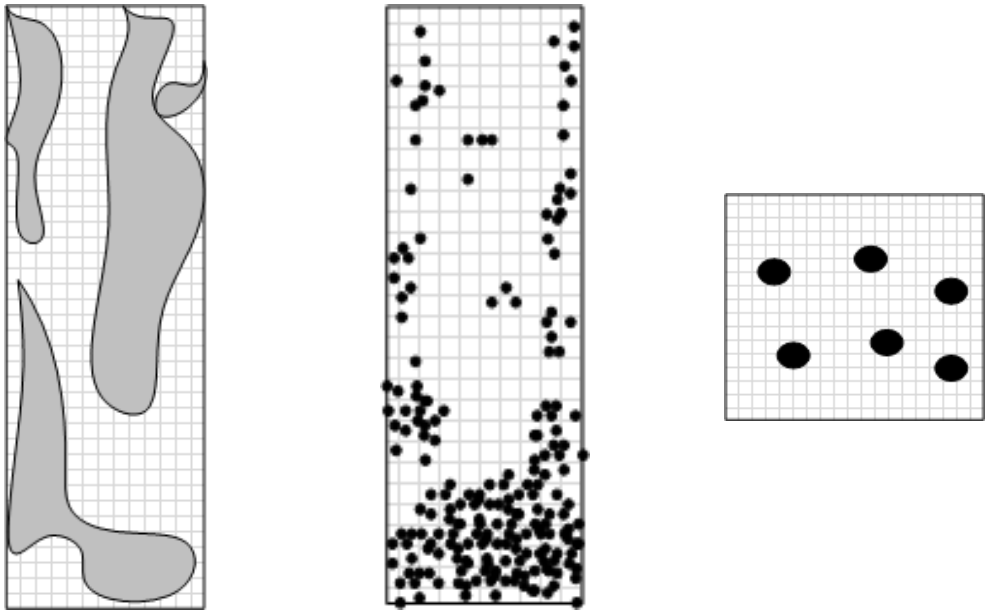

(a) EE model (b) EL model (c) DNS

Figure 1.2: Resolution of gas-solid flows using (a) EE model (b) EL model and (c) DNS (Van der Hoef et al., 2008)

Table 1.1: Comparison of gas-solid flow models (Van der Hoef et al., 2008)

Model	Gas phase	Solid phase	Gas-solid coupling	Scale
EE	Eulerian	Eulerian	Drag closure	Engineering (m)
EL	Eulerian	Langrangian	Drag closure	Laboratory (0.1 m)
DNS	Eulerian	Langrangian	Boundary conditions at particle surface	Laboratory (0.01 m)

Clearly, the gas-solid flow models are significantly different from each other in their ability to capture the flow physics, requirement of the computational effort and in turn their applicability. Table 1.1 gives a brief comparison of these models and scale at which they can be applicable. In the EL model, the Newtonian equations of motion for each individual particle are solved, and the accuracy of simulation is dependent on the number of particles tracked, which in turn is dependent on the computational resource employed. Therefore, for realistic industrial scale simulations, this approach is computationally intensive and can only be applied to laboratory-scale simulations.

In the EE model, both the solid and gas phases are represented as continuous and interpenetrating. Such continuous assumption for the solid particle phase allows use of coarse grid, which can have size many times larger than the length scales of the flow structures. Therefore, this representation is computationally less intensive and is well suited for modelling of engineering-scale flows (Ranade, 2001).

The comparison between different available models clearly indicates that the EE model is the obvious choice for simulations of industrial flows, which generally have high solid inventory. However, it should be noted that the predictability of the EE model is largely dependent on the empirical constants such as collision restitution factors and correlations such as solid phase closures and drag models. The EE model, in combination with the KTGF, has been applied extensively to study the hydrodynamics of the riser (Neri and Gidaspow, 2000; Benyahia et al., 2001; Huilin et al., 2003; Jiradilok et al., 2006; Vaishali et al., 2007; Almuttahar and Taghipour, 2008). In these studies, the effect of different boundary conditions, closure models, drag models, and even simulation parameters such as time step, grid size and domain considerations has been reported. Despite of several studies on the hydrodynamics of the riser, there are many shortcomings:

1. Most of the simulations have considered a 2D domain, in which inlet and outlet boundary configurations are significantly altered to approximate the gas-solid flows inside the 3D riser (Neri and Gidaspow, 2000; Benyahia et al., 2001). These boundary configurations do not reflect the 3D boundary configurations and carry significant assumptions. Thus, many of previous studies have emphasized the 3D simulations of the riser (Benyahia et al., 2001), which are computationally intensive.

2. Almost all the previous studies restricted themselves to a narrow set of operating regimes, either high or low mass flux conditions. Furthermore, the model has been validated using few selected quantities such as either holdup or velocity. In addition, the model validation for all experimental data measured on a single riser system is not available.

3. In EE model, the solid phase closure models and drag model are dependent on the flow system (Sundaresan, 2000). As a result, several models have been proposed in the literature to cater specific flow conditions. There is no consensus amongst previous studies on a single set of models, and clear guidelines on the selection of the drag model.

4. The gas-solid flows of fine particles (FCC catalyst) shows complex heterogeneity due to the formation of clusters. To capture this heterogeneity, the drag models based on the multiscale approaches (Li and Kawauk, 1994; Andrews Iv et al., 2005) have been proposed. These studies have showed considerable improvements in flow predictions using these drag models. However, these models are in developing stage and are applied to only particular flow conditions. Thus, they need to be evaluated for a wide range of flow conditions and experimental evidences.

5. Application of the model to simulate industrial-scale equipment has been challenging because of (i) complex geometry with many internals, (ii) large-scale, and (iii) existence of multiple flow regimes such as dense fluidization and dilutes fast fluidization within a single flow domain. As a result, only very few studies have reported on the application of the gas-solid flow model to simulate industrial equipment.

Thus, the EE model needs to be evaluated by studying the effects of different modelling aspects such as boundary conditions and closure models on the hydrodynamic predictions of the riser.

1.3. Objectives of this research

The current research addressed some of the shortcomings discussed in the previous section by evaluating the effect of boundary conditions, drag models and solid phase closure models on the hydrodynamics predictions. In this study, the EE gas-solid flow models were developed for different flow conditions by selecting appropriate modelling parameters. They were then used to simulate riser in both 2D and 3D domains. The hydrodynamic predictions were compared with the relevant

experimental data for necessary validations and to make conclusions on the effect of modelling and operating parameters on the flow predictions. The specific objectives of this research are:

1. To evaluate the EE model by comparing the hydrodynamics predictions from both 2D and 3D simulations of the flow in risers with experimental data.

2. To study the effect of inlet and wall boundary conditions on the flow predictions using the EE model.

3. To study the performance and applicability of structure-based drag model using the energy minimization multiscale (EMMS) model against the conventional Gidaspow drag model for predicting the hydrodynamics of the riser under different flow conditions.

4. To investigate the effect of cluster diameter correlations using the current framework of the EMMS model on the structure-based drag and hydrodynamics predictions.

5. To simulate industrial-scale catalyst lift engager, and conduct a parametric study such to assess the effect of lift gas velocities on the catalyst lift rate.

1.4. Contributions of this thesis

As a consequence of addressing above objectives, significant contributions have been made in this study by conducting coarse grid simulations of risers. Specific contributions are:

1. Different types of boundary conditions from previous studies were investigated in 2D simulations, and their effect on so-called “fully developed zone” was also studied.

2. The EMMS drag model was critically evaluated for predicting the flows in riser with different flow conditions.

3. The use of the EMMS model was further extended by using different cluster diameter correlations.

4. As a case study, the EE model was systematically applied to simulate an industrial-scale lift engager.

1.5. Outline of this thesis

The objectives were addressed by undertaking a systematic research program that is described in three parts, which are summarised below:

Part 1. Effect of Boundary Conditions.

CFD simulations were conducted for both 2D and 3D risers. The impacts of boundary conditions on the hydrodynamic predictions were investigated using three different types of inlet arrangements for both gas and solid phases for a 2D riser. The effect of wall boundary condition was studied by considering no-slip and partial-slip wall for the solid phase. Finally, a 3D simulation was also conducted by implementing the boundary configuration mimicking the experimental setup. The hydrodynamics model was qualitatively validated by comparing the radial profiles of solid velocity and volume fractions with the experimental data.

Part 2. Using EMMS drag model.

A structure-based EMMS drag model (Li and Kwauk, 1994) was used with the EE model to simulate the flow in risers under different flow conditions. The simulation results using the EMMS drag models were compared with those using the Gidaspow models (Gidaspow, 1994). The numerical predictions using both drag models were also compared with the published experimental data and simulation results. In addition, the effects of cluster diameter correlations on the structure-based drag coefficient and its impact on the hydrodynamic predictions were also investigated.

Part 3. Hydrodynamics of an industrial-scale lift engager

After evaluating the EE gas-solid flow model, it was then applied to simulate a 3D industrial-scale Lift engager, which transports the catalyst between a reactor and regenerator in continuous catalytic reforming (CCR) unit. A parametric study on the effect of lift gas velocities on the catalyst lift rate was carried out to characterise the hydrodynamics of the lift engager

The activities have been described in three chapters i.e. Chapter 3, 4 and 5 and form the core of this thesis. Chapter 2 consists of a literature review on the hydrodynamics studies of the riser. The EE model along with the governing equations and the concept of KTGF has been discussed in the Chapter 3. Finally, Chapter 6 provides a closure to the thesis summarizing different studies, their conclusions and discussions on the scope for future research.

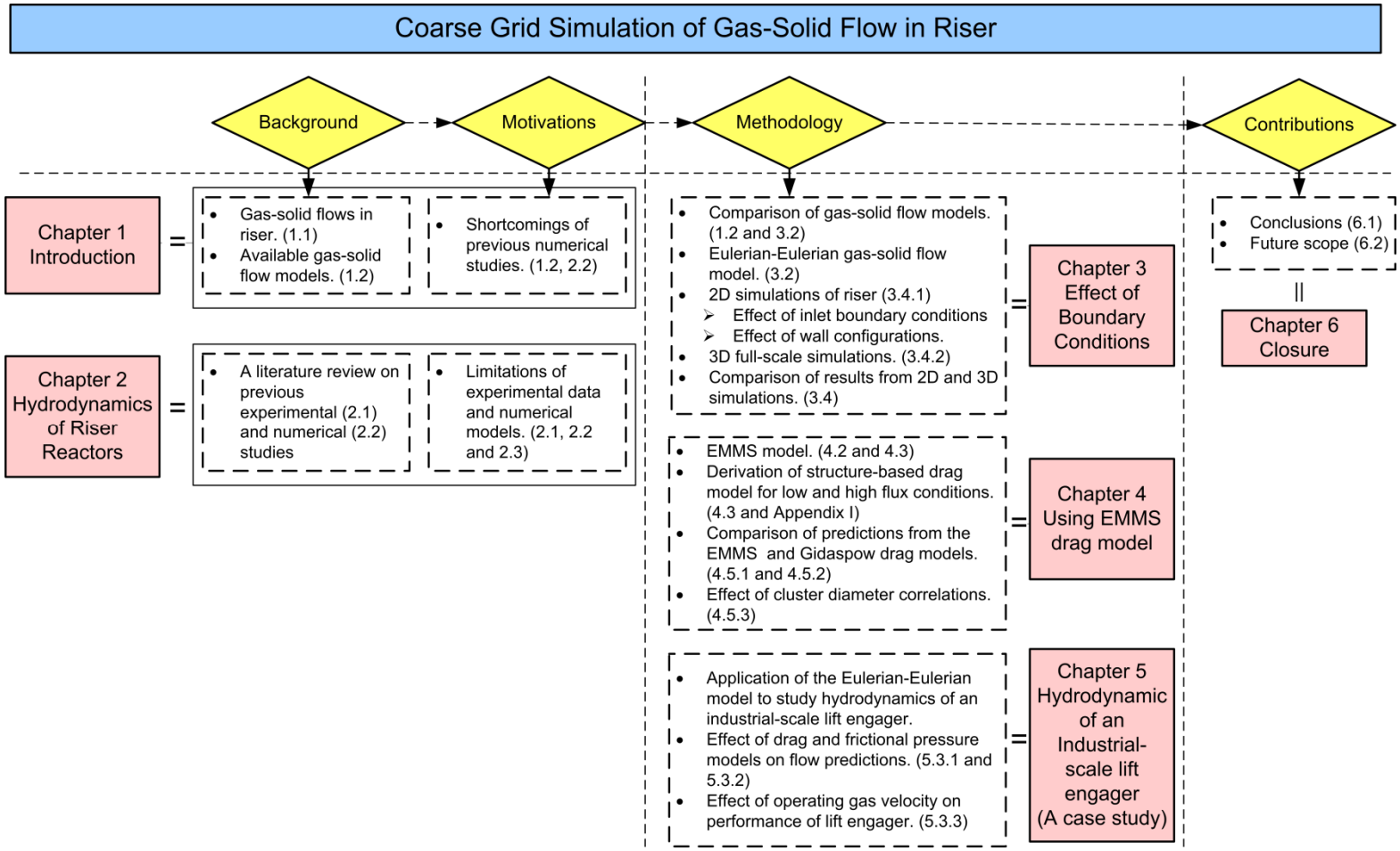

Figure 1.3 Thesis structure.

2. Hydrodynamics of Riser Reactors

A better understanding of the gas-solid flow hydrodynamics in riser is of critical importance for designing and improving the performance of the circulating fluidized bed (CFB) systems. In fluid catalytic cracking (FCC) units, the conversion reactions take place in the riser where the hot catalyst comes in contact with the heavy vacuum gas oil. The hot catalyst vaporises the liquid feed and cracking reaction occurs as the oil vapour and catalyst flow concurrently in the riser. Residence time and distribution of catalyst in the riser reactor can govern the performance of the reactor and ultimately specification of products. Another example is circulating fluidized bed combustion (CFBC). The CFBC gives flexibility to use a wide range of coal without compromising efficiency and with reduction in pollution. In CFBC units, the combustion of coal takes place in the riser. The intense mixing action in a splash zone of the riser immediately mixes the fresh coal and sulphur-absorbing chemical such as limestone with bed of solids. This results in uniform distribution of the temperature and less emission of pollutants. After the splash zone, the solids fluidizes in a plug flow manner in a transport zone at the top of the riser (Peirano and Leckner, 1998). The understanding of the state of fluidization and different flow structures is extremely necessary to improve the efficiency of CFBs. Hence a need to study the effects of operating and designing parameters on the heterogeneous flow structures in the riser has resulted in several hydrodynamic studies, including both experimental and numerical investigations.

2.1. Experimental Studies

Most of the experimental studies on the hydrodynamics of the riser have been conducted on the cold-flow CFB setups (Miller and Gidaspow, 1992; Knowlton et al., 1995; Nieuwland et al., 1996b; Ibsen, 2002; Bhusarapu et al., 2005). The focus of these experimental studies has been to capture time-averaged as well as fluctuating instantaneous values of the solid velocity, volume fraction and pressure at multiple locations inside the riser. A brief review of experimental studies on riser is summarised in Table 2.1.

Table 2.1: Summary of experimental studies.

Reference	Measurement technique	Experimental setup	Operating conditions	Important observations
Yerushalmi et al. (1976)	Pressure taps High-speed photography Butterfly valves	D_t = 3 inch H = 24 ft d_p = 60 μm ρ_s = 31.9 lb/ft^3	G_s = 1200 CFM U_g = 12 ft/s	Pressure drop along the height of the riser at different solid fluxes was measured. From high speed photography, the solid segregation was observed both in dilute and dense flows. Particles in segregation (Clusters) moved upward surrounded by a faster moving leaner phase. By increasing the solid loading, solid back mixing was observed. Dense strands were observed to fall and drift from the side, whereas, the bulk of the column was found to be occupied by particles moving upward in a dilute environment.
Rhodes and Geldart (1986)	Pressure taps	D_t = 0.152 m H = 6 m d_p = 64 μm ρ_s = 1800 kg/m^3	G_s = 8.5-107 kg/m^{2}s U_g = 2.5-4.5 m/s	Axial profiles of solid volume fractions at different solid circulation fluxes and superficial gas velocities were reported. A higher concentration at the bottom and a dilute flow top was reported. Solid volume fraction at the bottom increased with increase in solid circulation rate.

Reference	Measurement technique	Experimental setup	Operating conditions	Important observations
Li et al. (1988)	Pressure taps Optical probes Butterfly valves	D_t = 9 cm H = 10.5 m d_p = 54 μm ρ_s = 1654 kg/m^3	G_s = 14.3 kg/m^{2}s U_g = 1.52 m/s	Two regions in an S-shape axial profile were identified: a dilute top and dense bottom. The existence of the transition at the inflection point of the voidage was located. Dependence of the axial and radial voidage profiles on the gas velocity, solid inventory was also investigated.
Louge and Chang (1990)	Pressure taps Gate valve Capacitance probes	D_t = 19.7 cm H = 7 m d_p = 61 μm	G_s = 17 kg/m^{2}s U_g = 2 m/s	Voidages were recorded using capacitance probes at different regions of the riser. With these observations, fluctuations in voidages at dilute top, dense bottom and transition regions were recorded. Furthermore, time-averaged fluctuating voidages were found to be agreed with the existence of core-annular regions in radial profiles.

Reference	Measurement technique	Experimental setup	Operating conditions	Important observations
Miller and Gidaspow (1992)	X – ray densitometer Extraction probe	D_t = 7.5 cm H = 6.58 m d_p = 75 μm ρ_s = 930 kg/m^3	G_s = 12 kg/m^{2}s U_g = 2.89 m/s	Direct measurement of radial solid volume fraction was observed using X-ray densitometer probe, and solid flux was measured using extraction probe. Results were used to determine the solid velocity profile, axial pressure profile and also viscosity of the suspension.
Knowlton et al. (1995)	Pressure taps	D_t = 20 cm H = 14.2 m d_p = 76 μm ρ_s = 1712 kg/m^3	G_s = 485 kg/m^{2}s U_g = 5.2 m/s	Radial profiles of solid flux and density showed core-annulus profiles. The axial pressure drop profile showed higher pressure drop in the bottom and lower at the top section of the riser.
Nieuwland et al. (1996)	Optical probes Pressure taps	D_t = 5.4 cm H = 8 m d_p = 129 μm ρ_s = 2540 kg/m^3	G_s = 100-300 kg/m^{2}s U_g = 10 m/s	Radial profiles of velocity and volume fraction were reported for different operating conditions. Both increase in solids flux and decrease in gas velocity gave a higher segregation of solids towards wall. Average solids mass fluxes from the measured local values exceeded an imposed solids mass fluxes. This was explained by a down flow of solids at wall.

Reference	Measurement technique	Experimental setup	Operating conditions	Important observations
Wei et al. (1998)	Laser doppler anemometry	D_t = 18.6 cm H = 8 m d_p = 54 μm ρ_s = 1398 kg/m^3	G_s = 200 kg/m^{2}s U_g = 2.3-6.2 m/s	Development of core-annular flow was shown by plotting the radial profiles of solid velocity and volume fractions at different height of riser. Results showed similarity between the profiles in the dense bottom and dilute top of the riser. An S-shape axial profile of solid volume fractions was also observed. The radial profiles were found to be only a function of cross-sectional averaged solid fraction, but independent of gas velocity or solid flux.
Bai et al. (1999)	Optical fibre probes	D_t = 7.62 and 10.2 cm H = 6.1 and 8.2m d_p = 70 μm ρ_s = 1600 kg/m^3	G_s = 425 kg/m^{2}s U_g = 8 m/s	Voidage signals at two different locations were obtained and used to calculate averaged-voidage distribution and also chaotic analysis. Differences in the flow structures for different flow regimes such as bubbling, turbulent and fast fluidization regimes were identified.

Reference	Measurement technique	Experimental setup	Operating conditions	Important observations
Mathiesen et al. (2000)	Laser and Phase doppler anemometry	D_t = 3.2 cm H = 1 m d_p = 120 and 185 μm ρ_s = 2400 kg/m^3	U_g = 0.8, 1 and 1.2 m/s	Mean and fluctuating velocity for different particle sizes were measured at different flow conditions. Core-annulus flow with a relative velocity between particles of different sizes showed significant radial segregation of the mean diameter in the riser.
Pärssinen and Zhu (2001)	Fibre optic probes	D_t = 7.6 cm H = 10 m d_p = 67 μm ρ_s = 1500 kg/m^3	G_s = 100 and 300 kg/m^{2}s Ug = 8 m/s	Effects of variations in solid flux and gas velocity on the radial and axial distributions of solids at different heights were investigated.
Ibsen (2002)	Laser doppler anemometry Particle image velocimetry (PIV)	D_t = 2 cm H = 2 m d_p = 6. To 250 μm ρ_s = 2400 kg/m^3	U_g = 0.45 m/s	Mean particle velocity, particle RMS velocity and particle kinetic shear stresses were obtained from the PIV measurements.

Reference	Measurement technique	Experimental setup	Operating conditions	Important observations
Zhang et al. (2003)	Optical fibre density probe Laser Doppler velocimeter (LDV)	D_t = 41.8 cm H = 18 m d_p = 77 μm ρ_s = 1398 kg/m^3	G_s = 19-180 kg/m^{2}s U_g = 1.8-8 m/s	Transient signals of solid fraction were analysed using particle density distribution functions. PDD curves exhibited bimodal distribution, which were observed as an indication existence of two phases i.e. dilute dispersed phase and dense cluster phase.
Pandey et al. (2004)	Laser Doppler velocimetry (LDV)	D_t = 30.5 cm H = 15.2 m d_p = 812 μm ρ_s = 189 kg/m^3	G_s = 3.4-17.1 kg/m^{2}s U_g = 3.75-5.4 m/s	Effects of solid loading and gas velocity on the solid velocity distribution near the wall were reported. As solid circulation rate increased, the particle downward velocity also increased. The increase in gas velocity resulted in increase in particle velocity near the wall. Fluctuations in instantaneous velocity, was used to identify the formation of clusters. Criteria of clusters formation were proposed and then data was analysed to find presence of cluster.

Reference	Measurement technique	Experimental setup	Operating conditions	Important observations
Bhusarapu et al. (2005)	Computer-automated radioactive particle tracking (CARPT) Computer tomography (CT)	D_t = 15.2 cm H = 7.9 m d_p = 150 μm ρ_s = 2550 kg/m^3	G_s = 33.7 and 36.9 kg/m^{2}s U_g = 3.9 and 4.5 m/s	Non-invasive measurement technique provided not only a time-averaged velocity map and various turbulence parameters, but also particle trajectories. Solids velocity field data were obtained in two different risers with different operating solids fluxes and superficial gas velocity to span both the fast-fluidized (FF) and dilute phase transport (DPT) regimes. Core-annulus radial profiles as well as residence time distribution curves were reported.
Mabrouk et al. (2007)	Radioactive particle tracking (RPT)	D_t = 52 cm H = 1 m d_p = 250 and 170 μm ρ_s = 2500 and 3400 kg/m^3	U_g = 2 and 12 m/s	RPT measurement technique was used to obtain particle trajectories in the riser. Particle velocity, its fluctuations and acceleration were calculated to develop a new drag model considering effects of velocity fluctuations and Basset force.

Reference	Measurement technique	Experimental setup	Operating conditions	Important observations
He et al. 2006	Particle image velocimetry	2D riser W = 0.05 m D = 1.5 m H = 1 m d_p = 335 μm ρ_s = 2500 kg/m^3	G_s = 5,10 amd 20 kg/m^{2}s U_g = 2 – 2.3 m/s	Movements of clusters were analysed using PIV images. The clusters were observed to move downward faster along the wall. A wake was observed following the clusters, in which particles move downward quickly. Radial profiles of solid volume fractions and velocities were also observed at different axial locations
Van de Velden et al. (2007)	Positron emission particle tracking (PEPT)	D_t = 10 cm H = 6.5 m d_p = 90 μm	G_s = 25 and 89.7 kg/m^{2}s U_g = 3.6 and 9 m/s	Residence time distribution (RTD) curves were obtained from both stimulus response and continuous particle tracking. From RTD curves and particle velocity plots, a transition from core-annulus flow (mixed flow) to dominant core (plug flow) was identified.

Reference	Measurement technique	Experimental setup	Operating conditions	Important observations
Kim et al. (2008)	Pressure taps	D_t = 5 cm H = 4.5 m d_p = 70 μm ρ_s = 1740 kg/m^3	G_s = 7-300 kg/m^{2}s U_g = 0.2-9 m/s	Effects of different solid inlet configurations such as loop-seal type, J-valve, L-valve, as well as the outlet arrangements such as C-shape, L-shape and T-shape on solid circulation rate, solid inventory and pressure signals were investigated.
Yan et al. (2009)	Pneumatic phosphor tracer technique	D_t = 18.6 cm H = 10 m d_p = 78 μm ρ_s = 1225 kg/m^3	G_s = 40.8 and 229.4 kg/m^{2}s U_g = 3.156 and 5.989 m/s	RTD curves obtained at different operating conditions were used to analyse the solid mixing. The peak height of the RTDs were analysed to conclude the co-existence of two mechanisms in axial direction: the dispersion of dispersed particle and that of clusters.
W. Chan et al. (2010)	Positron emission particle tracking (PEPT)	D_t = 16 cm H = 7.9 m d_p = 120 μm ρ_s = 2260 kg/m^3	G_s = 5 and 622 kg/m^{2}s U_g = 1 and 10 m/s	Radioactively labelled single particle was tracked to determine particle motion, population densities in the riser. Links between the particle velocities and overall solid mixing were identified. The average particle velocity and the velocity distributions were used to determine the RTD of solids.

In early 1980s and 1990s, several experimental studies (Yerushalmi et al., 1976; Rhodes and Geldart, 1986; Louge and Chang, 1990) were conducted by measuring static pressures at different axial and radial positions. Yerushalmi et al. (1976) conducted the experiments on fast fluidization of the FCC catalyst particles using a 2D riser. The pressure readings were taken at several locations using pressure taps, and high speed cameras were used to film the gas-solid flows. They observed several important aspects i.e. (i) the existence of high solid segregation at both low and high solid loadings; (ii) movement of particles in the segregation within fast moving lean phase; (iii) rise, fall and drift of dense strands and ribbons from side to side at high speed; (iv) the bulk of the column occupied by dilute flow moving upward; (v) makeup and breakup of dense strands and (vi) higher pressure gradient at the bottom and lower values at the top of the bed. Furthermore, the study also discussed the effect of operating parameters on the fast fluidization regimes and several advantages of the fast fluidization bed. The observations of Yerushalmi et al. (1976) yielded an insight on the flow structures in the CFB risers, and provided ground for further experimental investigations.

Rhodes and Geldart (1986) measured the pressure drop, and reported axial profiles of solid volume fractions along the height of the riser. They observed higher volume fractions at the bottom and a dilute top section. Furthermore, they observed that the solid volume fraction in the dense bottom section increased with the solid circulating fluxes. Li et al. (1988) also measured pressures at different axial and radial locations using pressure taps. Recorded pressures were then used to calculate averaged voidages. The observations showed axial variation of the voidages having an S-shape profile with a dense bottom and dilute top region. They also recorded a transition height between dense and dilute regions. The sensitivity of axial profiles as a function of parameters such as the gas velocity and solid inventory were also reported. Louge and Chang (1990) conducted experiments using non-intrusive capacitance probe to measure the voidages. Their observations confirmed the presence of a dense annulus of solids near the wall. Furthermore, cross-sectional averaged voidages at different elevations also showed dense bottom and dilute top sections. By now, a broad picture of the fast fluidization in the riser and different flow structures inside it was clear. But further observations were necessary for capturing the local velocity and voidage distribution in different parts of the riser. These observations could provide a reasonable validation of the

gas-solid flow models, which would then be used to understand an effect of design and operating parameters on the flow structures. However, all of these observations were based on the pressure drop data measured using pressure taps, which were inserted into the flow domain and could influence the nearby hydrodynamics. Thus, in later studies more emphasis was laid on the use of non-invasive measurement techniques.

Miller and Gidaspow (1992) used an X-ray densitometer in which the detectors were used to capture the intensity of X-rays reflected from the particles. The X-ray intensity data was then used to calculate the solid volume fractions. This non-invasive measurement technique gave quantitative values of the solid velocity and volume fractions at different radial positions and heights. The radial profiles clearly indicated the existence of the core-annulus flow having higher solid volume fraction near the wall and lower in the bulk of the riser. In addition, the observations were also made on the effect of solid flux and gas velocity on the radius of the core region. Nieuwland et al. (1996b) used optical fibre probes to record the local solid concentration and velocity. In this measurement method, the reflection of light emitted from the laser source by the particles was measured using the photo diodes. The detected optical signal was converted into the electric signal, which was correlated to the solids concentration. The results showed the core-annulus profile of radial distributions for different operating conditions. It also showed that the increase in the solids mass flux at constant superficial gas velocity, or alternatively the decrease in the superficial gas velocity at constant solid mass flux, the lateral solids segregation became more pronounced. Furthermore, the axial solids velocity profile showed a weak dependence with respect to solids mass flux. Decreasing the superficial gas velocity caused a decrease in the solids velocity although the shape of the profiles was relatively unaffected.

Zhang et al. (2003) used a Laser-Doppler Velocimetry (LDV) measurements technique to measure the fluctuating local solid velocities. In LDV, two light signals i.e. the one coming from the reference source and (ii) the other being reflected from the tracer particles were compared to measure the Doppler frequency shift. The ratio of the two signals was then used to measure the solid fractions and velocity signals. In this study, transient signals of solid fractions at multiple locations were analysed to study the differences in cluster formation

patterns in both riser and downer. Ibsen (2002) used a Particle Image Velocimetry (PIV) technique in which movements of tracer particles were captured using images taken from a high speed camera. The image processing gave a velocity maps inside the equipment and could provide the observations on the movement of clusters. Isben (2002) reported particle velocity near the wall region at different superficial gas velocities. The optical measurement techniques such as LDV and PIV require the riser to be made of transparent materials such as glass, acrylic or PVC which allow the detectors or high speed cameras to capture the reflection or images respectively. These techniques provide only the Eulerian measurements at certain elevation of the riser. However, in reality the CFB systems are opaque and have high solids mass fluxes and solids holdup. Hence, these measurements using optical technique could not describe the flows properly and non-invasively.

Recently, non-invasive measurement techniques such as radioactive particle tracking (RPT) (Roy et al., 1997; Bhusarapu et al., 2004; Mabrouk et al., 2007) and positron emission particle tracking (PEPT) (Van de Velden et al., 2007; W. Chan et al., 2010), have been developed to record time-averaged values, along with the Langrangian trajectories of the tracer particles. In these methods, a radioactive particle is used as a tracer, and the emission from this particle is detected at multiple locations. The data on the particle position can be used to construct probability density functions (PDF) which lead to time-averaged map of solids velocity and volume fraction, and residence time distribution (RTD) curves. Bhusarapu et al. (2005) used RPT to map the flow regimes of dilute gas-solid flows in the riser. From the experimental data, the radial distribution of solids volume fractions, velocity and fluctuating component of solids velocity, along with RTD curves were reported. Van de Velden et al. (2007) used PEPT to carryout experiments under different superficial gas velocities and circulating solid fluxes. Then, the flow conditions inside the riser were characterised as mixed or plug flows from the RTD curves, and a range of operating conditions were recommended for required degree of back-mixing.

The above experimental studies captured radial profiles, axial profiles, fluctuations in velocity and volume fractions and RTD curves. They also demonstrated a continual advancement in our measurement ability. With current experimental techniques, it is now possible to explain

the macro-scale heterogeneity and the back-mixing in the gas-solid flows in riser. However, it is still not possible to access many important properties such as an accurate measurement of the cluster properties. Furthermore the effect of operating parameters and riser dimensions on the clustering phenomena still need more investigations. Therefore, fundamentals of formation of heterogeneous flow structures remain largely unknown. In addition, both axial and radial profiles at multiple locations in a single CFB riser set-up have also been rarely reported. A validated CFD model can provide a valuable insight into parameters not currently accessible through experiments.

2.2. Numerical studies

CFD studies can facilitate endless number of trials to evaluate alternate design configurations and optimal operating parameters. It can also be used to understand various flow structures and inherent heterogeneity of flows in riser. CFD models of varying degree of complexity such as the EE model (two-fluid model), the EL model (discrete particle model) and direct numerical simulations (DNS) have been used in the past to capture the underlying physics of the gas-solid flows. However, the EE model offers computational edge over other models especially in case of systems operating with high solid holdup and those involving large industrial/complex geometries (Van der Hoef et al, 2008). Consequently, the EE models have been used in several previous hydrodynamics studies (Arastoopour et al., 1990; Miller and Gidaspow, 1992; Nieuwland et al., 1996a; Ranade, 1999; Benyahia et al., 2001; Ibsen, 2002; Yang et al., 2004; Benyahia et al., 2005; Jiradilok et al., 2006; Vaishali et al., 2007; Almuttahar and Taghipour, 2008; Benyahia, 2009; Chalermsinsuwan et al., 2009; Naren, 2009). Since the objective of this study was to enhance the predictions from the EE model so that it can be reliably used to simulate large-scale equipment. Therefore, this review (as summarised in Table 2.2) focuses only on those simulation studies which were conducted using the EE model.

Table 2.2: Summary of simulation studies.

Reference	Model	Computation	Code	Validation	Comments
Arastoopour et al. (1990)	2D riser, Two-phase model, Gibilaro drag model (Gibilaro et al., 1985)	D_t = 0.152 m H = 0.33 m d_p = 64 μm, ρ_s = 1800 kg/m^3	FORSIM	Quantitative validation with the experimental data of Geldart and Rhodes, (1986).	Effect of superficial gas velocity on the radial profiles of the solid velocity and volume fractions at different height was studied. Need of more research to obtain suitable gas-solid interaction model, solid viscosity model were expressed.
Pita and Sundaresan (1993)	2D axisymmetrical, EE model, Wen-Yu drag	D_t = 0.152 m, H = 10 m d_p = 76 μm, ρ_s = 1714 kg/m^3	In house		Effects of inlet boundary conditions on the solid flow patterns were investigated using three different inlet boundaries for both gas and solid phases. Effects of restitution factor, inlet granular temperature and column diameter were also investigated.

Reference	Model	Computation	Code	Validation	Comments
Nieuwland et al. (1996)	2D axisymmetrical, two-fluid (EE) model, Gidaspow drag model	D_t = 0.0536 m, H = 8 m d_p = 129 μm, ρ_s = 2540 kg/m^3	-	Predicted radial profiles of the solid velocity and volume fraction were compared with the experimental data of Nieuwland et al. (1996), Bader et al. (1988) and previous numerical results of Ding and Gidaspow (1990).	Interaction between the gas-phase eddies and dispersed particles were modelled using a modified Prandlt mixing length model. The results showed a reasonable qualitative agreement with the experimental data.
Ranade (1999)	2D axis-symmetrical periodic domain, EE model, Wen-Yu drag model	D_t = 0.14 m, d_p = 54 μm, ρ_s = 1545 kg/m^3	Fluent	Numerical predictions were compared with the experimental data of Yang et al. (1991) and van Bruegel et al. (1969)	2D periodic domain had been used to predict fully-developed flow profiles. Effects of gas and solid fluxes and riser diameter on the hydrodynamics predictions were studied.
Mathiesen et al. (2000)	2D domain having full CFB loop, EE model, Gidaspow drag model	D_t = 0.032 m, H = 1 m d_p = 120 μm, ρ_s = 2400 kg/m^3	Spalding	Radial distributions of the solid velocity and volume fraction were compared with the experimental data.	Simulations predicted good agreement with the experimental data showing core-annulus radial profile.

Reference	Model	Computation	Code	Validation	Comments
Benyahia et al. (2001)	2D riser, EE model, Arastoopour drag model (Arastoopour et al., 1990)	D_t = 0.2 m, H = 14.2 m d_p = 76 μm, ρ_s = 1740 kg/m^3	Fluent	Simulation results of radial profiles of solid flux and density were compared with the experimental observation of Knowlton et al. (1995). Axial pressure drop profile was also compared with the experimental data.	Only qualitative agreements for both radial and axial profiles were achieved. Effect of initial solid inventory was found to have no impact on the steady state results. Effect on inlet boundary conditions was studied by implementing two solid inlets at side walls and one solid inlet as appearing in the experimental set-up. The simulation with one solid inlet gave higher solid segregation towards the one wall.
Neri and Gidaspow (2000)	2D Cartesian and axis-symmetric, EE model, Gidaspow drag model	D_t = 0.075 m, H = 6.58 m d_p = 75 μm, ρ_s = 1654 kg/m^3	MFIX	Radial profiles of the solid velocity and volume fraction were compared with the experimental data of Miller and Gidaspow, (1992)	Different solid inlet velocity profiles such as uniform and trapezoidal profiles were simulated and found to have significant impact on the flow patterns in the riser. Effect of particle cohesive forces and wall restitution factor was also studied.

Reference	Model	Computation	Code	Validation	Comments
Agrawal et al. (2001)	2D periodic domain, EE model, Gidaspow drag model	FCC particles	MFIX		Importance of resolving meso-scale structures, "clusters", was discussed. These structures were too small to capture in coarse grid simulation. However, they still affected the overall hydrodynamics. Effects of meso-scale structure on the gas-particle interaction (drag) force and solid stresses were discussed.
Yang et al. (2003)	2D domain, EE model, EMMS drag	D_t = 0.09 m, H = 10.5 m d_p = 54 μm, ρ_s = 930 kg/m^3	CFX	Both axial and radial profiles of voidages were compared with the experimental data of Li and Kwauk, (1988).	The Structured-based drag from the EMMS model was incorporated in the EE model to simulate 2D domain of the riser. Effect of solid inventory was investigated by implementing cycle boundary conditions for solid inlets and outlets. Both axial and radial heterogeneity of voidage profiles was captured, but only quantitatively.

Reference	Model	Computation	Code	Validation	Comments
Huilin et al. (2005)	2D riser, EE model, Cluster-based drag model	D_t = 0.076 m, H = 10 m d_p = 67 μm, ρ_s = 1500 kg/m^3	KFIX	Radial profiles of solid velocity and volume fractions were compared with the experimental data Manyele et al. (2002).	Simulations were conducted with different operating conditions and using the cluster-based drag model. The predictions showed significant improvements in capturing experimental observations of solid velocity and volume fraction distribution in the flow domain.
Andrews Iv et al. (2005)	2D periodic and cartesian geometry, EE model, Sub-grid closure models	D_t = 0.1562 m, H = 6.164 m d_p = 75 μm, ρ_s = 1500 kg/m^3	MFIX	Results were not compared with the experimental data.	Sub-grid closures were constructed from the results of high resolution simulations of periodic domain to account for micro-scale flow structures. These closures were then applied to coarse grid simulations, which showed significant qualitative improvements using the sub-grid closures than those performed without the sub-grid corrections.

Reference	Model	Computation	Code	Validation	Comments
Jiradilok et al. (2006)	2D riser, EE model, EMMS drag model	D_t = 0.186 m, H = 8 m d_p = 54 μm, ρ_s = 1398 kg/m^3	In house	Simulation results were compared with high density riser experiment of Wei et al. (1998).	Simulations of riser having high solid flux were carried out using the EMMS drag derived by Yang et al. (2003).Radial profiles, granular temperature, solid pressure, viscosity and frequency of oscillation were compared with the experimental data.
Almuttahar and Taghipour (2008)	2D riser, EE model, Gidaspow, Syamlal and O'Brien, Arastoopour drag	D_t = 0.762 m, H = 6.1 m d_p = 70 μm, ρ_s = 1600 kg/m^3	Fluent	The experimental studies of Liu, (2003) were used to evaluate the simulation results.	Core-annulus gas-solid inlet was used in the riser simulations. A separate simulation for the J-valve was conducted, and the results were then used to justify the selection of core-annulus inlet. The effect of different drag models, restitution coefficients, specularity coefficient and gas phase turbulence was investigated.
Vaishali et al. (2007)	2D riser, EE model, Wen-Yu drag model	D_t = 0.152 m, H = 8.9 m d_p = 150 μm, ρ_s = 2550 kg/m^3	Fluent	Radial profile of solid velocity, volume fraction and granular temperature were compared with the experimental data of Bhusarapu et al. (2005)	Effects of drag models on the hydrodynamics predictions were discussed. Radial profiles of solid velocity volume fraction and granular temperature were also compared with the experimental data.

Reference	Model	Computation	Code	Validation	Comments
Wang et al. (2007)	2D domain, EE model, EMMS drag	D_t = 0.09 m, H = 10.5 m d_p = 54 μm, ρ_s = 930 kg/m^3	CFX	Both axial and radial profiles of voidages were compared with the experimental data of Li and Kawauk, (1988).	Proposed an extended version of the EMMS model which calculated the Structure-based drag in each computational cell using local flow conditions..
Igci et al. (2008)	2D and 3D periodic domain, EE model, Sub-grid closure models	D_t = 0.1562 m, H = 6.164 m d_p = 75 μm, ρ_s = 1500 kg/m^3	MFIX	Results were not compared with the experimental data.	Sub-grid closures were developed using high resolution simulations of 2D and 3D periodic domain. The study considers a need for modifications in the two-fluid equations to introduce the effect of unresolved structures. It also shows an effect of filter grid size on the sub-grid closures.
Naren (2009)	3D periodic domain, Wen-Yu drag model	D_t = 0.0536 m, H = 8 m d_p = 129 μm, ρ_s = 2540 kg/m^3	Fluent	Computational results were compared with the experimental data of Nieuwland et al. (1996).	Very fine mesh was used in 3D periodic domain to study an effect of different model parameters such as drag models, granular temperature conservation equations, restitution coefficient and specularity coefficient on the numerical predictions.

Reference	Model	Computation	Code	Validation	Comments
Benyahia (2009)	2D and 3D riser, EE model, Both EMMS and Sub-grid drag models	D_t = 0.2 m, H = 14.2 m d_p = 76 μm, ρ_s = 1740 kg/m^3	MFIX	Numerical predictions of radial voidage profiles and axial pressure drop profile were compared with the experimental data of Knowlton et al. (1995)	Drag models were derived using both EMMS and Sub-grid approach to simulate both 2D and 3D domains of the riser. It was concluded that both drag models still give only qualitative agreements with the filtered model giving reasonably better agreement with the experimental data.

.

Arastoopour et al. (1990) used a continuum model to simulate the flows in 2D riser, and reported radial distributions of solid velocity and volume fraction at various height of the riser using different gas velocities. The profiles showed non uniformity as captured in the experimental data. The authors validated their model using the experimental data (Rhodes and Geldart, 1986). Ding and Gidaspow (1990) showed the formulation of the EE model as a generalised Navier-Stokes equation proposed by Jackson (1963), and derivation of the solid phase constitutive equations from the KTGF (Jenkins and Savage, 1983; Lun et al., 1984) starting from the Boltzmann equation for the velocity distribution of particles. However, they simulated a bubbling fluidized bed but the model description was quite useful in understanding the EE model applied to the gas-solid flows in the riser. Neri and Gidaspow (2000) used the two fluid model presented by Ding and Gidaspow (1990), and compared the hydrodynamics predictions with the experimental data of Miller and Gidaspow (1992). In their model, the interaction between the gas and solid phases was modelled using the Gidaspow drag (Gidaspow, 1994) model, which is a combination of the Wen-Yu and Ergun equations for the dilute and dense flows respectively. They also studied the effect of inlet boundary conditions and cohesive forces between the particles on the hydrodynamics predictions, and also utilised different geometrical considerations such as axis-symmetry simulation.

Nieuwland et al. (1996) conducted both experiments and CFD simulations using the EE model. In this study, the interaction between the gas-solid phases was modelled using the turbulence model. The predictions were compared with their experimental data showing only qualitative agreements. Ranade, (1999) simulated 2D periodic domain of the riser and showed that the results were in good agreement with the experimental data of Yang et al. (1991). However, their results showed wide disagreements with the experimental data of Bruegel et al. (1969). Benyahia et al. (2001) conducted 2D simulation and compared the results with the experimental data of (Knowlton et al., 1995). The study showed considerable disagreements with the data for both radial profiles of the solid density and velocity, as well as the axial profile of the pressure drop. The effects of boundary conditions and time-averaging on the flow predictions were also evaluated. The results showed negligible effect of duration of the time-averaging on the radial profiles, whereas the boundary conditions such as single inlet

and multiple side inlets in 2D domain had profound effect on the flow predictions. Numbers of studies were performed using various boundary conditions, drag models and solid phase closure models, however, the agreements with the experimental data for both the radial and axial profiles could not be achieved. To remove this limitation of the model, the focus was shifted towards the multi-scale approaches, which could capture different flow structures such as clusters. The simulations were conducted using the structure-based drag models derived from the multi-scale approaches instead of using the drag model derived for the single particle (Wen and Yu,) or that modified for multi particle system (Gidaspow, 1994 and Syamalal and O'Brien, 1993). The structure-based drag models accounting for the effect of cluster formation have been derived using two approaches, namely, the energy minimization multiscale (EMMS) and sub-grid scale (SGS) approach.

Li and co-workers (Li and Kawauk, 1994; Ge and Li, 2002; Wang et al., 2007; Yang et al., 2003a, b; 2004) developed an EMMS approach to derive structure-based drag models, which were then used with the EE model to simulate the riser. Yang et al. (2003b. 2004) used a structure-based drag from the EMMS approach to simulate low mass flux FCC riser. The results showed significant improvements in the flow predictions especially the axial profiles of voidage compared to those using the Gidaspow drag model. Naren et al., (2007) critically reviewed the EMMS model and raised several questions on the solution criteria of minimum energy and its sensitivity on different structure parameters models. Their study showed that the minimum energy could only be achieved at the lowest possible value of the cluster diameter. Furthermore, the study also revealed excessive sensitivity of the solution to different flow structure parameters such as the cluster diameter correlations and assumptions such as maximum voidage. However, further advancement in the EMMS model was proposed by Wang et al. (2007) which also showed better predictions for the axial and radial heterogeneity.

Another approach called Sub-grid scale (SGS) model has been developed by Sunderasan and co-workers (Agrawal et al., 2001; Andrews Iv et al., 2005; Igci et al., 2008). Agrawal et al. (2001) conducted highly resolved simulations using continuum model in 2D and 3D periodic domains with grid size of an order less than ten particle sizes, and observed non-uniformity in

the flows caused by the formation of the clusters. They found a significant effect of the clusters on the gas-solid drag and the solid viscosity, and concluded that unresolved flow structures could contribute to results predicted by coarse-grid simulations. Andrews Iv et al. (2005) used the results of high resolution periodic simulations to derive the gas-solid drag, solid phase viscosity and pressure accounting for the effect of the clusters on the flows. Igci et al. (2008) studied the effect of grid size (known as filter size) on the sub-grid closures. Authors also considered a need for modifications in the two-fluid equations to introduce the effect of unresolved structures. The coarse grid simulations using sub-grid closures gave considerable insight into hydrodynamics of riser. Recently, Benyahia, (2009) applied a structure-based drag derived using both the EMMS and SGS approach to simulate the high flux flows in the riser and concluded considerable improvements in the hydrodynamics predictions using both approaches, however, those using the SGS model showed better agreement with the experimental data.

The above literature review clearly shows that the simulations have been performed using different geometrical configurations such as 2D-Axisymmetric (Pita and Sundaresan, 1993; Nieuwland et al., 1996a; Ranade, 1999), 3D-fullscale (Zhang et al., 2008; Benyahia, 2009) and 3D periodic domains (Agrawal et al., 2001; Naren, 2009). Most of the previous simulation studies were conducted using 2D risers instead of 3D cylindrical risers. In 2D simulations, different types of inlet and outlet boundary conditions have been used (Miller and Gidaspow, 1992; Benyahia et al., 2001; Almuttahar and Taghipour, 2008), and these boundary conditions have been quite different from the actual 3D boundary conditions. In the previous studies, the gas-solid interactions had been modelled using the drag models such as the Wen-Yu (Ranade, 1999; Benyahia et al., 2001; Vaishali et al., 2007) and Gidaspow (Miller and Gidaspow, 1992; Agrawal et al., 2001; Almuttahar and Taghipour, 2008) drag models. These drag models were generally derived from the experimental data such as pressure drops in packed bed and terminal velocity of a particle. Simulations (Benyahia et al., 2001; Yang et al., 2003b; Yang et al., 2004) using these drag models could only capture the qualitative trends of the radial profiles of voidages, but not the axial profiles. Therefore, multi-scale approaches have been developed in the recent past. Currently, most of the research has been carried out to develop structure-based drag models, which use multi-scale

approaches and their integration with the EE model to capture the heterogeneous flow structures (Yang et al., 2003b; Yang et al., 2004; Andrews Iv et al., 2005; Wang et al., 2007; Igci et al., 2008; Wang, 2008). Though, use of multi-scale approaches gave significant improvements in the hydrodynamics predictions (Yang et al., 2004; Andrews Iv et al., 2005) by capturing the qualitative trends of the axial and radial heterogeneity, the quantitative agreements still have not been achieved (Yang et al., 2004; Benyahia, 2009). Furthermore, these modelling approaches are still at the development stage, and rigorous evaluations of them are necessary before using them to simulate industrial- scale equipments.

2.3 Summary

Hydrodynamic studies on risers have revealed both inadequacies of experimental studies and an infancy of CFD models. The experimental studies do not give accurate measurements on heterogeneous flow structures such as clusters. In addition, a sensitivity of clusters on operating and designing parameters still has not been investigated. On the other hand, the CFD models largely rely on empirical coefficients and correlations, and therefore, many assumptions in geometrical configurations and different correlations for closure models were used. Subsequently, a clear disagreement on the boundary conditions, geometrical considerations, drag models and solid phase closure models used the EE gas-solid flow models has emerged. Furthermore, these models have been only validated by qualitative agreements with the experimental data, and quantitative agreements have not been achieved. Thus, there is a need for further investigation such as effect of modelling aspects on the hydrodynamics predictions, which can then lead to optimal modelling parameters and help to refine the flow predictions. In this work, both 2D and 3D simulations of riser were conducted for detail validation of the EE models, along with investigations on the effect of (i) boundary conditions (Chapter 3) to remove ambiguity on the selection of particular boundary conditions and (ii) multi-scale model (Chapter 4) to improve the current state of hydrodynamic predictions for a wide range of flow conditions.

3.1. Introduction

Computational fluid dynamics (CFD) has been extensively used to study hydrodynamic of riser using different modelling approaches. However, most of previous simulations on riser have been conducted using 2D risers because 3D simulations are rather computationally intensive. In previous 2D simulations, different boundary conditions have been used for the inlets and outlets. For example, inlet arrangements such as two-sided inlets (Pita and Sundaresan, 1993; Benyahia et al., 2001), core-annulus inlets (Almuttahar and Taghipour, 2008) and uniform gas-solid inlets (Neri and Gidaspow, 2000) have been used. None of these solid inlet arrangements are close to the actual 3D boundary conditions of an experimental setup, and they are merely assumed to approximate the solid entry into the 2D domain. Therefore, boundary conditions for gas and solid inlets in the 2D riser have been a subject of discussions in several previous studies (Pita and Sundaresan, 1993; Benyahia et al., 2001; Vaishali et al., 2007).

Pita and Sundaresan, (1993) examined three different inlet configurations, namely, uniform inlet, core-annulus flow at the inlet and circumferential injection of secondary gas. It was concluded that the inlet configuration had a profound impact on the segregation of particles towards the wall and their internal recirculation. In the simulation using the uniform inlets and core-annulus inlet, the segregation of particles towards the wall cause widespread internal recirculation of solids and gas Using the circumferential gas injection, the segregation of particles towards the wall occurred more slowly, and resulted in a drastic reduction in the recirculation of solids.

Benyahia et al. (2001) compared simulation results of a two-sided inlet with that having a single inlet as used in the experimental setup. The single inlet design lead the gas to flow towards the opposite side of the solid inlet, and therefore resulting in inadequate mixing throughout the height of the riser. The resulted radial distribution of the solid density was not symmetric with most of the solid particles being at one

side of the riser, and the opposite side of the riser remaining relatively dilute. The typical core-annular flow regime was also not clearly observed in these simulations. The author found that the two-sided inlet design gave the core-annulus profile closer to the experimental values. The study also concluded that the actual inlet and outlet conditions could only be implemented in 3D simulations. However, the 3D simulations would require high computational time, and therefore, was not included. Furthermore, an effect of initial solid inventory on flow predictions was also investigated using a patch of solids up to 3m height of the riser. The results showed that the initial inventory affected the radial distribution initially, but after running the simulations for adequately longer time, that effect became negligible.

Neri and Gidaspow (2000) used uniform gas and solid distribution at the inlet of a riser which was part of a CFB set-up with J-valve before the riser inlet. Contrary to this study, Almuttahar and Taghipour (2008) simulated a 2D geometry of the inlet section (J-valve) separate from the riser simulation to study the solid velocity and volume fraction profile at the riser inlet. Based on the simulation study, they used core-annulus type with the solids entering vertically upward along the walls and the air entering in the core of the riser. In both studies, the results of the radial profiles showed a reasonable qualitative and qualitative agreement with the experimental data.

The preceding discussion clearly indicates that there is a lack of agreement on the type of inlet boundary conditions in 2D riser simulations. Therefore, in this study, the impact of inlet boundary condition was investigated by conducting 2D simulations with three different types of inlet arrangements for the gas and solid phases. The effect of wall boundary conditions was also studied by configuring it as a no-slip and partial-slip wall. Finally, as recommended in several previous studies (Benyahia et al., 2001; Vaishali et al., 2007), a transient 3D simulation of full-scale riser was also conducted which used inlet and outlet boundary conditions close to the experimental setup. The results for both 2D and 3D simulations were compared with the experimental data to quantify the impact of different boundary conditions.

3.2 Eulerian- Eulerian gas-solid flow model

As discussed previously two approaches exists, namely EL and EE, for gas-solid flow modelling. The EL models, also known as discrete particle model (DPMs), can be adopted in simulations in which the number of particles in the system is rather low (i.e. less than 10^5 particles) (Van der Hoef et al., 2008). The EE models are more suitable for simulating large and complex industrial fluidized bed reactors containing billions of solid particles such as the riser. The interrelationship between various models is schematically shown in Figure 3.1. Due to its continuum description, the EE model requires additional information about solid phase rheology and particle-particle interaction laws. In theory, it is possible to deduce all the necessary closure laws and parameters required for the EE model using more fundamental approaches like Lattice Boltzmann Models (LBM), direct solution of Navier-Stokes equation (DNS) and contact theory. Nevertheless, LBM and DNS are computationally intensive.

The EL model solves the Newtonian equations of motion for each individual particle, taking into account the effect of particle collisions and forces acting on the particle by gas. Particle collisions are described by collision laws, that account for energy dissipation due to non-idea particle interactions by means of the empirical coefficient of restitution and friction (hard sphere approach) or an empirical spring stiffness and a friction coefficient (soft sphere approach). The EE model considers both the gas and solids phases to be continuous and fully interpenetrating. The equations employed are a generalization of the Navier-Stokes equations. Implicit to the continuum description of the discrete phase, Eulerian models require additional closure laws to describe the rheology of particle phase. In most recent continuum models constitutive equations according to the kinetic theory of granular flow are incorporated. This theory is basically an extension of the classical kinetic theory of gases to dense particle flow, which provides explicit closures that take energy dissipation due to non-ideal particle–particle collisions into account by means of the coefficient of restitution.

With the present state of knowledge, capturing different scales of interactions using the EE model on a standalone basis is not possible (Ranade, 2002). Therefore, it is necessary to use different models, theories and empirical correlations to derive different closure laws in the EE model (Figure 3.1). DNS and DPMs are generally used to gain an insight into various critical flow phenomenon such as bubble or cluster formations and their characteristics or segregation phenomena (Hill et al., 2001; Beetstra et al., 2006, 2007).

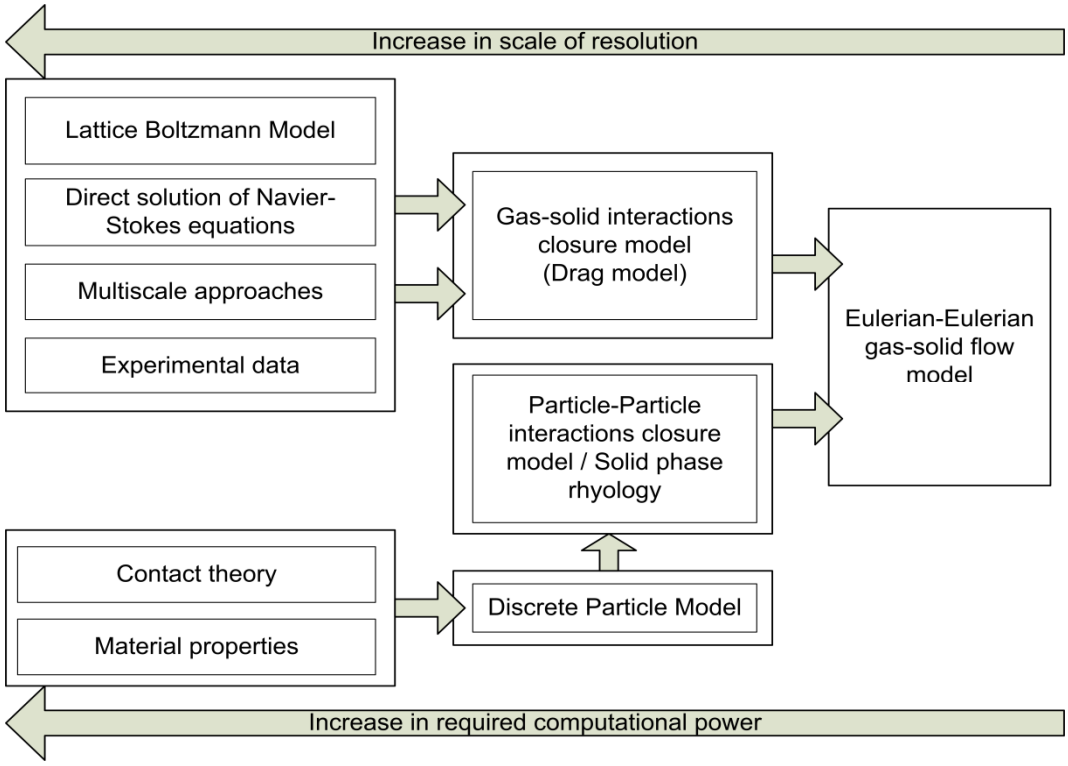

Figure 3.1: Interrelationship between various gas-solid flow models.

For full-scale simulations of industrial fluidized beds such as the riser, DPMs are computationally too demanding for the system involving many particles and the EE models should be preferred. Therefore, the EE model was used to carry out this research.

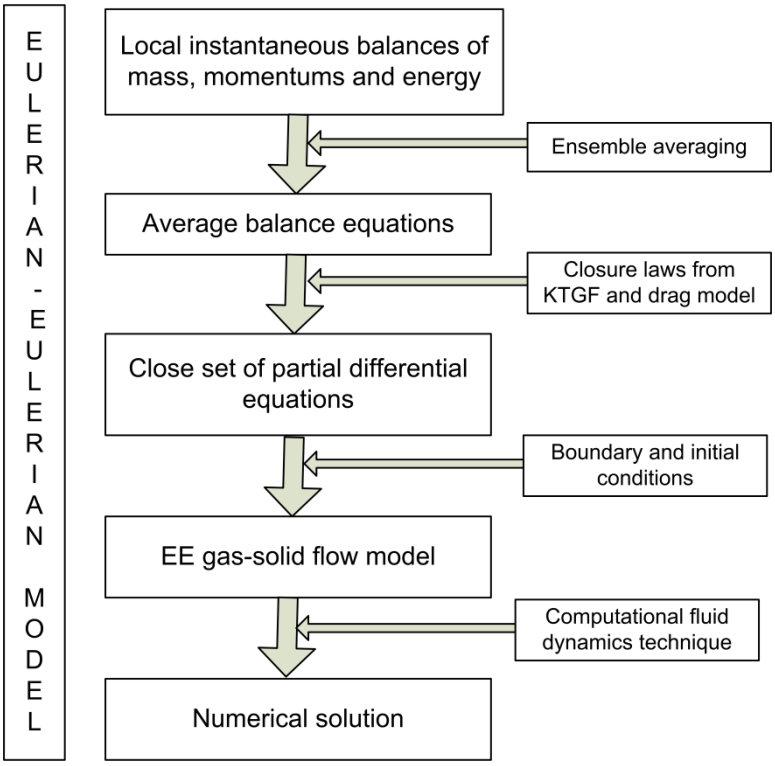

Figure 3.2: Formulation of the EE model.

The formulation of the EE model for the gas-solid flows was comprehensively discussed by Enwald et al. (1996) and is schematically represented in Figure 3.2. Initially, the local instantaneous equations are written for mass, momentum and energy balances for each phase in each control volume. These equations can be solved by direct simulation using a mesh finer than the smallest length scales of the flows and a time step shorter than the time scales of the fastest fluctuations. However, this direct simulation would be highly computational intensive. Thus averaging of local instantaneous equations is applied. Generally, ensemble averaging (Enwald et al., 1996) is applied to formulate averaged balance equations. The averaging of the balance equations leads to represent both phases as interpenetrating and continuous. As a result, this allows a coarser mesh and a longer time step to be used in the numerical simulations. The averaged equations then need extra closure laws to close the set of equations. The closure laws for the continuous solid phase are derived using the kinetic theory of granular flows (KTGF) (Lun et al., 1984). Using

KTGF, the correlations of solid phase viscosities and pressure are derived. In addition, the closures for the inelastic collisions of particles are also derived using the KTGF. Another required closure is for the gas-solid drag model which accounts for the interaction between the two phases. The closure relations derived using the KTGF and drag model are then incorporated into the balance equations for the solid phase to achieve a close set of partial differential equations (PDEs). These PDEs, along with the specified boundary conditions, are finally solved using computational fluid dynamics (CFD) techniques.

3.2.1. Averaged balance equations

The EE model includes mass and momentum conservation equations for each phase, which are then averaged over both length and time scales to formulate the averaged governing equations.

Continuity equation

The continuity equation for the gas may be written as:

$$\frac{\partial}{\partial t}\left(\varepsilon\rho_g\right) + \nabla.\left(\varepsilon\rho_g\vec{u}_g\right) = 0 \qquad \text{eq.(3.1)}$$

and that for the solid as:

$$\frac{\partial}{\partial t}\left(\varepsilon_s\rho_s\right) + \nabla.\left(\varepsilon_s\rho_s\vec{u}_s\right) = 0 \qquad \text{eq.(3.2)}$$

The continuity equation represents the balance of mass for a given phase. The volume fraction of the each phase is calculated from the continuity equations. Additionally, constraint on the volume fractions prescribes a sum of volume fraction of each phase should be equal to one. With this condition, the solution of continuity equation for the secondary phase allows for calculation of volume fraction of the primary phase.

Momentum conservation equation

The conservation of momentum for the gas and solid phases are given by equations 3.3 and 3.4 respectively:

$$\frac{\partial}{\partial t}\left(\varepsilon\rho_g\vec{u}_g\right) + \nabla.\left(\varepsilon\rho_g\vec{u}_g\vec{u}_g\right) = -\varepsilon\nabla P - \nabla.\bar{\bar{\tau}}_g + \varepsilon\rho_g g - \beta(\vec{u}_g - \vec{u}_s) \quad \text{eq.(3.3)}$$

$$\frac{\partial}{\partial t}\left(\varepsilon_s\rho_s\vec{u}_s\right) + \nabla.\left(\varepsilon_s\rho_s\vec{u}_s\vec{u}_s\right) = -\varepsilon_s\nabla P - \nabla.\bar{\bar{\tau}}_s + \varepsilon_s\rho_s g + \beta(\vec{u}_g - \vec{u}_s) \quad \text{eq.(3.4)}$$

The momentum exchange between the two phases is based on the value of the gas-solid exchange coefficient (β).

3.2.2. Interphase drag coefficient

For gas-solid flows, a predominant part of an exchange coefficient is the interphase drag. Generally, the drag depends on the voidage, particle diameter, difference between fluid and solid phase velocities and in turn, particle Reynolds number. Several drag coefficient functions (drag models) (Matsen, 1982b; Gibilaro et al., 1985; Matsen, 1988; Syamlal et al., 1993; Gidaspow, 1994; Yang et al., 2003a; van Sint Annaland et al., 2005) are available in literature for a specific multiphase flow conditions. These drag models are generally based on pressure drop measurements, bed expansion studies and numerical experiments (Mabrouk et al., 2007). The drag force is one of the dominant forces in multiphase flows; hence the selection of the model has significant impact on resulted flow predictions. Despite of several studies, there is no clear guideline for its selection in a specific flow condition, and therefore, evaluation of different drag models for a given flow condition is necessary before conducting simulations to investigate an effect of operating parameter on the hydrodynamics in any equipment.

In this part of study, the Gidaspow drag (Gidaspow et al., 1991a) model, which is conventionally used and applicable over a wide range of flow conditions, was used. The Gidaspow drag model (Gidaspow et al., 1991a) is a combination of the Ergun (Ergun, 1952) equation, which was derived from the pressure drop data in packed bed and the Wen-Yu (Wen and Yu, 1966) equation, which was derived from the

settling of solids in liquid. For the voidage less than 0.8, the Ergun equation is applied and for the voidage greater than or equal to 0.8, Wen-Yu equation is applied. A step change in drag value is realised at the crossover. Equations 3.5 to 3.8 describe this model:

$$\beta_{Wen-Yu} = \frac{3}{4}\frac{\varepsilon(1-\varepsilon)}{d_p}\rho_g|\vec{u}_g - \vec{u}_s|C_{D0}\varepsilon^{-2.7} \quad \text{-----} \quad \text{for voidage } > 0.8 \qquad \text{eq.(3.5)}$$

$$\beta_{Ergun} = 150\frac{(1-\varepsilon)^2\mu_g}{\varepsilon d_p} + 1.75\frac{(1-\varepsilon)\rho_g|\vec{u}_g-\vec{u}_s|}{d_p} \quad \text{----} \quad \text{for voidage <= 0.8} \qquad \text{eq.(3.6)}$$

$$C_{D0} = \frac{24}{\varepsilon Re_s}[1 + 0.15(\varepsilon Re_s)^{0.687}] \quad \text{If } Re_s < 1000 \qquad \text{eq.(3.7)}$$

$$= 0.44 \quad \text{If } Re_s \geq 1000$$

$$Re_s = \frac{d_p\rho_g|\vec{u}_g-\vec{u}_s|}{\mu_g} \qquad \text{eq.(3.8)}$$

3.2.3. Phase stress tensors

The stress tensors for gas and solid phase are given by equations 3.14 and 3.15 respectively.

$$\bar{\bar{\tau}}_g = \varepsilon\mu_g\{(\nabla.\vec{u}_g + \nabla.\vec{u}_g^T) - \frac{2}{3}\nabla.\vec{u}_g\bar{\bar{I}} \qquad \text{eq. (3.9)}$$

$$\bar{\bar{\tau}}_s = -P_s\bar{\bar{I}} + \mu_s(1-\varepsilon)(\nabla.\vec{u}_s + \nabla.\vec{u}_s^T) - \frac{2}{3}\nabla.\vec{u}_s\bar{\bar{I}} \qquad \text{eq. (3.10)}$$

The solid phase stress tensor has additional terms arising from a continuum assumption of the discrete granular phase. The solid phase stresses are derived by making an analogy between a random motion of particles and thermal motion of gas molecules; the kinetic theory of granular flows (KTGF) (Lun et al., 1984). Unlike the gas kinetic theory, the KTGF accounts for inelasticity of particle-particle collisions. The intensity of the particle velocity fluctuations determines the stresses, viscosity and pressure of the solid phase.

In KTGF, the solid particles are considered in a continuous and chaotic restlessness in a fluid. This random motion exists at very low concentration due to friction between the two phases, gas turbulence, pressure variations etc. or at higher concentration due to particle collisions. Taking the analogy with the thermodynamic temperature of the gas, this random motion of particles is represented by "granular temperature", which is proportional to the mean quadratic velocity of the particle:

$$\Theta_s = \frac{1}{3}\langle \vec{u}_s^2 \rangle \qquad \text{eq. (3.11)}$$

$$E_\Theta = \frac{3}{2}\Theta_s \qquad \text{eq. (3.12)}$$

where, Θ is the granular temperature, c is fluctuating velocity of particle and E_Θ is the fluctuating energy due to random motion of particles:

The solid phase stresses depends on the magnitude of this fluctuating particle velocity. Thus, conservation of granular temperature (or energy) associated with the fluctuating velocity is required. This conservation equation can be given as:

$$\frac{3}{2}\left[\frac{\partial}{\partial t}(\varepsilon_s \rho_s \Theta_s) + \nabla.(\varepsilon_s \rho_s \vec{u}_s \Theta_s)\right] = \left(-P_s\bar{\bar{I}} + \bar{\bar{\tau}}_s\right):\nabla\vec{u}_s + \nabla.(k_{\theta s}\nabla\Theta_s) - \gamma_{\theta s} + \phi_{ls} \qquad \text{eq. (3.13)}$$

$\left(-P_s\bar{\bar{I}} + \bar{\bar{\tau}}_s\right):\nabla\vec{u}_s$= generation of energy by solid stress tensor

$\gamma_{\theta s}$= Collisional energy dissipation (Lun et al., 1984)

$$\gamma_{\theta s} = \frac{12(1-e_{ss}^2)g_{o,ss}}{d_p\sqrt{\pi}}\rho_s\varepsilon_s\Theta_s^{3/2} \qquad \text{eq. (3.14)}$$

Diffusion coefficient for the granular energy (Gidaspow et al., 1992)

$$k_{\theta s} = \frac{15 d_p \rho_s \varepsilon_s \sqrt{\Theta\pi}}{4(41-33\eta)}\left[1 + \frac{12}{5}\eta^2(4\eta-3)\varepsilon_s g_{o,ss} + \frac{16}{15\pi}(41-33\eta)\eta\varepsilon_s g_{o,ss}\right] \qquad \text{eq. (3.15)}$$

$$\eta = \frac{1}{2}(1+e_{ss}) \qquad \text{eq. (3.16)}$$

ϕ_{ls}= energy exchange between l^{th} fluid or solid phase and s^{th} solid phase

Various correlations have been proposed in the literature for the solid phase transport closures (equations for solid pressures, solid viscosity, radial distribution functions etc.). A comparative study of these relations was presented by van Wachem et al. (2001) and Ahuja and Patwardhan (2008). The solids pressure (P_s) represents the normal solid phase forces due to particle-particle interactions. It is calculated independently and used for the pressure gradient term in the phase stress tensor. The solids pressure is composed of a kinetic term and a second term due to the particle collisions. The solids bulk viscosity (λ_s) is the resistance of particle suspension against the compression. For solids pressure and solid bulk viscosity, there is a general agreement in the literature on the relation proposed by Lun et al. (1984). The solid shear viscosity (μ_s) (given by equation 3.19) is made up of the colliosional, frictional and kinetic parts. All the models for solid shear viscosity yield practically the same solid shear viscosity at solid volume fraction greater than 0.25. For the lower volume factions, the models start deviating from one another (Ahuja and Patwardhan, 2008). However, there are no clear guidelines on selecting the solid shear viscosity model. The Gidaspow model (Gidaspow, 1994) for the solid shear viscosity neglects the inelastic nature of particle collisions in the kinetic contribution of the total stress and was used in this study. The frictional viscosity was calculated using Schaeffer's (Schaeffer, 1987) model. The model equations used in the present study are listed below (from Equations 3.17 to 3.22):

$$P_s = \varepsilon_s \rho_s \Theta_s (1 + 2(1 + e_{ss}) \varepsilon_s g_{o,ss}) \qquad \text{(Lun et al., 1984)} \qquad \text{eq. (3.17)}$$

$$\lambda_s = \frac{4}{3} \varepsilon_s^2 \rho_s d_p g_{o,ss} (1 + e_{ss}) \sqrt{\frac{\Theta}{\pi}} \qquad \text{(Lun et al., 1984)} \qquad \text{eq. (3.18)}$$

$$\mu_s = \mu_{s,col} + \mu_{s,kin} + \mu_{s,fri} \qquad \text{eq. (3.19)}$$

$$\mu_{s,col} = \frac{4}{5} \varepsilon_s^2 \rho_s d_p g_{o,ss} (1 + e_{ss}) \sqrt{\frac{\Theta}{\pi}} \qquad \text{(Gidaspow, 1994)} \qquad \text{eq. (3.20)}$$

$$\mu_{s,kin} = \frac{10 \rho_s d_p \sqrt{\Theta \pi}}{96 e_s (1 + e_{ss}) g_{o,ss}} \left[1 + \frac{4}{5} \varepsilon_s^2 (1 + e_{ss}) g_{o,ss}\right]^2 \qquad \text{(Gidaspow, 1994)} \qquad \text{eq. (3.21)}$$

$$\mu_{s,fri} = \frac{P_s sin\phi}{2\sqrt{I_{2D}}}$$ (Schaeffer, 1987)) eq. (3.22)

where, e_{ss} is the coefficient of restitution, which determines the degree of elasticity of particle-particle collisions. For typical gas-solid applications, the restitution coefficient has a value between 0.7 and 0.95. I_{2D} is the second invariant of the deviatoric stress tensor and ϕ is an angle of internal friction. P_s is the frictional solid pressure which accounts for the solid pressure in the frictional regime. The default frictional pressure model which is based on the KTGF was applied in this work. $g_{0,ss}$ is the radial distribution function, which is a correction factor that modifies the probability of collisions between particles when the granular phase becomes dense. Comparative studies show only a little difference between various models for the radial distribution function at different solid volume fractions. In this work, the model proposed by Lun et al. (1984) (Equation 3.23) was used for the radial distribution function.

Radial distribution function describes the probability of finding two particles in close proximity (Lun et al., 1984):

$$g_{o,ss} = \left[1 - \frac{\varepsilon_s}{\varepsilon_{s,max}}\right]^{-2.5 e_{max}}$$ eq. (3.23)

3.3.4. Boundary conditions

Boundary conditions have been used to specify the numerical values at the boundary cells in flow modelling. In this work, the velocity inlet boundary condition was used by specifying velocity and volume fraction of both phases at inlets. The average solid velocity at the inlet was calculated from the following relation based on the given solid mass flux:

$$u_s = \frac{G_s A_{riser}}{\rho_s \varepsilon_s A_{inlet}}$$ eq. (3.25)

At the outlet, pressure outlet boundary condition was used by specifying gauge pressure equal to zero, which meant that the pressure at outlet was equal to the atmospheric pressure.

At the wall, two alternatives, either no-slip or partial-slip boundary conditions, can be used for an individual phase. The no-slip boundary condition was used for the primary gas phase, whereas, each of wall boundary conditions was used for the solid phase in separate simulations. For the solid phase, no-slip boundary condition was set by equating the tangential and normal velocities to zero, while the partial-slip boundary condition can be configured using correlations developed by Sinclair and Jackson, (1989) for the wall shear and Johnson and Jackson, (1987) for granular energy.

The wall shear boundary condition for the solid phase was given by rate of axial momentum transferred to the wall by the particles in a thin layer adjacent to wall surface (Sinclair and Jackson, 1989):

$$\tau_{s,w} = \frac{\emptyset \pi u_{slip} \rho_s g_{o,ss} \Theta^{1/2}}{2\sqrt{3}\varepsilon_{s,max}} \qquad \text{eq. (3.26)}$$

where ∅ is specularity coefficient. Its value equal to zero denotes free slip or specular wall, and unity denotes diffusive transfer of particles through wall.

The granular energy at the wall can be obtained by using Johnson and Jackson, (1987) equation. The granular energy flux can be positive (wall as sink) or negative (wall as source) depending upon the relative magnitude of granular energy dissipation due to non-elastic collision between particle and wall and generation of granular energy due to shear at the wall. The granular energy dissipation due to inelastic collision with wall:

$$\gamma_{\Theta,s,w} = \frac{\sqrt{3}\pi \rho_s \varepsilon_s g_{o,ss} (1 - e_w^2) \Theta^{1/2}}{4\varepsilon_s^{max}} \qquad \text{eq. (3.27)}$$

Thus, the partials-slip condition for the solid phase requires two additional parameters i.e. specularity and wall restitution coefficients. The theoretical values of both these coefficients are unavailable and thus in this work, their values were set using those used in the previous studies (Benyahia et al., 2001; Jiradilok et al., 2006).

3.3. CFD simulations

The EE gas-solid model was applied to simulate the flows in the riser using CFD technique. Simulations were conducted in unsteady manner using commercial CFD package fluent v 6.3, which is based on the finite volume method. Transient simulations were carried out using a time step of 5 x 10^{-4} s. A second order discretisation scheme was used for the momentum equation and the QUICK scheme was applied to solve the volume fraction. Turbulent in the gas phase and its effect on the dispersed secondary phase was modelled using standard k-ε model. The pressure-velocity coupling was resolved using the SIMPLE algorithm. The under relaxation factors were reduced from their default values to maintain numerical stability in the simulations. The physical properties of both phases and the simulation parameters are listed in Table 3.1.

Table 3.1: Physical properties of gas and solid phases, and simulation parameters.

Phase properties		Simulation parameters	
Gas phase	Air	Riser diameter (D_t)	152 mm
Air density (ρ_g)	1.12 kg/m^3	Riser height (H)	7.9 m
Air viscosity (μ_g)	1.18e-05 kg/m.s	Inlet boundary	Velocity inlet
Air velocity (U_g)	4.5 m/s	Outlet boundary	Pressure outlet
Solid phase	Glass beads	Discretisation	Second order
Particle diameter (d_p)	150 μm	Turbulent model	k-ε model
Solid density (ρ_s)	2550 kg/m^3	2D simulation	
Solid flux (G_s)	37 kg/m^{2}s	Grid size	9.5 x 25 mm
Restitution factor		Time step	5×10^{-4} s
Particle-particle (e_{ss})	0.95	3D simulation	
Particle-wall (e_w)	0.9	Time step	2×10^{-4} s
Max. packing limit	0.6		

In this work, previous experimental study conducted by Bhusarapu et al. (2005) was considered for comparing the simulation results. The detail explanation of the experimental setup, measurement techniques and results can be found in various publications of Bhusarapu (Bhusarapu et al., 2004; Bhusarapu et al., 2005; Bhusarapu et al., 2006). The dimensions of the riser and flow conditions from

Bhusarapu's experimental set-up (Bhusarapu et al., 2005) are summarised in Table 3.1 and have been used in simulations presented in this chapter. In Bhusarapu's experimental set-up (Bhusarapu et al., 2005), solids entered from an inclined pipe attached to the cylindrical riser (Figure 3.3a). The gas entered at the bottom of the riser, and travelled through the air distributor into the riser (Figure 3.3a).

Beyahia et al. (2001) simulated 2D geometry with one solid inlet arrangement (Figure 3.3b) keeping the inlet configuration closer to 3D experimental setup of Knowlton et al. (1995). In their simulation, most of the solid particles were found to be concentrated at the inlet side of the riser causing unsymmetrical radial distribution of the solid density, which did not agree with the core-annulus profile. Thus, the authors used two symmetrical side inlets for the solids as shown in Figure 3.4(a). Furthermore, a literature review showed that the inlet arrangements have been generally changed from that of the experimental setup while conducting 2D simulations. As a result, several types of inlet arrangements have been used in previous studies.

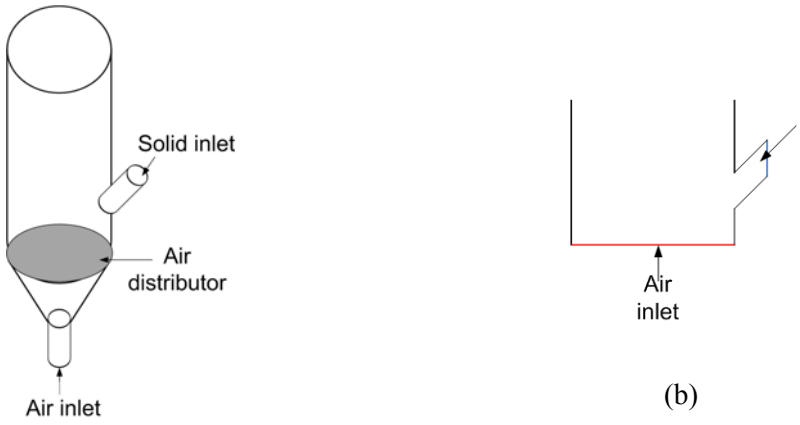

Figure 3.3: (a) Inlet arrangements in experimental set-up and (b) one solid inlet configuration simulated by Benyahia et al. (2001).

In this study, three different types of inlet arrangements (in 2D simulations) were used and are summarised below:

1. BC-A: Solid entering in radial direction from two side inlets and gas entering axially from the bottom inlet (Figure 3.4a) (Benyahia et al., 2001; Yang et al., 2004; Vaishali et al., 2007).

2. BC-B: Solid entering axially from two bottom inlets near the wall and gas entering axially from a bottom inlet at the centre (Figure 3.4b) (Pita and Sundaresan, 1993; Almuttahar and Taghipour, 2008).

3. BC-C: Axial solid entry from a single bottom inlet at the centre and gas entry from two bottom inlets near the wall (Figure 3.4c).

For outlets, the experimental set-up (Bhusarapu et al., 2005) had a single outlet at the top from which mixture of the gas and solid entered into the disengagement section. Therefore, the outlet of the riser was configured as a single outlet at the top. This outlet configuration was also different from those used in previous studies. For example, Benyahia et al. 2001 and Yang et al. 2004 used a two-sided outlets, whereas Neri and Gidaspow (2000) and Jiradilok et al. (2006) used single-sided outlet.

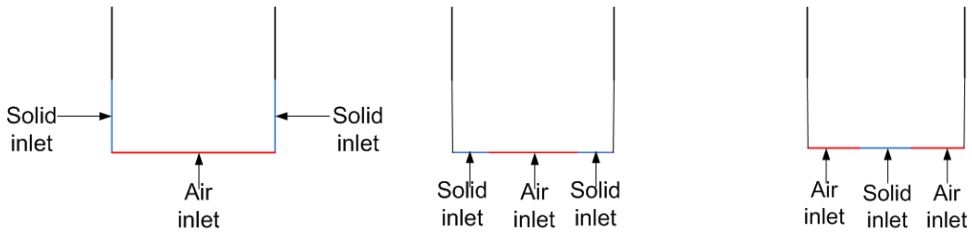

Figure 3.4: Inlet arrangements used in 2D simulations (a) BC-A, (b) BC-B and (c) BC-C

3.4. Results and discussion

3.4.1. 2D simulations

As a base case, a 2D simulation was conducted using the boundary condition type BC-A, in which, the inlet velocities of the gas and solid phases were set from experimental values of the solid mass flux (G_s = 37 kg/m^{2}s) and superficial gas velocity (U_g = 4.5 m/s). The mass flow rate at the outlet was plotted as a function of time for duration of 30 s (Figure 3.5a). It attained a dynamic steady state after 10 s where it fluctuated around the average value equal to the inlet mass flow rate (~ 6.4 kg/s). Therefore, to ensure that the system was in a dynamic steady state, the time-averaged data were collected. Figure 3.5(b) and (c) shows the effect of time averaging period on the radial profiles. A minor effect of time averaging period was noticed for the radial profiles of the mean solid volume fraction (Figure 3.5b), whereas only negligible effect was found on the mean solid velocity profiles (Figure 3.5c). The simulation predictions were time-averaged for the last 20 s of a simulation runs with a sampling frequency of 2 kHz to show the radial distribution of velocity and volume fraction of solid at riser height of 5.5 m.

The radial profiles of the time-averaged solid volume fraction (Figure 3.5b) showed a higher solid accumulation near the wall and lower value near the centre of the riser. The radial profile of the time-averaged solid velocity (Figure 3.5c) showed a maximum velocity at the centre with a zero velocity near the wall. These results were consistent with the core-annulus flow structure reported in previous simulation studies on the riser (Nieuwland et al., 1996a; Mathiesen et al., 2000; Neri and Gidaspow, 2000); and provided a preliminary evaluation of the model, which was then applied to simulate other types of boundary conditions.

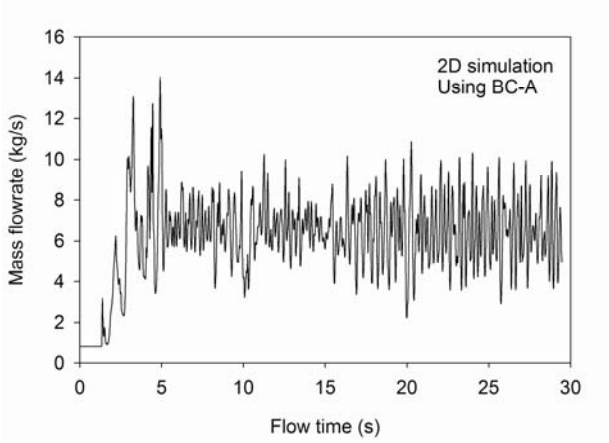

(a)

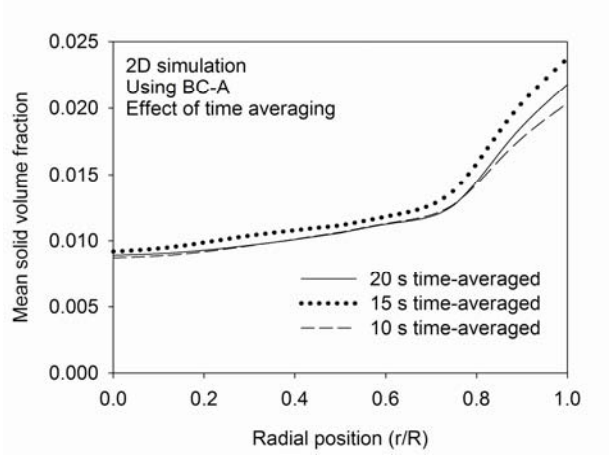

(b)

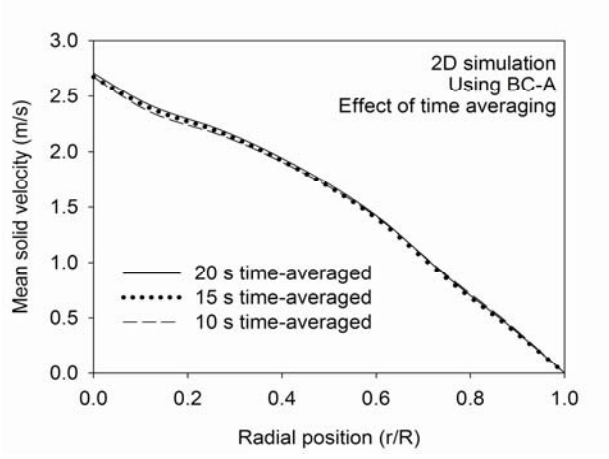

(c)

Figure 3.5: Base case simulation results: (a) Mass flow rate at outlet as a function of time; (b) and (c) Time-averaged radial profiles of mean solid volume fraction and velocity respectively (at 5.5 m height from the distributor).

3.4.1.1. Effect of solid inlet boundary conditions

The effect of the solid inlet boundary conditions was studied by using two types of solid inlet arrangements i.e. (i) BC-A (as simulated by Benyahia et. al., (2001), Figure 3.4(a)) and (ii) BC-B (as simulated by Alamuttahar and Taghipour, (2008), Figure 3.4(b)). Time-averaged radial profiles of mean solid velocity and volume fraction at the fully developed zone are shown in Figure 3.6(a) and (b) respectively, where it is clear that there were considerable disagreements between results from the two boundary conditions. The simulation using the BC-A gave higher volume fraction and lower velocity than those using the BC-B. The disagreements can be attributed to differences in the mixing of two phases at the entrance using different inlets. Figure 3.7 shows solid volume fraction contour and velocity vector plots near the entrance. Using BC-A (Figure 3.7a and b), the solids entered in the radial direction whereas the gas entered in the axial direction. Due to the perpendicular entries of two phases, the solids moved towards the centre region, and lifted upward with the gas flowing from the bottom and the mixing between the two phases was higher. In addition, this higher degree of mixing caused higher dissipation of energy. Therefore, the solid velocity was lower than that from BC-B (Figure 3.6).Using BC-B (Figure 3.7c and d), both gas and solid phases entered in the axial direction. The solid moved upwards with higher velocity and higher volume fractions near the wall, whereas the gas travelled with high velocity at the centre. Therefore, there was a lack of mixing between the two phases and as a result, the radial distribution of the solids was lower. This caused higher velocity and lower solid volume fractions in the radial profiles (Figure 3.6), when compared with BC-A.

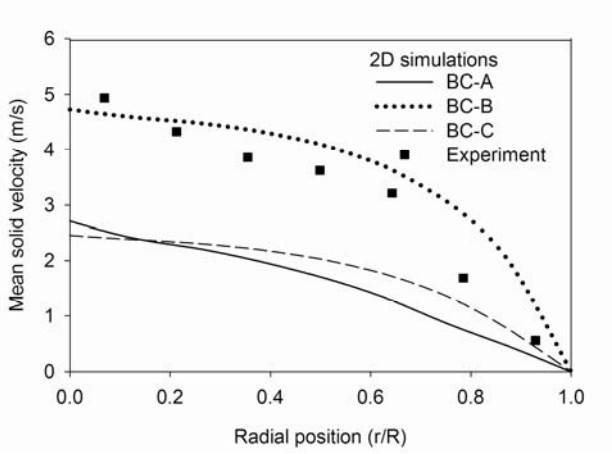

(a)

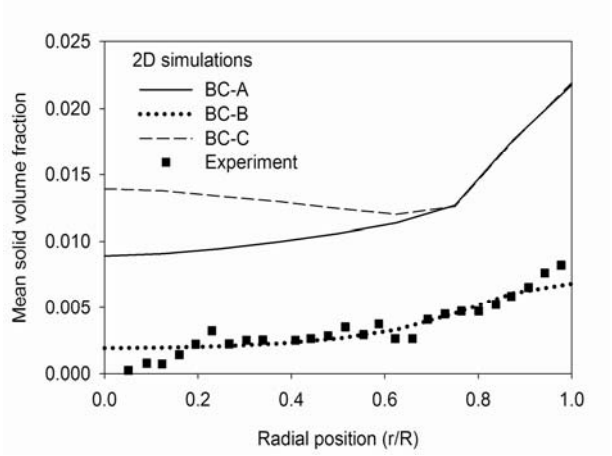

(b)

Figure 3.6: Effect of boundary conditions: (a) and (b) Radial profiles mean solid velocity and solid volume fraction respectively (at 5.5 m height from the distributor).

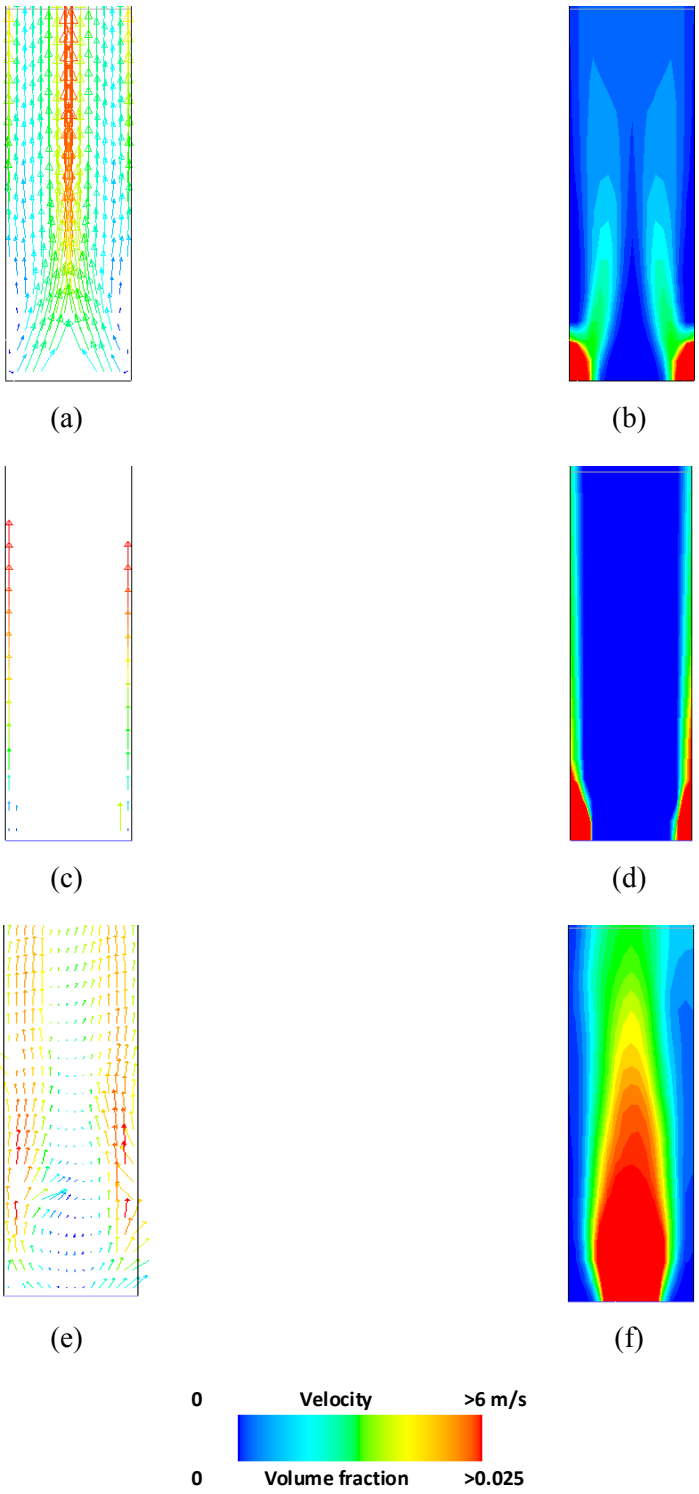

Figure 3.7: (a), (c) and (e) solid velocity vector plots for BC-A, BC-B and BC-C respectively and (b), (d) and (f) solid volume fraction contour plots for BC-A, BC-B and BC-C respectively near the entrance zone.

The disagreements between the radial profiles using two types of inlets were also investigated by comparing kinetic energies of two phases at the entrance. Figure 3.8 shows rate of kinetic energies for two phases at the inlets and those for the experimental 3D boundary conditions. The kinetic energies of both phases using BC-A and BC-B showed significant disagreements with those of 3D experimental boundary conditions. The kinetic energy of the solid phase using BC-A was lower than that of the experimental value, and contrary to this, BC-B gave higher values. Therefore, the kinetic energies at inlets did not represent the exact experimental values using either of these boundary conditions. Thus, despite achieving the mass balance by configuring the boundary conditions using the solid mass flux (G_s) and superficial gas velocity (U_g) from the 3D experimental operating conditions, the energy balances in the 2D simulations were quite different from that in the actual 3D conditions. Therefore, this aspect needs to be further investigated before using assumed 2D boundary conditions to simulate the riser.

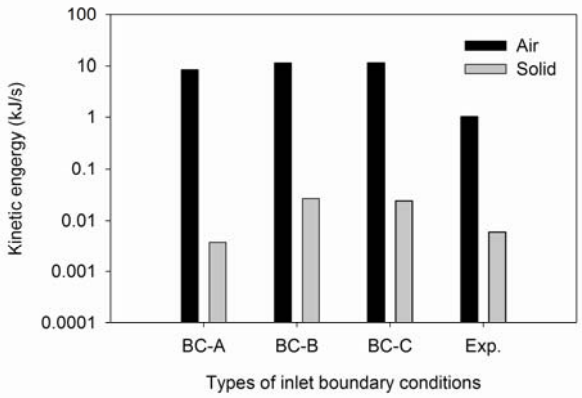

Figure 3.8: Kinetic energies of gas and solid phases using different inlet boundary conditions.

To further investigate the effect of the boundary conditions using the kinetic energies, the simulation was carried out using a third boundary condition (BC-C) as shown in Figure 3.4(c). In BC-C, the kinetic energies of the gas and solid phases at the inlets were equal to those in the BC-B, however, the positions of the gas and solid inlets were altered (Figure 3.4c). The time-averaged radial profiles of the solid volume fraction and velocity are shown in Figure 3.6(a) and (b) respectively. Despite

the same kinetic energies of two phases at the inlets, the simulation using the BC-C gave higher solid volume fraction and lower solid velocity compare to that using the BC-B. Furthermore, when the results using the BC-C were compared with those using the BC-A, they agreed well near the wall and showed disagreements near the centre, with the BC-C showing higher solid volume fraction. The agreements near the wall can also be explained by the mixing patterns in Figure 3.7b and f, which show time-averaged contours of solid volume fractions near the entrance region for BC-A and BC-C respectively. Both contour plots (for BC-C and BC-A) showed a lower solid volume fraction near the wall and higher values near the centre. Particularly in the contour plot for BC-C, the solid volume fraction near the centre was even higher. Therefore, the radial profile of the solid volume fraction using BC-A and BC-C showed agreement near the wall, but not near the centre. The results clearly show that different directions and positions of the gas and solids inlets caused profound effect on the mixing of two phases, in turn on the radial profiles of velocity and volume fractions. Thus, the selection of inlet boundary conditions in 2D simulations a challenging task. Unfortunately, in the past, several authors assigned these boundary conditions in a rather arbitrary manner, thus misleading validations of their simulations. Therefore, this aspect of boundary conditions assignment needs more attention in future.

3.4.1.2 Effect of wall boundary condition

The effect of wall boundary condition was investigated by configuring the wall as no-slip and partial-slip for the solid phase. In the EE model, the conservation of the granular temperature (eq. 3.17) can be modelled using two types of equations i.e. (i) algebraic and (ii) partial differential equations. In the algebraic equation, convection and diffusion of the granular temperature are neglected, and the wall can only be configured as a no-slip for both phases. Whereas, the partial differential equation accounts for dissipation terms such as the conduction of granular temperature, dissipation of granular temperature due to the inelastic granular collisions and rate of transfer of fluctuating energy between the gas and solid phases. Using the partial differential equation, the wall can be configured using a partial-slip boundary

condition, which was derived by Johnson and Jackson (Johnson and Jackson, 1987). In this wall boundary condition, the solid tangential velocity and wall granular temperature have been calculated using a specularity coefficient and particle-wall restitution coefficient respectively. The specularity coefficient is a measure of fraction of collisions, which transfers momentum to the wall, and the restitution coefficient specifies the collision dissipation rate between particle and wall. The specularity coefficient and particle-wall restitution factor were set to 0.6 and 0.9 respectively using previous simulation studies (Benyahia et al., 2001; Jiradilok et al., 2006).

The simulation using both inlet types BC-A and BC-B were conducted to investigate the effect of the wall boundary conditions, and time-averaged mean solid velocity and volume fraction are shown in Figure 3.9. Using the BC-A (Figure 3.9a and b), the simulation with the partial-slip wall gave higher solid concentration and lower solid velocity than those with a no-slip wall. The higher solid segregation near the wall using the partial-slip wall can be attributed to the dissipation due to collisions between solids and wall, which were neglected in the simulation with the no-slip wall boundary condition. Furthermore, it was found that the predictions with the no-slip wall boundary condition were closer to the experimental data than those using the partial-slip wall (Figure 3.9a and b). However, the results also disagreed with the experimental data quantitatively, particularly near the centre of the riser. Hence, a change in wall boundary configuration gave radial profiles closer to the experimental values using the inlet type BC-A, which showed considerable disagreements with the experimental data in the previous section of this study. The improvement using no-slip wall boundary condition can be attributed to exclusion of dissipation caused by the particle-wall collisions, which is a reasonable assumption for a dilute phase transport. Figure 3.9(c) and (d) shows the effect of wall boundary conditions on the radial profiles using the inlet type BC-B. Interestingly, for this type of inlet arrangement, only a minor effect of wall boundary condition was noted with radial profiles for no-slip and partial-slip walls being similar to each other. This similarity

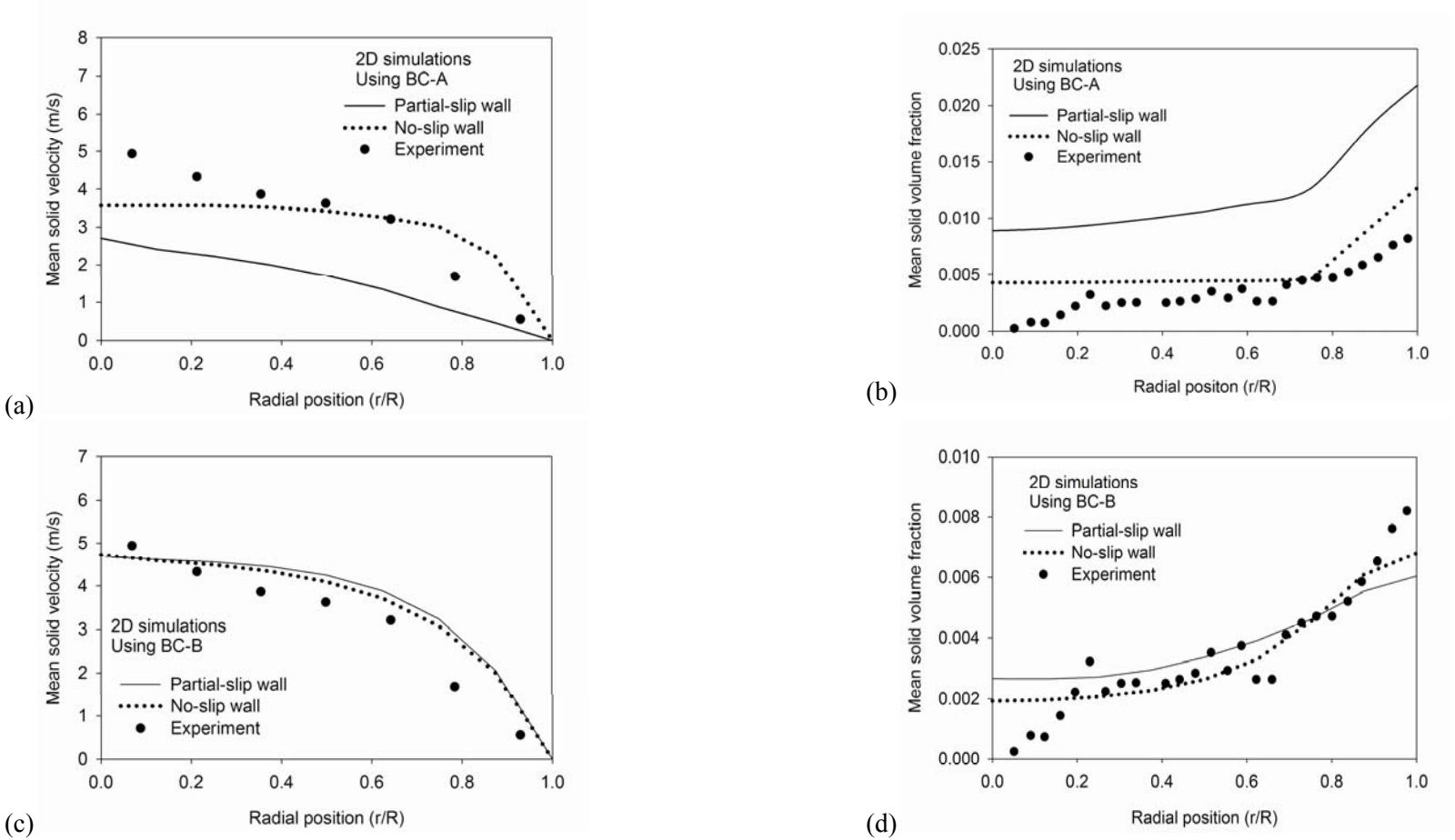

Figure 3.9: Effect of wall boundary conditions: (a) solid velocity and (b) volume fraction profiles using BC-A; (c) solid velocity and (d) volume fraction profiles using BC-B (at 5.5 m height from the distributor).

can be attributed to predicted dilute flow using this inlet type in which effect of dissipation at the wall becomes negligible.

It is clear from the above discussion that due to inconsistent effect on the simulation results using different inlet boundary conditions, 2D simulations is highly unreliable. Therefore, a full-scale 3D simulation of Dudukovic and co-worker's (Bhusarapu et al., 2005) riser was also conducted in this study.

3.4.2. 3D full-scale simulation

Most of previous studies on risers have been confined to 2D simulations due to computational limitations. However, these studies (Benyahia et al., 2001; Vaishali et al., 2007) have also emphasized on using 3D simulations instead of 2D simulations. In this work, a 3D simulation was conducted using inlet boundary conditions similar to experimental setup. Figure 3.10(a) shows a schematic of the 3D geometry of the riser, which was meshed with a total of 210216 cells. A computer machine with a cluster of eight processors was used to conduct the CFD simulations. Since a small time step size of 0.0002 s was used to carry out the simulation, it took more than three weeks for a 30s of real flow time. Figure 3.10(b) and (c) show the time-averaged radial profiles of the solid velocity and volume fraction. The predicted values showed a reasonable qualitative agreement with the experimental values. However, near the centre, the simulation slightly over predicted the solid volume fraction and under predicted the solid velocity, and an opposite trend was predicted near the wall.

Vaishali et al. (2007) conducted simulations on 2D riser, in which authors evaluated two drag correlations by comparing not only the radial profiles of the solid velocity and volume fraction but also the fluctuating solid velocity (granular temperature). Although, the authors successfully compared their predictions with the experimental data for the fast fluidization of solids but could not even predict the basic core-annulus nature of the riser flow for the dilute phase transport. They had emphasised a need for a better combination of solid phase closure models and 3D full scale

simulation to eliminate the reported discrepancies. A comparison between the predictions from current study with that of Vaishali et al., (2007) is shown in Figure 3.11. It is evident from the comparison that both 2D and 3D simulations in the current study consistently predicted a qualitative trend for the core-annulus flow.

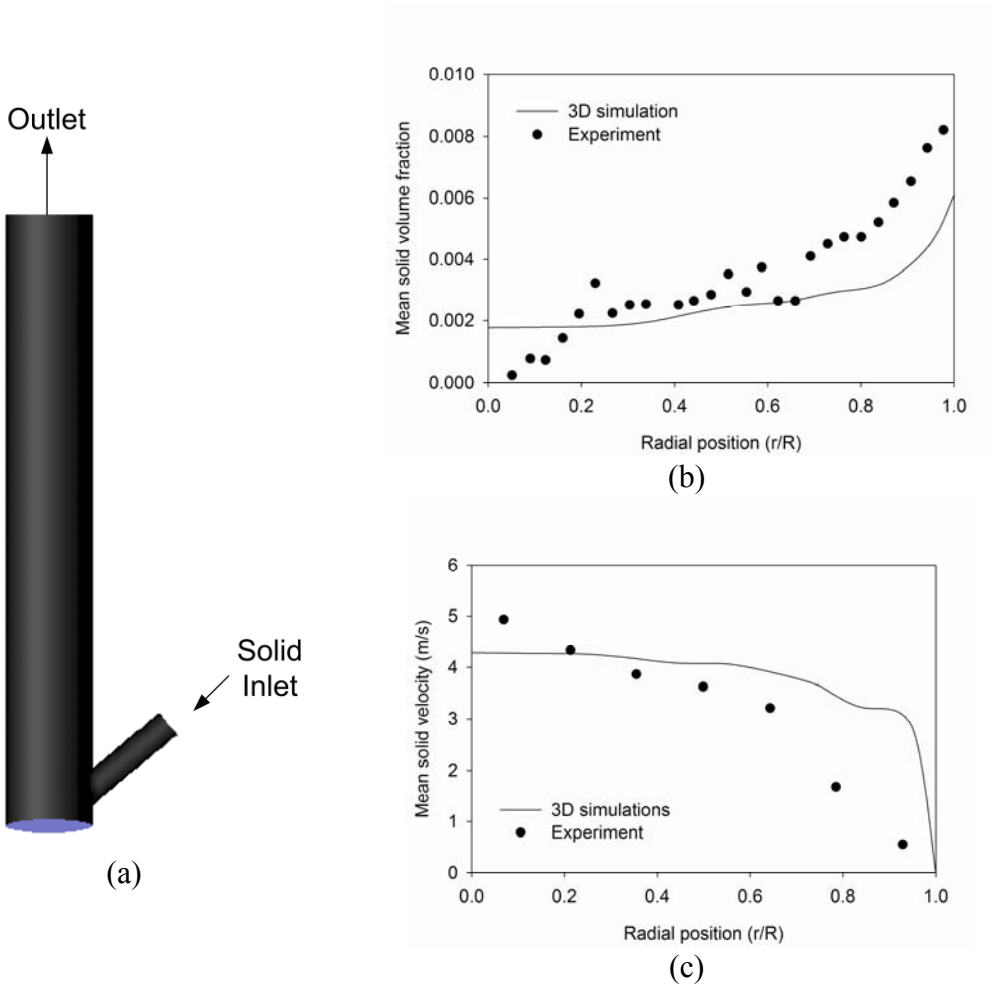

Figure 3.10: (a) Schematic diagram of 3D riser; (b) and (c) Radial profiles of mean solid volume fraction and velocity respectively (At 5.5 m height from the distributor).

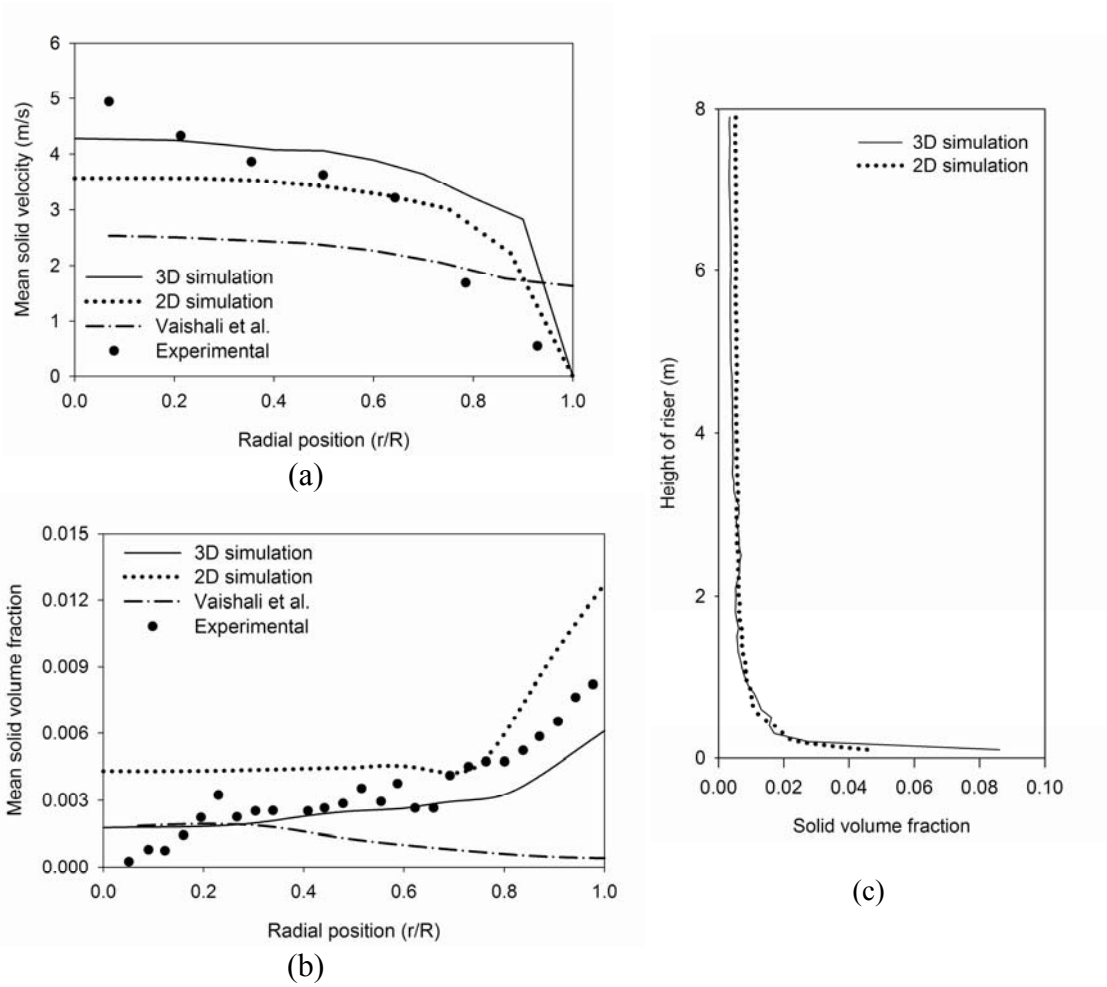

Figure 3.11: Comparison of results from 2D and 3D simulations along with those from previous study: (a) and (b) Radial profiles of mean solid velocity and volume fraction respectively; (c) Axial profile of solid volume fraction

The flows in the riser also exhibit axial variations in the solid volume fractions. Previous experimental studies (Rhodes and Geldart, 1986; Li and Kwauk, 1994) have shown two distinct regions with dense bottom and dilute top sections of the riser. Benyhai et al. (2001) compared the predictions of the axial pressure drop with the experimental data of Knowlton et al. (1995). However, their predictions did not agree with the experimental data. Yang et al. (2003b) concluded that the conventional drag models such as the Gidaspow drag model could not predict the axial variations in the voidage. To evaluate the ability of the current gas-solid flow model to capture the axial profile, the mean solid volume fractions at different axial position from both 2D

and 3D simulations have been plotted in Figure 3.11(c). It is clear that profiles from both 2D and 3D simulations were identical. In both cases, after an initial drop in the volume fraction, it remained constant along the height of the riser. This uniformity in voidages was in contradiction with the experimental S-shape profiles (Knowlton et al., 1995, Li and Kwauk, 1994).

3.5. Conclusions

In this work, the EE model was evaluated by comparing results from both 2D and 3D simulation with the experimental data of Bhusarapu et al. (2005). In 2D simulations, the effect of the inlet boundary conditions was studied by using three different types of inlet arrangements. Furthermore, the effect of wall configurations was also investigated. Inlet arrangements were found to have significant impact on the radial profiles of solid velocity and volume fractions in even the top section. The top section of the riser has been generally described as a fully developed zone and believed to be immune to any entry effect. Interestingly, the core-annular inlet for the solid and gas phases gave reasonable agreement with the experimental data; however, those for two-sided inlets over predicted the solid volume fractions compared to the experimental data (Figure 3.6). This profound effect of inlet arrangements was attributed to two possible causes, i.e. (i) the mixing and (ii) kinetic energies of two phases at the entrance. The contour plots of solid volume fractions (Figure 3.7) at the entrance clearly indicated that the mixing of two phases was poor in the core-annular inlets, whereas that in two-sided solid inlets was better due to the orientation of the flow from the inlets. These mixing patterns were directly correlated to the radial distribution of the solids in the fully developed zone. The kinetic energies of both phases at the inlets (Figure 3.8) were widely differed with those in the 3D experimental case for either of 2D boundary conditions. Thus, using assumed boundary conditions in 2D simulations, energy balances inside the domain did not reflect that in the 3D conditions. The effect of boundary conditions was further investigated using a third inlet arrangement by keeping the flow directions of each phase and kinetic energies at inlets identical to the core-annulus inlet, but the position of the gas and solid inlets were altered. The third inlet arrangements gave

the radial profiles (Figure 3.7) inconsistent with those resulted using the core-annulus inlets. Thus, the position of inlets also showed significant impact on the radial profiles even in the so-called fully-developed region.

The effect of the wall boundary conditions using two different types of inlets was also investigated by considering it as partial-slip or no-slip conditions. Using the two-sided solid inlets boundary conditions, a change in the wall condition from the partial-slip to no-slip wall, gave results closer to the experimental data (Figure 3.9). This could be attributed to exclusion of the dissipation caused by particle-wall collisions. Interestingly, the effects of wall configuration on the radial profiles using the core-annulus inlet were negligible, and both profiles were similar. This could also be attributed to predicted lower solid volume fractions using this boundary condition. Thus, the effect of wall boundary conditions on the radial profiles using different boundary conditions was inconsistent. Due to these inconsistencies, the selection of boundary conditions in 2D simulations was found to be challenging, and the use of a particular type of boundary conditions could mislead in judging the validation of the EE model.

3D full-scale simulations were conducted by implementing the inlet and outlet boundary conditions similar to the experimental setup. The results from 3D simulation agreed reasonably well with the experimental data, but only qualitatively and showed quantitatively disagreements (Figure 3.10) near the centre and walls. In addition, the axial profiles of the solid volume fraction for both 2D and 3D simulations showed uniform axial solid distribution after a sudden drop at the bottom of the riser (Figure 3.11). This axial profile was contrary to the existence of dense bottom and dilutes top sections observed in the experimental studies. Therefore, it was concluded that although both 2D and 3D simulations could predict the radial profiles qualitatively by tweaking the parameters such as inlet arrangements and wall configuration, the current gas-solid models could not capture the axial variations in the solid volume fractions, even qualitatively. Thus, further simulations with improved modelling parameters such as drag model were required. In the next chapter, a drag model using a multi-scale approach has been studied.

4.1 Introduction

In previous chapter, it was observed that the EE model could not capture an inherent heterogeneity of the gas-solid flows in risers, particularly the axial profile of voidages. Therefore, further improvements in the EE model were necessary, and one of the possible improvements can be the interphase drag model which is one of the most critical closure parameters in the EE gas-solid flow model. The drag model has been generally used to model the interactions between the gas and solid phases. Previous studies (Yang et al., 2004; Andrews Iv et al., 2005) have shown that the EE model with the drag derived from multi-scale approaches is more effective in capturing both axial and radial heterogeneity of the flows in risers. In this work, we have evaluated the multi-scale approach based on the energy minimization concept for a wide range of flow conditions to find possible improvements in the flow predictions.

Several gas-solid drag models have been proposed in the literature for different flow conditions (Matsen, 1982a; Gibilaro et al., 1985; Syamlal et al., 1993; Gidaspow, 1994; Li et al., 1999). The available drag models can be broadly classified into two categories; (i) conventional drag models and (ii) structure-based drag models. The conventional drag models such as those of Gidaspow (Gidaspow, 1994) and Syamlal-O'Brien (Syamlal et al., 1993), are derived using the terminal velocity data for a single particle and pressure drop data from a dense packed bed. The Gidaspow drag model is a combination of the Wen-Yu (Wen and Yu, 1966) and Ergun (Ergun, 1952) equations. However, the flow conditions in the riser lead to the formation of particle aggregates or clusters (Yerushalmi and Cankurt, 1979; Subbarao, 1986) which coexist and interact with the dilute phase. These clusters are dynamic entities and affect the flow structures in the riser. The formation of clusters affects the slip velocity, and in turn the gas-solid drag. Agrawal et al. (2001) concluded that a contribution of solid stress obtained from KTGF was negligible, and the effect of clusters played a dominant role in the gas-solid simulation. Thus, accounting for

particle clusters is very critical for accurate modelling of gas-solid flows in the riser. The conventional drag models do not represent the cluster formation appropriately (Ranade, 1999; Makkawi and Wright, 2003; Yang et al., 2003a; Andrews Iv et al., 2005), and need to be corrected to account for the clusters. Direct application of these models can lead to unrealistic predictions. Therefore, the structure-based drag models derived using the multi-scale approaches such as the Sub grid scale (SGS) and Energy minimization multiscale (EMMS) approaches have been developed in the recent past.

In the SGS approach, the drag has been derived using an extremely fine grid (Andrews Iv et al., 2005) or Lattice Boltzmann (Beetstra et al., 2007) simulations. Agrawal et al. (2001) concluded that the high grid resolution simulations using the conventional drag model was also capable of capturing the clusters because the heterogeneity got weakened by use of very fine grid. Andrew Iv et al. (2005) conducted high resolution simulations of a section of riser using periodic boundary conditions, and the results were then used to derive different solid phase closures and gas-solid drag models. Igci et al. (2008) extended the above work, and showed the effect of grid size, known as filter size, on the closures derived from the high resolution simulations. These closures were then used in coarse grid simulation of a full-scale riser, and the results showed significant improvements by capturing both radial and axial profiles of voidages. However, the use of the fine grid simulations has made this approach computationally intensive. An alternative approach is the energy minimization multi-scale (EMMS) model, in which various flow structure parameters such as the fraction of solids in the cluster phase, cluster diameter and superficial velocities in the cluster phase are calculated using the overall mass flux and superficial gas velocity. These structure parameters can then be used to calculate a structure-based drag model, which can be easily incorporated in the EE model. This method has also been very effective in improving the flow predictions in the riser (Yang et al., 2004; Huilin et al., 2005; Jiradilok et al., 2006; Wang et al., 2007). Due to its relative simplicity and computational feasibility, there has been a growing interest in the EMMS model.

Several hydrodynamics studies using the EMMS model have been published in the literature. Yang et al. (2003b, 2004) simulated a low flux FCC riser with a drag correlation derived using the EMMS model. Those hydrodynamic predictions were compared with that using the Gidaspow drag model. The authors concluded that the EMMS gave more consistent results for the axial and radial heterogeneity than Gidaspow's drag model. Wang and Li (2007) made further advancements in the EMMS model by introducing multiple acceleration terms for individual phases. The solution of this extended EMMS model resulted in a huge matrix of drag coefficients (known as an EMMS/matrix) for different local solid flux and gas velocities. Naren et al. (2007) critically evaluated the formulation of EMMS model. Their study revealed that it is not possible to obtain minima under all flow conditions as postulated by the EMMS model. Qi et al. (2007) applied the EMMS approach to modify the drag correlation of Syamlal-O'Brien (Syamlal et al., 1993), which the authors then used to simulate the flow of a riser, and concluded that the results using the modified drag model gave better agreement with the experimental data. Jiradialok et al. (2006) and later Chelermsinsuwan et al. (2009) used the drag formulation for the low flux flow to simulate the flow in high solid flux risers. This was a major drawback in these two studies because the solution of the EMMS model depends on the flow parameters, and the drag calculated for a particular flow system cannot be used in another flow system (Naren et al., 2007). Most of the previous studies on the EMMS model used Chavan's correlation (Chavan, 1984) for the cluster diameter to calculate the structure-based drag. Naren et al. (2007) studied the sensitivity of the EMMS drag coefficient with different cluster size correlations and concluded that appropriate correlation needed to be used with the EMMS model. However, they restricted their study to the solution of the EMMS model and did not study its effect on the hydrodynamics. Several cluster diameter correlations have been proposed in the literature. Chavan (1984) correlated the cluster diameter with the energy consumed for the suspension and transportation. Harris et al. (2002) used experimental data collected using different particle properties and operating conditions to derive an empirical correlation for the cluster size as a function of solid volume fraction. Recently, Subbarao (2010) proposed a cluster diameter correlation

based on a conceptual model for fully developed gas-solid flow in dilute phase transport and also considered effect of the column diameter.

Although there have been several studies on the EMMS model over the past several years, it is clear from the preceding discussion that most of the previous studies on the EMMS model considered either low solid flux flows or used the drag derived from the low solid flux flows. A rigorous evaluation is, therefore, necessary before these models can be adopted for industrial scale simulations. In this work, we have used the EMMS and Gidaspow models for conducting 2D CFD simulations for both low and high solid flux FCC risers. The simulation predictions for the axial and radial profiles of voidages using both drag models were compared with experimental data. The performance and applicability of the drag models has also been evaluated for predicting the hydrodynamics of low and high solid flux conditions. The literature review revealed that the previous studies offer insight into the complex gas-solid flow in the riser; however the effect of the cluster diameter correlations on the hydrodynamics remains largely unknown. The EMMS model provides a framework to access the effect of cluster diameter on the hydrodynamics. Therefore in this work, the sensitivity of drag coefficient and simulation predictions to different cluster diameter correlations was also evaluated.

4.2. Energy minimization multi-scale (EMMS) model

The EMMS model was originally proposed by Li and Kwauk, (1994) and subsequently investigated by member of researchers from the Chinese Academy of Science and their collaborators (Wei et al., 1998; Xu and Li, 1998; Yang et al., 2003a; Wang et al., 2007; Wang, 2008; Zhang et al., 2008). Earlier works on the EMMS model have been focused on the development of the model, its solution methodology and incorporation of the EMMS drag into CFD model. Table 4.1 summarised various contributions to the EMMS model and its application to the hydrodynamics studies on the riser.

Table 4.1 Contributions to the EMMS model and its applications to the hydrodynamics studies on risers.

Reference	Contribution to the EMMS model
Li and Kwauk, (1994)	A detail explanation on the formulation of the EMMS model was discussed. The gas-solid flow in riser was represented by two pseudo phases i.e. the cluster and dilute phase. Governing equations of the EMMS model were derived using the mass and momentum balances for the cluster phase, dilute phase and interface between the two phases. Generalized Reduced Gradient (GRG) algorithm was used for analytical solution of the model which yielded flow structure parameters such as cluster diameter, cluster fraction and superficial gas velocities.
Xu and Li, (1998)	An alternative analytical solution scheme was represented by avoiding a convergence problem of the GRG algorithm. However, use of experimental curve of C_{d0} – Re (Lapple and Shepherd, 1940) resulted in rather complicate calculations involving several intermediate parameters. Using the solution scheme, the calculated flow structure parameters such as cluster diameter, cluster fraction and energy consumed for suspension and transportation were plotted as a function of superficial gas velocities, which were compared well with those calculated using the GRG algorithm.

Li et al. (1999)	A simplified numerical solution method of the EMMS model (Cheng, 1999) was summarised, and solutions calculated using this method were compared with those from the GRG algorithm and Xu and Li's method. Furthermore, the EMMS model was reiterated in this contribution along with recent developments and ongoing research comprehensively.
Ge and Li (2002)	Difficulties in finding the solution of the EMMS model using both analytical and numerical methods were identified. Furthermore, significance of possible roots and their theoretical implications was also explained. Roots of the EMMS models were used to map different flow regimes of the flows in the riser.
Yang et al. (2003a, 2003b, 2004)	Series of contributions showed calculation of flow structure parameters, drag coefficient, correction factors to account for the drag reduction and combining the structured based drag to the CFD simulations. In first study (Yang et al., 2003a), structure parameters were calculated at a constant superficial gas velocity but using different cluster voidages. The calculated values were plotted against the overall voidage. The stability condition was also modified in the solution method, and the ratio N_{st}/N_T equal to minimum was used instead of N_{st} in original EMMS model. Drag coefficient was calculated from the calculated structure parameters and compared with the Gidaspow drag model (Yang et al., 2003b; 2004).

	In the next part of the contribution (Yang et al., 2003b; 2004), which included the use of the structure-based drag in CFD simulations, a constant cluster voidage was used. This resulted in a decrease in total number of unknown variables, and this method resulted in a sharp drag reduction. Furthermore, simulations were conducted using so-called cycle boundary condition, which assumed a constant solid inventory at every instance, to study an effect of gas-solid drag model and initial solid inventory on hydrodynamic predictions. Simulation results showed capability of the EMMS of capturing variations in the voidages in both radial and axial directions.
Wang and Li (2006)	A detail explanation was given on derivations of the mass and momentum balances in cluster and dilutes phases by considering the dynamic interactions between the clusters and dilute phase. The study gave two algorithms i.e. one for calculation of structure parameters and the other for structure-based drag coefficient. The solution of the model was calculated using both global and local flow variables, which resulted in a huge matrix of the drag coefficients. Hydrodynamics simulations were conducted using the drag from the EMMS-matrix, and the results were compared with those using the Wen-Yu drag model. The results showed reasonable qualitative agreements for the axial profiles of voidages with the experimental data. The results also showed significant impact on the initial solid inventory on both voidage profiles and outlet solid mass flux.

Naren et al. (2007)	The authors used the solution scheme of Xu and Li, (1999) with modifications for the acceleration terms to solve the EMMS model. Then, the solution of the EMMS model was critically evaluated. An energy minimization criterion was examined by plotting the energy as a function of the cluster voidage. They considered the possibility of the formation of the cluster with the voidage lower than the minimum fluidizing voidage. It was found that the solution of minimal energy was obtained at the lowest possible value of the cluster voidage. In addition, sensitivity of the solution of the EMMS model with different cluster diameter correlations and the value of the maximum voidage were also found to be very significant.
Benyahia et al. (2009)	Both the multiscale approaches, the EMMS and SGS, were used to conduct 2D and 3D simulations of risers. The predictions showed improvements in the results using drag from both approaches. However, the results from the SGS model showed better agreements with the experimental data than those from the EMMS model.

In this section, the EMMS model has been briefly described by explaining basic considerations for the flow regimes and scales of interactions in the gas-solid flows in the riser.

Li and Kawauk, (1994) classified the prevailing flow regimes into three types namely; particle dominant, fluid dominant and particle-fluid compromise (Figure 4.1). The gas-solid flow can be termed as particle dominance (PD) when the motion of the fluid has negligible effect in dictating the motion of the particle and the fluid motion is governed by the particles. This regime corresponds to the fixed bed regime. The fluid dominant (FD) regime is characterized by the distinctive motion of the fluid, and the particle motion is governed by the fluid flowing around the particle. This corresponds to the dilute flows in the riser. The particle-fluid compromise (PFC) regime is neither fluid dominant nor particle dominant; instead, both PD and FD regimes co-exist in the PFC.

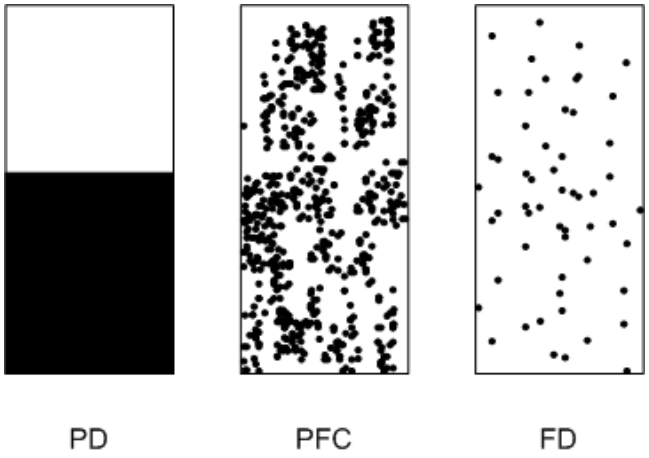

Figure 4.1: Flow regimes in gas-solid flows (Li and Kwauk, 1994).

In the EMMS model, three scales of fluid-particle interactions can be identified, namely, micro, meso and macro scale (Figure 4.2). The micro-scale is at the scale of observation of particle size, which is about 100-500 microns. The particle can be found inside the cluster or in the dilute fluid phase. In the cluster, the particle is under the influence of the surrounding particles and experiences the particle dominance mechanism. In the dilute phase, the particle is surrounded by the fluid and

is under the fluid dominance mechanism. The meso-scale interactions are those taking place between the cluster as a whole entity and the dilute phase surrounding it. The scale of observation for the meso-scale interaction is about 10 to 500 times the particle scale. The particle along the cluster boundary which defines the cluster as an entity is experiencing the paticle-fluid compromise mechanism, as it is under the effect of neighbouring particles from inside of the cluster and also the surrounding fluid of the dilute phase. The macro-scale is observed at the system level, and it deals with the interaction between the gas-solid flows as a whole and the system boundaries. Such interactions result in both axial and radial heterogeneity. The effect of wall boundary results in radial distribution patterns, whereas, the pressure drop consideration and inlet and outlet effects cause an axial heterogeneity.

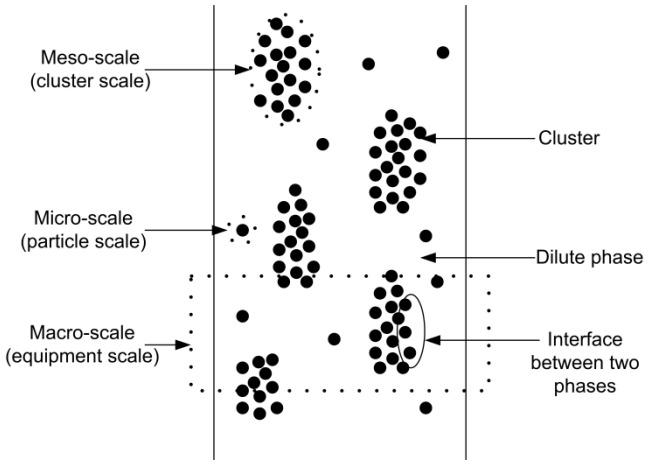

Figure 4.2: Schematic of riser flow.

The EMMS model addresses the spatial heterogeneity arising from different scales of interactions by representing the flow to be made up of two pseudo phases, namely the “cluster” and “dilute” phases (Figure 4.2). In the EMMS model, the total energy of the system is divided into two parts i.e. (i) the energy required for the suspension and transportation and (ii) dissipated energy (Li and Kwauk, 1994). The energy required for the suspension and transportation of these pseudo phases is the sum of the energies of individual phases (i.e. cluster and dilute phases) and their interface. The EMMS model ensures that this energy is minimized for a given set of flow conditions and a stable state of clusters. Applying the minimum energy condition, a

set of flow structure parameters such as the cluster diameter, cluster fraction and slip velocities can be calculated. These flow structure parameters are then used to derive a structure-based drag force for the overall gas-solid flow.

4.3. Calculation of EMMS based drag model

The drag coefficient is calculated using the EMMS model from the overall voidage (ε), total drag force (F_D) and overall slip velocity (U_s) according to the following equation (Yang et al., 2004):

$$\beta_{EMMS} = \frac{\varepsilon^2}{U_s} F_D = \frac{\varepsilon^2}{U_s}\left(m_c F_c + m_f F_f + m_i F_i\right) \qquad \text{eq (4.1)}$$

where, m_c, m_f and m_i are the number of particles per unit volume of the cluster, dilute phases and the ineterface between the two phases respectively. F_c, F_f and F_i are the forces per unit volume in the cluster, dilute phases and the interface between the two phases respectively. These forces are derived from the momentum conservation of the individual phases (equations 4.2 -4.4):

$$m_c F_c = \frac{(1-\varepsilon_c)}{\pi d_p^3/6} C_{Dc} \frac{\pi d_p^2}{4} \frac{\rho_f}{2} U_{sc}^2 = (1-\varepsilon)\left(\rho_p - \rho_f\right)(g+a) \qquad \text{eq (4.2)}$$

$$m_f F_f = \frac{(1-\varepsilon_f)}{\pi d_p^3/6} C_{Df} \frac{\pi d_p^2}{4} \frac{\rho_f}{2} U_{sf}^2 = \left(1-\varepsilon_f\right)\left(\rho_p - \rho_f\right)(g+a) \qquad \text{eq (4.3)}$$

$$F_i m_i = \frac{f}{\pi d_{cl}^3/6} C_{Di} \frac{\pi d_{cl}^2}{4} \frac{\rho_f}{2} U_{si}^2 = (\varepsilon - \varepsilon_c)\left(\rho_p - \rho_f\right)(g+a) f \qquad \text{eq (4.4)}$$

where, ε_c and ε_f are the voidage of the cluster and dilute phases respectively; C_{Dc}, C_{Df} and C_{Di} are the drag coefficients for the cluster, dilute phases and the interface between the two phases respectively, g is the gravitational acceleration, a is the average particle acceleration, ρ_p and ρ_f are the densities of particle and gas respectively; U_{sc}, U_{sf} and U_{si} are the superficial solid velocities in the cluster, dilute phases and the interface between two phases respectively; d_p is the particle diameter; and d_{cl} is the cluster diameter. It is noteworthy that the original EMMS model did not include the particle acceleration term which was later included by Yang et al. (2003).

The mass balance equations are also derived for the overall flow, the gas and particle phase:

$$\varepsilon = \varepsilon_c f + \varepsilon_f (1 - f) \quad \text{eq (4.5)}$$

$$U_p = f U_{pc} + (1 - f) U_{pf} \quad \text{eq (4.6)}$$

$$U_g = f U_c + (1 - f) U_f \quad \text{eq (4.7)}$$

where U_p and U_g are the superficial gas and particle velocities respectively; U_{pc} and U_{pf} are the superficial particle velocities in the cluster and dilute phases respectively; U_c and U_f are the superficial gas velocities in the cluster and dilute phases respectively.

The cluster diameter used in the above momentum balance equation is given by Chavan, (1984):

$$d_{cl} = \frac{d_p\left(\frac{U_p g}{(1-\varepsilon_{max})} - \left(U_{mf} + \frac{U_p \varepsilon_{mf}}{(1-e_{mf})}\right) g\right)}{N_{st}\frac{\rho_p}{\rho_p - \rho_f} - \left(U_{mf} + \frac{U_p \varepsilon_{mf}}{(1-\varepsilon_{mf})}\right) g} \quad \text{eq (4.8)}$$

where, U_p is the superficial solid velocity; ε_{mf} is the minimum fluidization voidage voidage; ε_{max} is the maximum voidage of the dilute phase and N_{st} is the energy consumed for the suspension and transportation which is calculated by minimizing equation (4.9) for a given set of operating conditions:

$$N_{st} = \left[U_g - \frac{\varepsilon_f - \varepsilon}{1-\varepsilon} f(1-f) U_f\right](g + a)\,\frac{\rho_p - \rho_f}{\rho_p} \quad \text{eq (4.9)}$$

where, U_g is the superficial gas velocity.

For minimizing eq (4.9), the maximum voidage of the dilute phase is set to 0.9997 (Matsen, 1982a) and the voidage of the cluster phase is assumed to be the minimum fluidizing voidage, 0.5. The solution yields f, ε, d_{cl}, U_{sc}, U_{sf} and U_{si} for a given U_g and G_s. However, applying the conventional EMMS model in CFD calculations directly requires that a minimum solution be obtained in each of the computational

cells at every iteration for the calculation of the local drag force, and thus, it is computationally intensive. Alternatively, an overall drag coefficient for the system can be obtained from the solution of the EMMS model using the superficial gas velocity and solid flux. This drag coefficient is then only dependent on the local voidage and can be easily incorporated in CFD calculations without any computational penalty. Details of computing drag coefficient using the modified EMMS model are given in Appendix I.

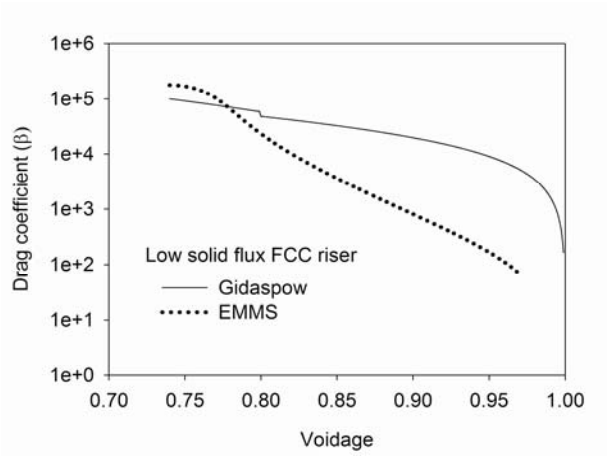

(a)

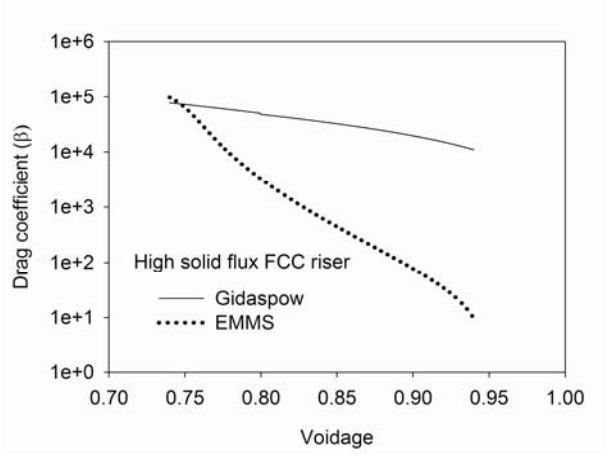

(b)

Figure 4.3: Drag coefficient calculated using the Gidaspow and EMMS models for (a) low solid flux (b) high solid flux conditions.

In this study, the EMMS model was solved for two flow conditions i.e. a low and high solid flux flow conditions. The flow parameters and phase properties for these

flow conditions are summarised in Table 4.3. The drag coefficient calculated using the modified EMMS model (Appendix I) was compared with that calculated using the Gidaspow model (Gidaspow, 1994). A comparison between the values of the two drag coefficient as shown Figure 4.3(a) and (b), which clearly indicates that the drag coefficient computed using the EMMS model was considerably lower than that calculated using the Gidaspow's model. This reduction in the value of the drag coefficient calculated using the EMMS model can be attributed to the energy minimization assumption which implies that the effective drag is reduced due to the lesser resistance caused by the flow of clusters.

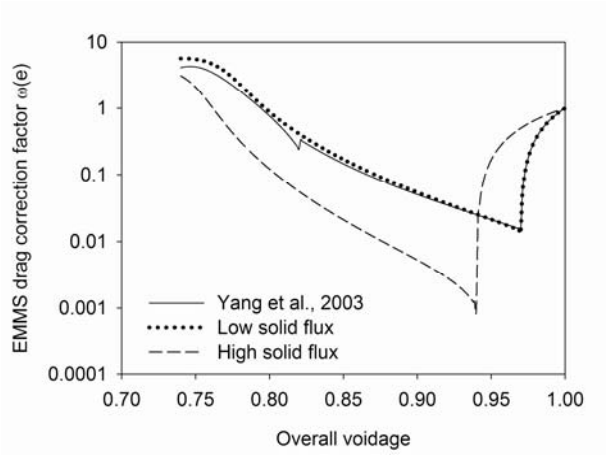

Figure 4.4: Correction factor of the EMMS drag model for both low and high solid flux conditions.

The correction factor (ω) was defined as a ratio of the drag coefficient calculated using a particular drag model (β) to a standard drag coefficient (β_0). For example, the correction factor for the Wen-Yu drag model is $\varepsilon^{-2.7}$. Figure 4.4 shows the correction factor plots for the EMMS drag model for both low and high solid flux conditions as a function of the voidage. For both the conditions, the plots were qualitatively similar; however, the values of the correction factors were significantly different. This can be attributed to the difference in the flow structure parameters for two flow conditions. The correction factor plots show a steep decline until the voidage was equal to 0.97 for the low solid flux, and 0.94 for the high solid flux conditions. This decline can be attributed to reduction in the drag coefficient due to the formation of

clusters, as well as because of an increase in the voidage. The steeper decline in the correction factor under high solid flux conditions can be attributed to the larger drag reduction due to the higher rate of cluster formation. After this steep decline, further increase in the voidage results in breakup of clusters. Therefore, at the higher voidages, the solution of the EMMS model could not be achieved and the correction factors were assumed to be approaching to unity.

Once a correction factor graph for a given system was obtained, the drag was calculated:

$$\beta_{EMMS} = \beta_0 \omega(\varepsilon) \qquad \text{eq. (4.10)}$$

Where, $\beta_0 = \frac{3}{4}\frac{\varepsilon(1-\varepsilon)}{d_p}\rho_g|u_g - u_p|C_{D0}$ is the standard drag coefficient.

The algebraic function of the correction factors as a function of the voidage (See Table 4.2) was then derived using a curve fitting.

4.4. CFD simulation

2D unsteady state CFD simulations were conducted for both low and high solid flux conditions using Fluent 6.2. The computational geometry used in simulations (see Figure 4.5) consisted of two-sided inlet for solid entry, bottom gas inlet and two side outlets. A velocity-inlet boundary condition was used for both gas and solid inlets whereas a pressure-outlet boundary condition was applied for the outlet. For both low and high flux conditions, the initial solids inventory in the riser was set using the available experimental data. The Johnson-Jackson boundary condition, which assumes no slip for the gas phase and partial slip for the solid phase, was applied to the wall. Transient CFD simulations were carried out using a time step of 5×10^{-4} s. Second order and QUICK discretization schemes were used for the momentum and volume fraction equations respectively. The turbulence in the gas phase and its effect on the dispersed secondary phase was modelled using the standard k-ε model. The pressure-velocity coupling was resolved using the SIMPLE algorithm. Each

simulation was carried out for at least 40 s and predictions were time-averaged for the last 20 s. The list of simulation and model parameters is shown in Table 4.3.

Table 4.2: EMMS drag equations with corresponding correction factors

For the low solid flux riser,

$\beta_{Ergun} = 150\frac{(1-\varepsilon)^2\mu_g}{\varepsilon d_p} + 1.75\frac{(1-\varepsilon)\rho_g|u_g-u_p|}{d_p}$ ----- for ε <= 0.78

$\beta_{EMMS} = \frac{3}{4}\frac{\varepsilon(1-\varepsilon)}{d_p}\rho_g|u_g-u_p|C_{D0}\omega(\varepsilon)$ ---- for ε > 0.78

Where ω(ε) = correction factor

$\omega(\varepsilon) = -3.867\times10^{-2} + \frac{6.893\times10^{-3}}{4(\varepsilon-0.761)^2+1.599\times10^{-3}}$ ---- For 0.78 < ε <= 0.86

$\omega(\varepsilon) = -1.283\times10^{-2} + \frac{3.940\times10^{-3}}{4(\varepsilon-0.782)^2+2.711\times10^{-3}}$ ---- For 0.86 < ε <= 0.97

$\omega(\varepsilon) = -31.859 + 32.859\varepsilon$ ---- For ε > 0.97

For the high solid flux riser,

$\beta_{Ergun} = 150\frac{(1-\varepsilon)^2\mu_g}{\varepsilon d_p} + 1.75\frac{(1-\varepsilon)\rho_g|u_g-u_p|}{d_p}$ ----- for ε <= 0.748

$\beta_{EMMS} = \frac{3}{4}\frac{\varepsilon(1-e)}{d_p}\rho_g|u_g-u_p|C_{D0}\omega(\varepsilon)$ ---- for ε > 0.748

Where ω(ε) = correction factor

$\omega(\varepsilon) = -3.379\times10^{-2} + \frac{2.187\times10^{-3}}{4(\varepsilon-0.744)^2+8.909\times10^{-4}}$ ---- For 0.748 < ε <= 0.83

$\omega(\varepsilon) = -1.186\times10^{-2} + \frac{1.327\times10^{-3}}{4(\varepsilon-0.7510)^2+9.252\times10^{-4}}$ ---- For 0.83 < ε <= 0.86

$\omega(\varepsilon) = -6.223\times10^{-3} + \frac{1.023\times10^{-3}}{4(\varepsilon-0.752)^2+8.151\times10^{-4}}$ ---- For 0.86 < ε <= 0.94

$\omega(\varepsilon) = -15.650 + 16.650\varepsilon$ ---- For ε > 0.94

Table 4.3 Simulation and model parameters

	Low solid flux	High solid flux
Particle dia. (d_p)	54 μm	76 μm
Density	930 kg/m^3	1712 kg/m^3
Solid mass flux (G_s)	14.3 kg/m^{2}s	489 kg/m^{2}s
Superficial gas velocity (U_g)	1.52 m/s	5.2 m/s
Grid size	2.5 mm × 35 mm	11 mm × 67 mm

Modelling parameters

Modelling approach	Eulerian-Eulerian
Gas-solid drag	Gidaspow drag (Gidaspow, 1994), EMMS drag (Li and Kwauk, 1994)
Shear viscosity	Gidaspow et. al., (1994)
Bulk viscosity	Lun et al. (1984)
Frictional viscosity	Schaeffer et al. (1987)
Frictional pressure	KTGF based (Lun et al., 1984)
Solid pressure	Lun et al. (1984)
Radial distribution	Lun et al. (1984)
Restitution coefficient	0.95
Granular temperature	Lun et al. (1984)

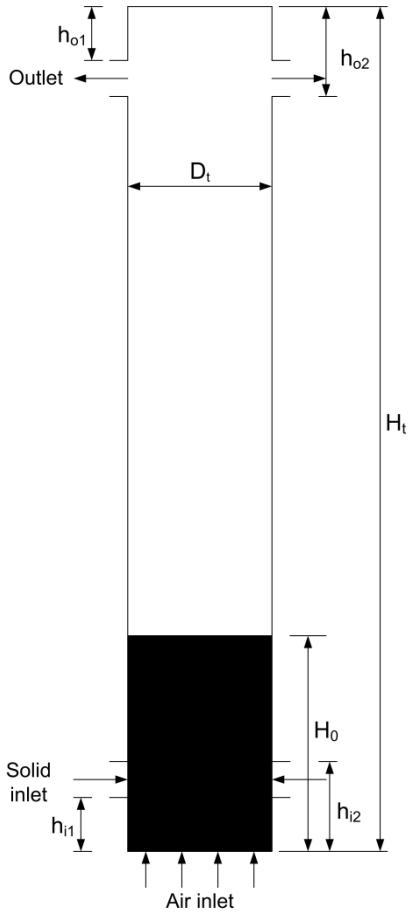

	Low solid flux	High solid flux
H_t	10. 5 m	14.2 m
D_t	0.09 m	0.2 m
H_0	1.225 m	2 m
h_{i1}	0 m	0.25 m
h_{i2}	0.14 m	0.35 m
h_{o1}	0 m	0.25 m
h_{o2}	0.14 m	0.35 m

Figure 4.5: Schematic diagram of FCC riser with corresponding dimensions for a low and high solid flux conditions.

4.5. Results and discussion

4.5.1. Hydrodynamics of low mass flux FCC riser

For low solid flux conditions, CFD simulations were performed using the calculated drag coefficient (from EMMS) and results were compared with those using the Gidaspow model as well as with the experimental data of Li and Kwauk (1994) and the numerical predictions of Yang et al. (2003b, 2004).

Figure 4.6 shows a comparison of time-averaged axial and radial profiles of voidages from CFD simulations with experimental data. In the experimental data, the riser exhibited a distinctive S-shaped axial voidage profile having a lower voidage at the bottom and a higher value at the top (Figure 4.6a). The Gidaspow drag model was unable to capture this profile both quantitatively and qualitatively, and predicted a uniform voidage along the height of the riser. Although the EMMS model did not show a quantitative agreement with the experimental data, it did show a reasonable qualitative agreement with the experimental profile. The experimental data showed a transition from higher to lower voidages at an approximate height of 4.5 m. The simulation using the EMMS model predicted this transition at 8 m height. After this height, the results with the EMMS model were in reasonable quantitative agreement with the experimental data. Figure 4.6(b) and (c) show radial profiles of the voidage using both drag models at two different axial locations (3.5 m and 8.75 m height). The radial profiles for both drag models showed a basic core-annulus structure with respect to phase hold-up with higher voidage near the centre and lower voidage near the wall. At 3.5 m height, the predictions using both drag models showed moderate to high quantitative disagreements with the experimental data, particularly near the wall, where only the EMMS drag could predict the rapid drop in voidages, albeit only qualitatively. In the dilute section of the riser (at 8.75m height) near the wall, the results using the EMMS drag model showed a reasonable qualitative agreement with the experimental data, whereas, those for the Gidaspow model were closer to the experimental data at the centre of the riser. Therefore, it was concluded that the EMMS model always gave better agreements near the wall, which can be attributed

to the EMMS model's ability to capture the formation of clusters near the wall, where high solid concentration prevail.

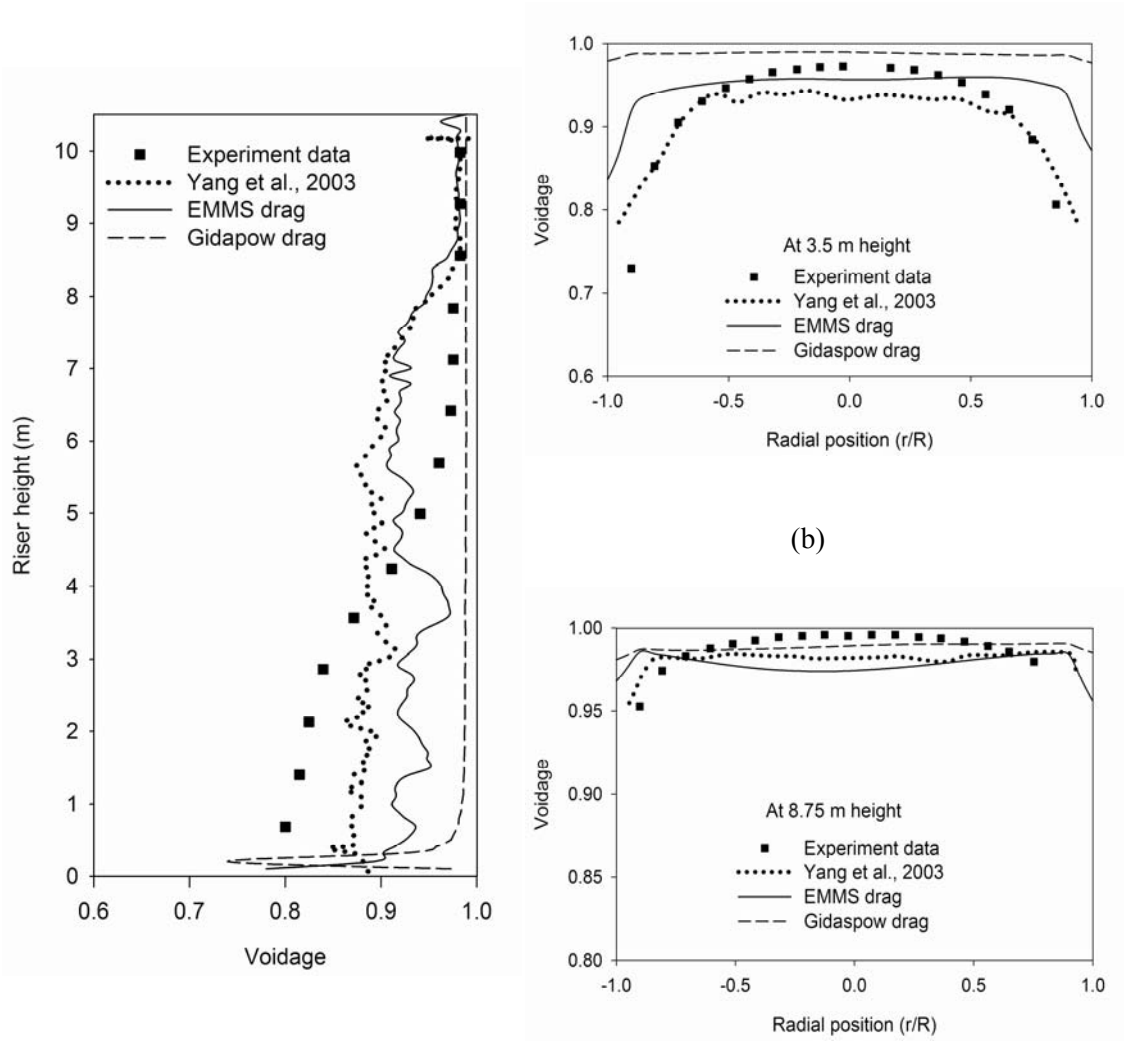

Figure 4.6: Hydrodynamics of low solid flux riser: (a) Axial profile of voidages along height; (b) and (c) Radial profiles of voidages at 3.5 and 8.75 m height respectively (Experimental data from Li and Kwauk, 1994).

Figure 4.7 shows fluctuations in the solid mass flux and solid inventory using the two drag models. Using the Gidaspow drag model, simulations predicted a very high solid flux with sharp decline in the solid inventory for initial 20 s. After that, the solid inventory achieved a dynamic steady state at which the value of the mass flux

fluctuated around the experimental value of 14.3 kg/m^{2}s. The initial peaks in the solid flux can be attributed to higher solid inventory in the beginning, as well as the over prediction of drag force using the Gidaspow model. Using the EMMS model, the solid flux at the outlet always remained close to the experimental value, whereas the solid inventory remained at a higher value. Thus, it was concluded that for a given solid flux the EMMS model predicted a higher solid inventory than that with the Gidaspow model.

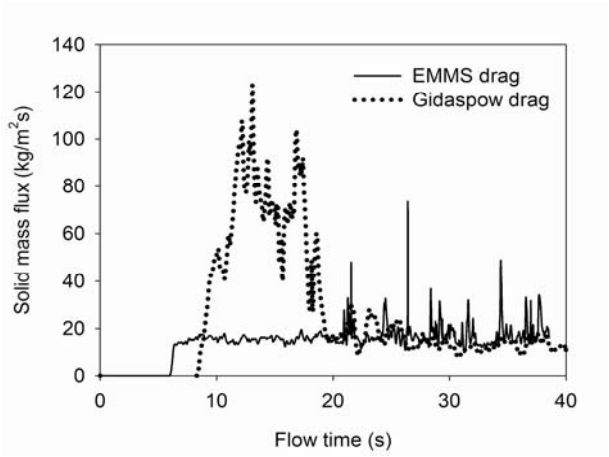

(a)

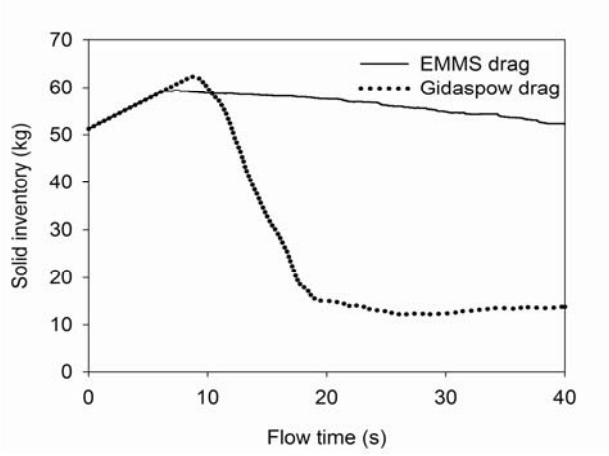

(b)

Figure 4.7:For low solid flux conditions: (a) Circulating solid flux, and (b) Solid inventory.

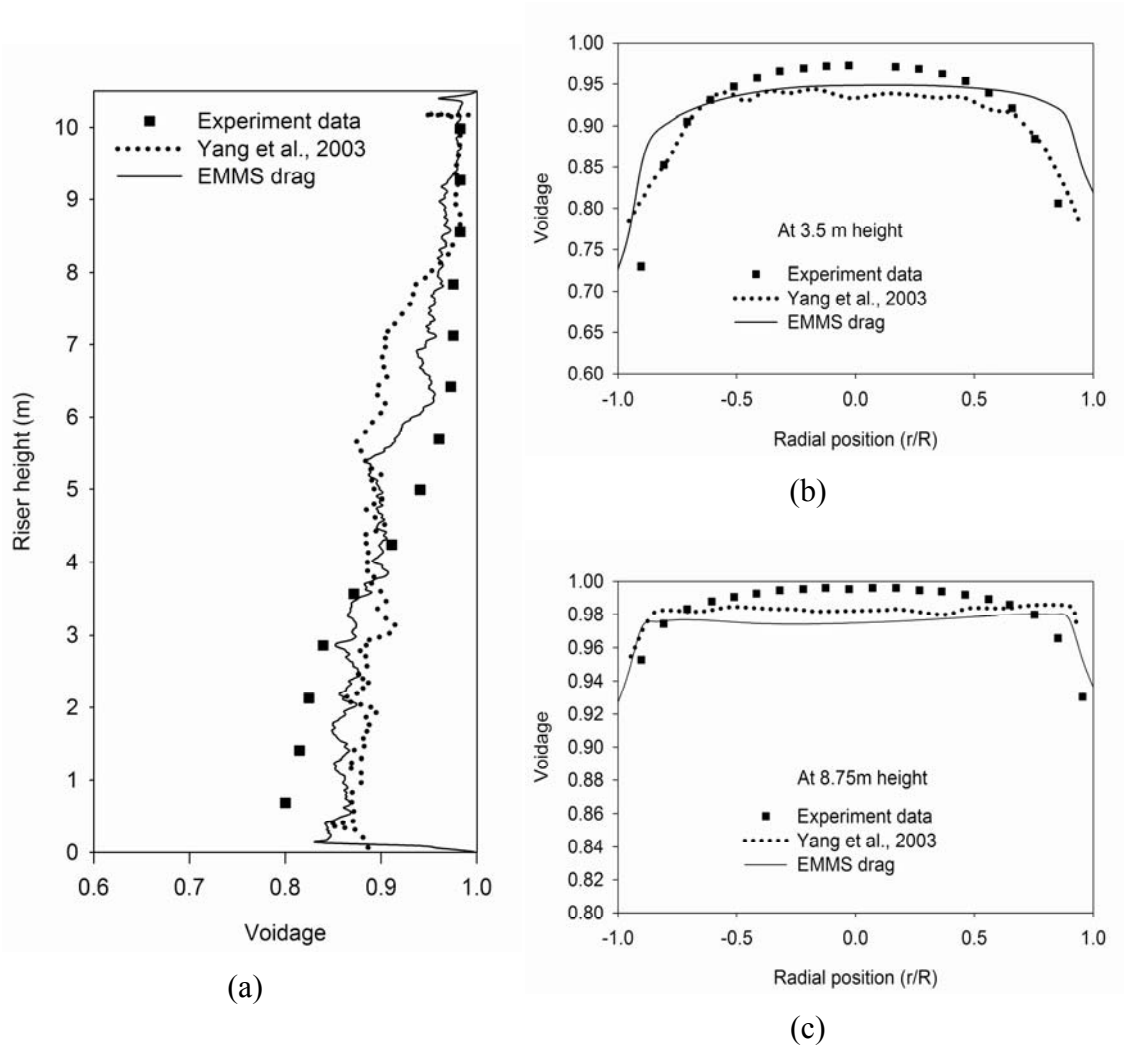

Figure 4.8: Hydrodynamics of low solid flux riser using a constant solid inventory on a time-averaged basis: (a) Axial profile of voidages along height; (b) and (c) Radial profiles of voidages at 3.5 and 8.75 m height respectively (Experimental data from Li and Kwauk, 1994).

The predictions from the current study showed some disagreements when compared with the results of previous numerical studies (Yang et al., 2003b; Yang et al., 2004). These apparent discrepancies can be attributed to the differences in types of boundary conditions for the solid inlet and outlet. In the previous studies, Yang et al. (2003b, 2004) maintained a constant solid inventory in the riser at each time step by imposing a cyclic boundary condition for solids. This boundary condition although allowed author to match their solid flux conditions to experimental values, it is

somewhat unrealistic as the inventory in the riser fluctuates continuously. Therefore, in this study, the solid inlet boundary condition was implemented using a constant solid flux, which was evaluated by carrying out a time averaging of outlet solid flux. This boundary condition ensured a constant solid inventory on the time-averaged basis and was used in the present work. The time-averaged axial and radial profiles of voidage using this boundary condition are shown in Figure 4.8. Both axial (Figure 4.8a) and radial profiles (Figure 4.8b and c) showed a reasonable qualitative and quantitative agreement with Yang et al., 2003b, 2004. It can also be observed that the height, where the transition from higher to lower voidages takes place, was predicted more accurately in the current study (Figure 4.8a). The circulating solid mass flux was also plotted as a function of flow time (Figure 4.9). The solid flux showed large scale fluctuations with Gidaspow's model predicting very high time-averaged value of 78.09 kg/m^{2}s, which is approximately five times greater than the experimental value. On the other hand, the EMMS drag predicted a time-averaged value of 16.48 kg/m^{2}s being close to experimental value of 14.3 kg/m^{2}s. These predictions of the circulating solid flux were also consistent with those reported in Yang et al. (2003b, 2004).

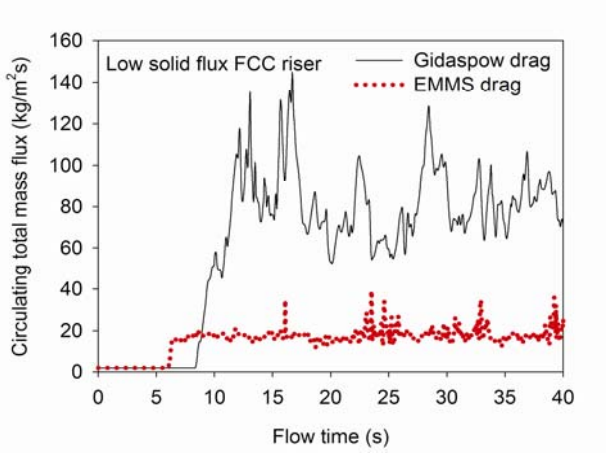

Figure 4.9: Circulating mass flux for simulations using constant solid inventory boundary conditions

4.5.2. Hydrodynamics of high mass flux FCC riser

For high solid flux conditions, simulations were conducted using the EMMS and Gidaspow drag models, and results were compared with the experimental data of Knowlton et al. (1995) and numerical predictions of Benyahia et al. (2001).

The axial profile of the pressure drop and radial profiles of voidages are shown in Figure 4.10. The simulations using the Gidaspow drag model gave higher pressure drops in the bottom section, after which it remained at a lower value without any significant variation along the height. A similar qualitative trend was predicted using the EMMS model; however, qualitatively, higher pressure drops were predicted (Figure 4.10a). For the EMMS drag model, the pressure drop profile showed a reasonable qualitative and quantitative agreement with only about 10 % discrepancy when compared with the experimental data, and also showed a better agreement with the experimental data than the results of previous numerical study (Benyahia et al., 2001). Figure 4.10(b) and (c) show the radial profiles of voidages at two different axial locations (3.9 m and 8.1 m height). At of 3.9 m height (Figure 4.10b), both drag models captured only qualitative trend of the experimental data with the results using Gidaspow's model showing a reasonable quantitative agreement near the centre. Additionally, it should also be noted that the predictions in this study showed a qualitative profile of the experimental data more accurately than those in Benyahia et al. (2001), which had used the Arastoopour drag model. At 8.1 m height (Figure 4.10c), the simulation using both drag models gave a reasonable qualitative and quantitative agreement with the experimental data near the wall. However, at the centre, only the Gidaspow drag model showed a quantitative agreement with the experimental data, whereas, the EMMS drag showed wide discrepancies.

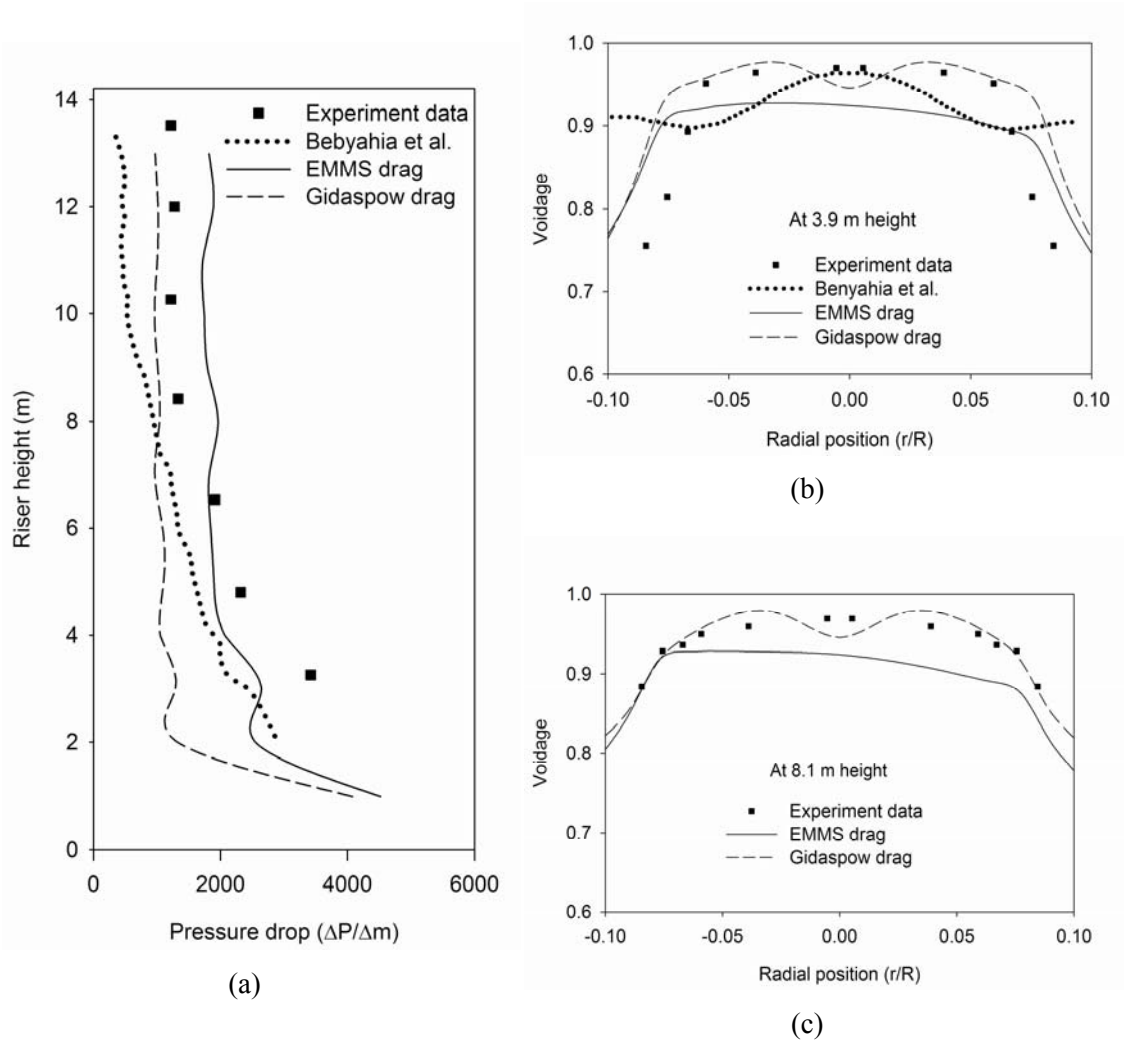

Figure 4.10: Hydrodynamics of high solid flux riser: (a) Axial profile of pressure drop along height; (b) and (c) Radial profiles of voidages at 3.9 and 8.1 m height respectively (Experimental data from Knowlton et al., 1995).

Figures 4.11(a) and (b) show the solid flux at the outlet and solid inventory inside the flow domain as a function of time. The solid flux (Figure 4.11a) fluctuated around the time-averaged value of 481.98 kg/m^{2}s using the EMMS model and that for the Gidaspow's model at 488.69 kg/m^{2}s. Both of these values were close to the experimental value of 489 kg/m^{2}s (Figure 4.11a). For the solid inventory (Figure 4.11b), the simulation using the EMMS model gave higher value of 594.31 kg, being approximately twice of that predicted by the Gidaspow's model. In case of high flux

condition also; the EMMS model predicted a higher solid inventory than that calculated using the Gidaspow's model.

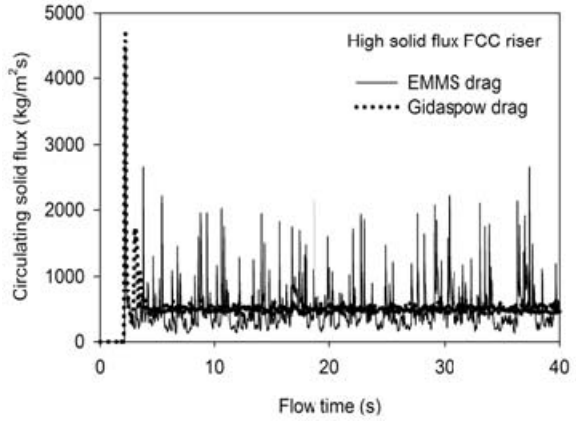

(a)

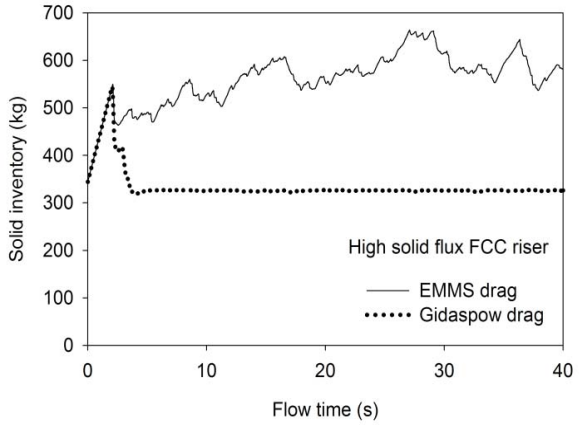

(b)

Figure 4.11: For high solid flux conditions: (a) Circulating solid flux, and (b) Solid inventory.

4.5.3. Effect of cluster diameter correlation

The cluster diameter is one of the important flow structure parameters in the EMMS model and directly affects its solution. In the orginial formulation of the EMMS model, the cluster diameter equation proposed by Chavan, (1984) is used. This correlation was derived by imposing constraints on its value at two extremes of the voidages; i.e. (i) its value approaches to infinity at the minimum fluidization voidage,

and (ii) to particle diameter at the maximum voidage. This cluster diameter correlation does not account for the effect of the column diameter, particle-particle interaction and the shape of the cluster. As a result, different cluster diameter correlations have been proposed (Harris et al., 2002; Subbarao, 2010). Harris et al., (2002) gave an empirical correlation for the cluster diameter near the wall of the riser as a function of the solid volume fraction. The correlation resulted in reasonable fit to the experimental data with the correlation coefficient (R^2) being 0.77:

$$d_{cl} = \frac{\varepsilon_s}{40.8-94.5\varepsilon_s} \qquad \text{eq (4.11)}$$

Recently, Subbarao, (2010) proposed a cluster diameter correlation considering the effect of the column diameter. The correlation was derived from a conceptual model for the fully developed gas-solid flow, which assumes that ratio of the volume of cluster to that of void is equal to the ratio of the cluster to gas volume fraction. In this model, the void size is restricted to the column diameter and the rise velocity is restricted to slug rise velocity, which again depends on the column diameter. The final equation of the cluster diameter is:

$$d_{cl} = \left[\frac{(1-\varepsilon)}{(\varepsilon-\varepsilon_c}\right]^{1/3} \frac{2u_t^2}{g}\left(1+\frac{u_t^2}{u_{sr}^2}\right)^{-1} + d_p \qquad \text{eq (4.12)}$$

where, u_t is the terminal velocity of the particle, u_{sr} is the slug rise velocity:

$$u_{sr} = 0.35(gD_t)^{1/2} \qquad \text{eq (4.13)}$$

The cluster diameter was calculated using different correlations and plotted as a function of the voidage in Figure 4.12(a). The plot shows wide disagreements in the values, with the correlation proposed by Subbarao (2010) yielding the lowest value for the voidage range from 0.6 to 0.98; whereas, correlation of Harris et al. (2002) gave the lowest value for the voidage near unity. The cluster diameter using Subbarao's and Chavan's correlation showed qualitative similar profile, which was constant over almost entire range of the voidage and then as the voidage approached the unity, its value dropped to the particle diameter (Figure 4.12a). The correlation of Harris et al. (2002) gave very high value of the cluster diameter which gradually

decreased with increase in the voidage. It should be noted that Harris et al.'s correlation was developed for regions near the wall, where higher solid concentration prevails and thus, the correlation resulted in higher values for the cluster diameter. The EMMS model was solved as described in Appendix I using these cluster diameter correlations to calculate the structure-based drag coefficient.

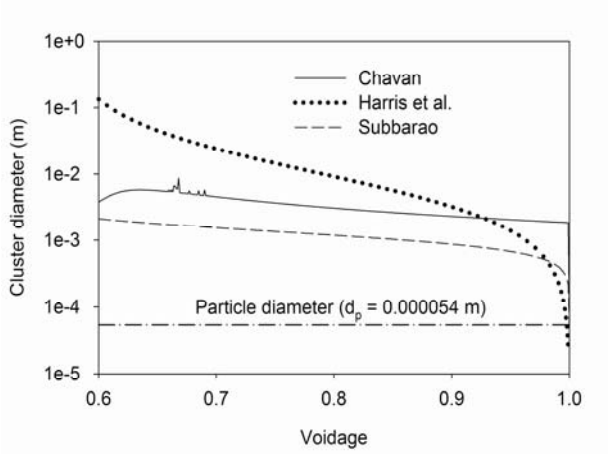

(a)

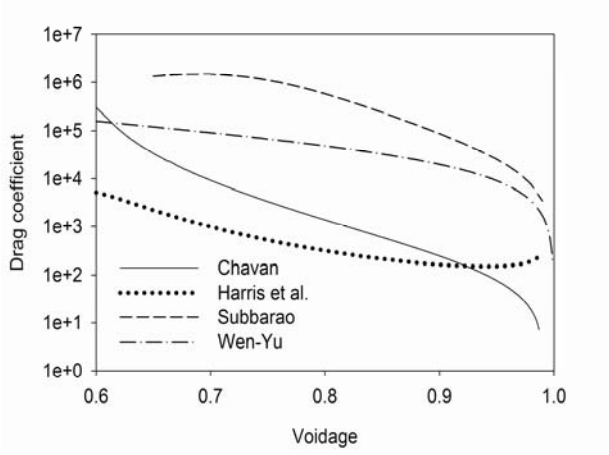

(b)

Figure 4.12: Effect of cluster diameter correlations on values from EMMS model: (a) Cluster diameters, and (b) Drag coefficients.

Figure 4.12(b) shows the calculated drag coefficients using three cluster diameter correlations. The correlation of Harris et al. (2002) gave higher drag reduction at lower voidages because of higher values of the cluster diameter. The drag coefficient

calculated using Harris et al.'s correlation approached to that calculated using the Wen-Yu correlation as the voidage approached to unity. Interestingly, Subbarao's correlation gave values higher than that calculated using the Wen-Yu correlation, which can be attributed to lower value of the cluster diameter and higher acceleration. Therefore, for Subbarao's correlation, the solution of the EMMS model did not gave drag reduction, contradicting with the basic essence of the EMMS model that the effective drag reduces and becomes less than that calculated using the Wen-Yu model due to the formation of the clusters. Thus, CFD simulations were only performed using the drag coefficient calculated using the cluster diameter correlations given by Chavan (1984) and Harris et al. (2002), and the results were compared with the experimental data.

Figure 4.13(a) shows the time-averaged axial profile of voidages from CFD simulations with the experimental data. Significant improvement in the axial profile of voidages was achieved using the cluster diameter correlation of Harris et al. (2002), particularly for voidages in the bottom dense region and height of the transition from higher to lower voidages. However, the results using Chavan's correlation showed reasonable agreement in the dilute top. Harris et al.'s correlation predicted higher drag reduction for lower voidages (from 0.6 to 0.93); however, at higher voidages, it predicted an increase in the drag coefficient. On the other hand, at higher voidages, Chavan's correlation predicted a further drop in the drag coefficient. This contradicting behaviour at lower and higher voidages might be responsible for the disparity in the results in the bottom and top sections. Figure 4.13(b) and (c) show radial profiles of the voidages using the two cluster diameter correlations at two different axial locations (3.5 m and 8.75 m height). At 3.5 m height, the results using Harris et al.'s correlation showed lower voidages than the experimental values (Figure 4.13a). At the same height, the results using Chavan's correlation gave reasonable agreement with the experimental data near the centre, however, near the wall, the results showed higher voidages than the experimental values. The under prediction of voidages by the correlation of Harris et al. (2002) can also attributed to higher cluster diameter and lower drag coefficient values in the dense bottom. In the dilute section of the riser (at 8.75m height), the results using Harris et al.'s

correlation showed a reasonable qualitative agreement with the experimental data near the centre, whereas, those using Chavan's correlation were closer to the experimental data near the wall of the riser (Figure 4.13b). At lower voidages, because of increase in the drag coefficient using Harris et al.'s correlation, it resulted in more dilute flow and gave reasonable agreement near the centre.

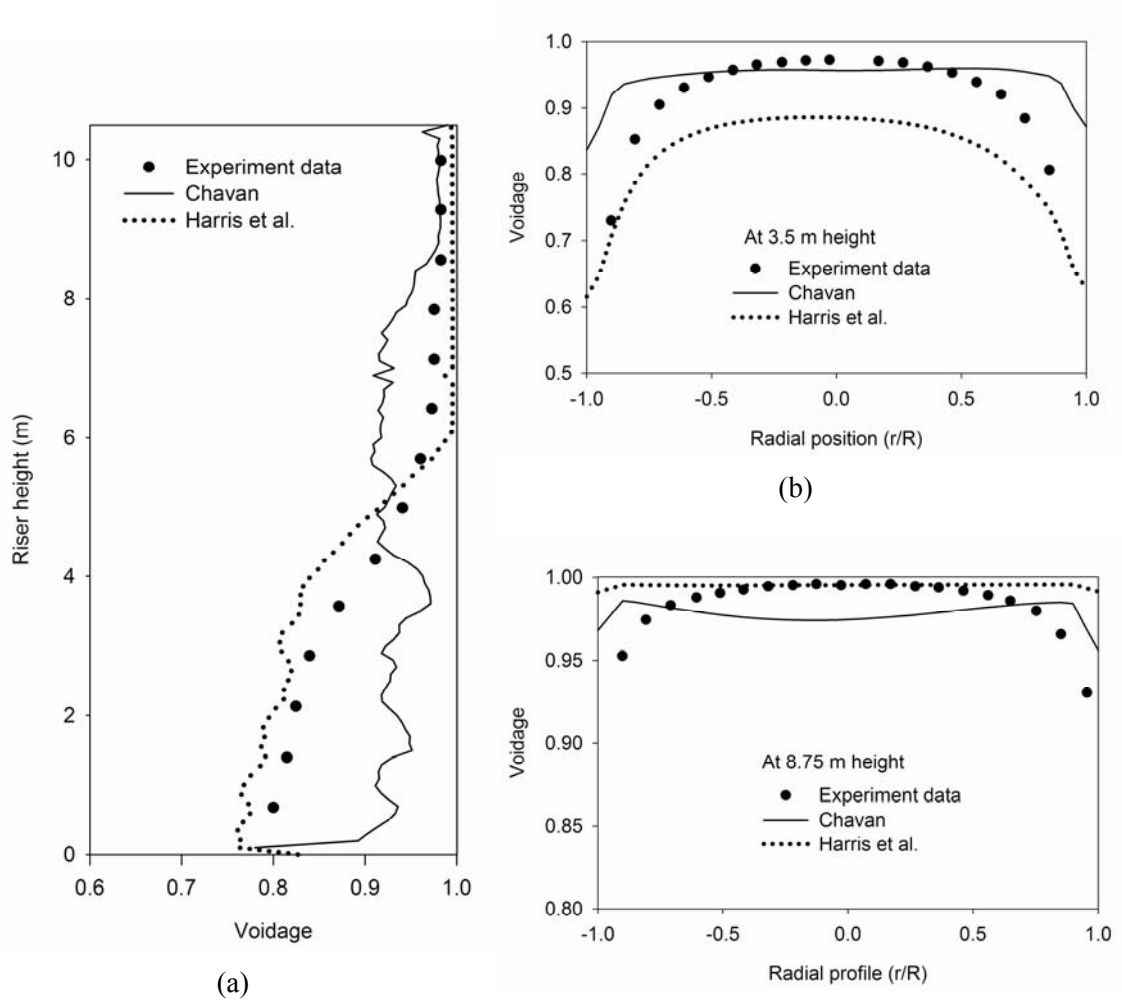

Figure 4.13: Effect of cluster diameter correlations on hydrodynamics of low solid riser: (a) axial profile of voidages along height; (b) and (c) Radial profile of voidages at 3.5 and 8.75 m height respectively (Experimental data from Li and Kwauk, 1994).

It is now clear from the above results that the cluster diameter correlation has significant effect on the hydrodynamics predictions and should be selected carefully for the prevailing flow conditions. The correlation proposed by Harris et al. (2002)

gave better results in the dense region, whereas, that of Chavan (1984) performed better in the dilute section. It will also be interesting to formulate a voidage dependent cluster diameter correlation that can be applied to the structure-based drag coefficient. Furthermore, depending on the relative performance in different ranges of voidages, a combination of different cluster diameter correlations can be used with the EMMS framework to find possible improvements in the hydrodynamics predictions. A validated structure based drag model that accounts for the effect of cluster diameter will be useful to remove some quantitative disagreements with the experimental data, particularly in the radial profiles of voidages. It will also help in providing more insight into gas –solid flows in risers.

4.6. Conclusions

In this chapter, the performance and applicability of the EMMS model was evaluated by comparing its hydrodynamics prediction with those using the Gidaspow drag model, as well as with the experimental data and the results of the previous numerical simulations for both low and high solid flux conditions. Only the simulations using the EMMS model captured the S-shape of the axial profile of voidage. However, the EMMS drag model did not compare well with experimental observation for the height at which a transition from lower to higher voidages occurs. For higher solid flux conditions, both the Gidaspow and EMMS drag models gave qualitatively similar results for the pressure drop with the EMMS model predicting higher quantitative value. For both drag models, the radial profiles of the voidages showed the basic core-annulus structure, with those predictions using the EMMS drag model showing a reasonable quantitative agreement with the experimental data near the wall of the riser. However, at the centre of the riser, the predictions using the Gidaspow drag model showed a reasonable agreement with the experimental data. Therefore, the EMMS drag model was able to capture the axial and radial heterogeneity of the riser hydrodynamics for both low and high solid flux conditions.

When simulations were conducted using a constant inlet solid flux, the solid inventory using the EMMS model was higher than that using the Gidaspow drag model. However, when a constant solid inventory was imposed, the Gidaspow drag

model gave several times higher time-averaged value of solid flux than experimental values, whereas that using the EMMS model was close to experimental values.

In addition, the drag coefficients were calculated using three different cluster diameter correlations using the EMMS model, and then simulations were conducted using these drag coefficients. The results using widely used cluster diameter correlation proposed by Chavan (1984) did not compare well with experimental observation for the height at which the transition from lower to higher voidages occurs. However, the correlation proposed by Harris et al. (2002) could capture qualitative profile of axial profile of voidage with reasonable quantitative agreement with the experimental data, particularly in the dense bottom. At dilute top section, the cluster diameter correlation of Chavan (1984) gave better agreement with the experimental data. Despite the use of different cluster diameter correlations, the disagreements in radial profiles of voidages between predictions and experimental data could not be explained. Therefore, alternative formulation of the cluster diameter correlations should be evaluated for calculating the drag coefficient.

5. Hydrodynamics of an Industrial-Scale Lift Engager

5.1. Introduction

In the previous chapters, several challenges have been identified while applying the EE model to simulate a dilute gas-solid flow in rather simple equipment such as riser. However, efforts are also necessary to apply the model to simulate more complex industrial-scale equipment. Such study can be useful in analysing qualitative nature of a state of fluidization in the equipment, and provide insight on the effect of operating as well as design parameters on the hydrodynamics. In this chapter, a catalyst lift engager of catalytic reformer has been studied by conducting CFD simulations.

Catalytic reforming is a process of great interest to petroleum refinery and petrochemical industry for the production of aromatic compounds which are raw materials for several petrochemical products and gasoline additives. Typically, the reforming units are of two types; semi-regenerative reforming (SSR) unit (older) and continuous catalyst regeneration reforming (CCR) (newer) unit, which is characterized by an in-situ regeneration of the reforming catalyst. One of the key aspects of the CCR is the catalyst circulation between the reactor and regenerator. It is important to maintain a sufficient rate of circulations as inefficient catalyst circulations may lead to retardation of reforming reaction rate. Generally, to compensate for the reduced reaction rate, make up catalyst must be added which affects the economy of the whole plant. The catalyst circulation is controlled by the lift engagers situated at the bottom of the reactor and regenerator. The efficiency of the lift engager in terms of catalyst lift rate depends on various operating and design parameters such as the lift gas velocity, lift line gap and catalyst feed rate. The hydrodynamics of the gas solid flow plays an important role in governing the performance of the lift engager. Higher gas velocities in the lift line can result in excessive catalyst attrition, whereas low gas velocities can produce an unstable lifting. In this study, the hydrodynamics of a lift engager has been characterized using the EE gas-solid flow model.

A schematic diagram of a lift engager and catalyst circulation circuit of CCR is shown in Figure 5.1. The Lift Engagers (LE1 and LE2) shown in Figure 5.1 hold, fluidize and transport the catalyst between the reaction and regeneration zones of the CCR. Typically, the recycled hydrocarbon gas and hydrogen are used as the lifting fluid. The spent catalyst flows from the bottom of the last stacked reactor bed through a lock hopper to a lift engager. The circulating lift gas enters through two inlets, namely, primary and secondary inlets and lifts the catalyst through a lift pipe to a disengaging hopper located above the regeneration tower. The catalyst is then fed to the regeneration tower from the bottom of the disengaging hopper. The regenerated catalyst follows a similar circuit and is transported to the reactor through another lift engager situated at the bottom of the regenerator. A typical lift engager is a cylindrical vessel with two concentric pipes, a catalyst inlet dip and a secondary gas inlet line (see inset Figure 5.1). The lift gas enters as two separate gas streams called the primary and secondary gas streams. The primary gas enters from the annular space between the two concentric pipes and the secondary gas enters separately from a side inlet. The secondary gas travels over a flow restricting baffle to the main body of the lift engager. The lifted catalyst is discharged through the extended centre pipe called the lift line.

Simulating the flows of lift engager is challenging because of the presence of multiple flow regimes within the equipment, as well as the scale of operation and complexity in geometry. The objective of this study was to investigate its hydrodynamics using CFD. The EE model, which can adequately represent the gas-solid flow hydrodynamics of a lift engager, was applied to simulate a 3D industrial-scale geometry. Initially, the effect of model parameters such as drag models (Gidaspow and Syamlal-O'Brien drag models) and solid pressure models was investigated. The evaluated model was then applied to conduct a parametric study. It should be noted that the flow regimes, reforming catalyst properties and the geometry of the lift engager are significantly different from the risers considered in the previous chapters. Consequently, this chapter serves as a case study for investigating complex industrial equipment using the EE model.

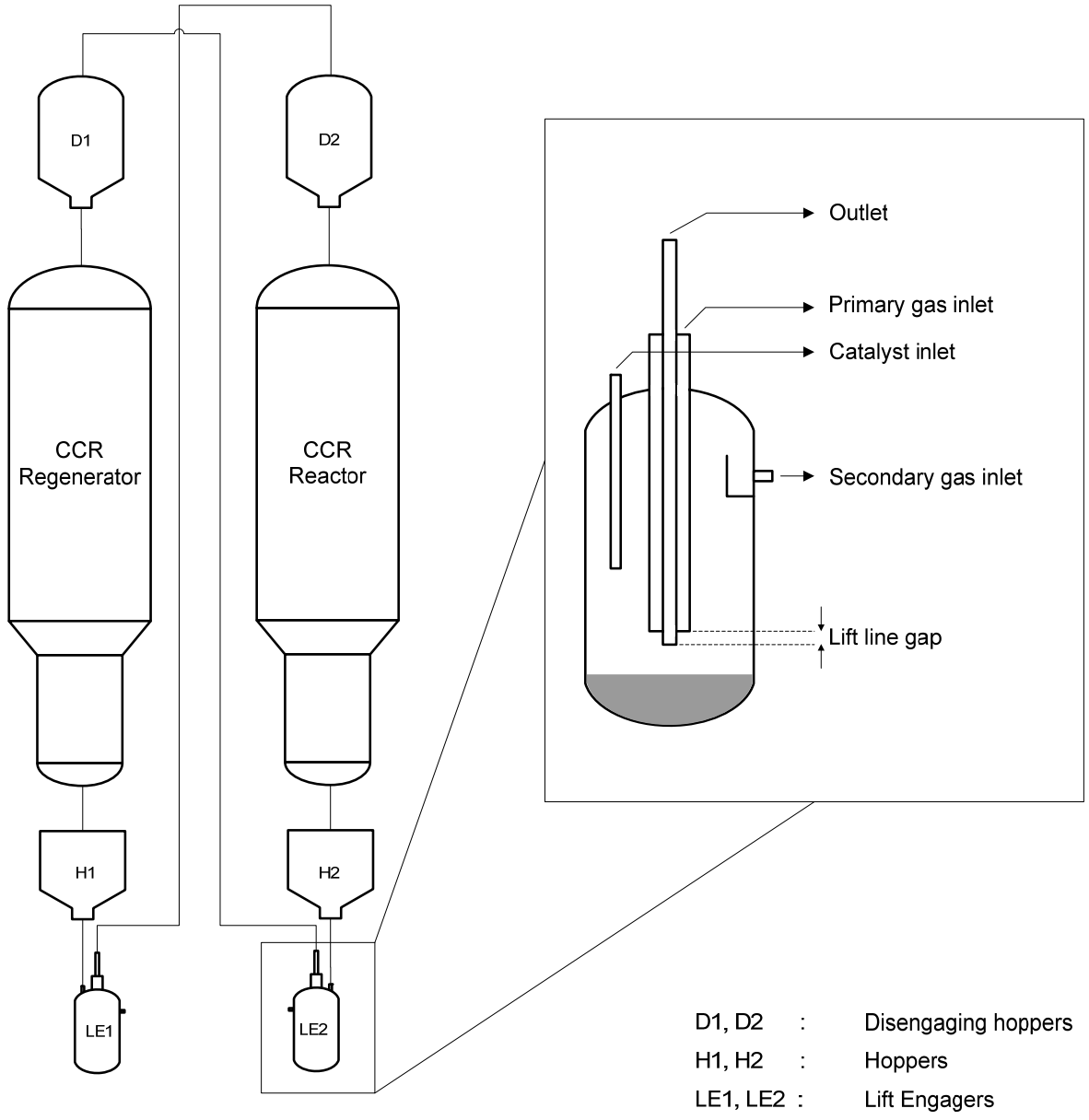

Figure 5.1: Schematic diagram of CCR and lift engager.

5.2. CFD simulations

The EE gas-solid flow model in FLUENT was used for simulating an industrial-scale 3D lift engager which was meshed using GAMBIT as shown in Figure 5.2a. Most of the flow domain was meshed using structured hexahedral-cooper grid scheme with unstructured tetrahedral meshing in other parts. Transient CFD simulations were carried out with a time step of 1×10^{-4} and approximately 435,000 grid points on a cluster of eight processor machines. A set of closure models used in this part have already been described in the previous chapter and are also summarized in Table 5.1 The lift gas (a mixture of hydrocarbons) and reforming catalyst have been the gas and solid phases respectively. Physical properties of both phases are also given in Table 5.1. Velocity-inlet boundary conditions were used for all inlets streams (solid, primary gas and secondary gas inlets). Simulations were performed for a constant catalyst flow rate of 0.19 kg/s for various flow rates for the primary and secondary gases. The walls were configured with no-slip conditions, and a pressure outlet boundary condition was applied for the outlet.

5.3. Results and discussion

The initial catalyst bed was patched with packed solids (volume fraction 0.63) up to the entrance of the lift line as shown in Figure 5.2b and simulations were commenced in an unsteady manner. As shown in Figure 5.2c, the total catalyst accumulation in the equipment gradually depleted during the course of simulation before stabilising. It is clear that it took about 15s or more for the system to come to a dynamic steady-state in-term of catalyst inventory. Even after this period the mass flow rate of solids at the outlet continuously fluctuated albeit with much smaller amplitudes with its time-averaged value being approximately equal to the inlet mass flow rate. The unsteady time-averaged statistics for the catalyst velocity, catalyst volume fraction and the slip velocity, discussed below were collected after this initial period (i.e. after 15s or more).

Table 5.1: Phase properties, modeling and simulation parameters.

Phase properties		
Gas phase (Hydrocarbon gas)		
Density	0.889 kg/m^3	
Viscosity	1.15×10^{-5}	
Solid phase (Reforming catalyst)		
Bulk density	933 kg/m^3	
Particle size	1.6 mm	
Modeling parameters		
Gas phase (eulerian approach)		
Turbulence		Standard k-ε model
Solid phase (eulerian approach)		
Shear viscosity		Gidaspow (1994)
Bulk viscosity		Lun et al. (1984)
Frictional viscosity		Schaeffer (1987)
Frictional pressure		Johnson and Jackson
Granular temperature		Lun et al. (1984)
Radial distribution		Lun et al. (1984)
Solid pressure		Lun et al. (1984)
Drag model		Gidaspow et al. (1991) Syamlal - O'Brien (1987)
Maximum packing limit	0.63	
Restitution coefficient	0.9	
Angle of internal friction	30^O	
Simulation parameters		
Number of mesh volumes	434966	
Average grid size	0.8359 cm^3	
Time step size	0.0001 s	
Discretization		Second order
Pressure-velocity coupling algorithm		SIMPLE

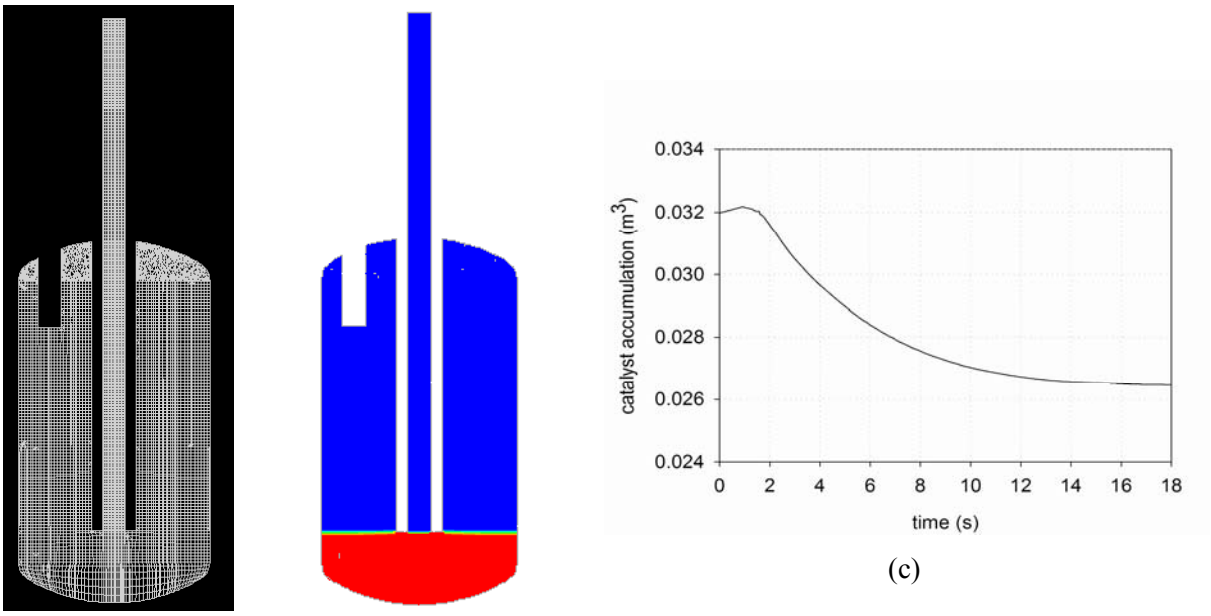

(a) (b) (c)

Figure 5.2: (a) Grid design, (b) Initial catalyst accumulation inside the lift engager, and (c) Change in catalyst accumulation as a function of time (Catalyst flow rate = 0.19 kg/s, Primary gas = 5 m/s, Secondary gas velocity = 7 m/s).

Initial numerical experiments were carried out to evaluate the effect of the grid size by conducting simulations on the lift engager with three different grid densities with average cell sizes being approximately 1.6914, 0.8359 and 0.6010 cm^3 (190,000, 435,000 and 530,000 grid points) respectively. Figure 5.3 shows the calculated pressure at the outlet as a function of time. It is clear that the behaviour for the first coarser grid was substantially different from the other two finer grids. Since there was minimal refinement in results with reducing the grid size 0.8359 cm^3 to 0.6010 cm^3, a grid size of 0.8359 cm^3 was used for the remaining simulations in this study.

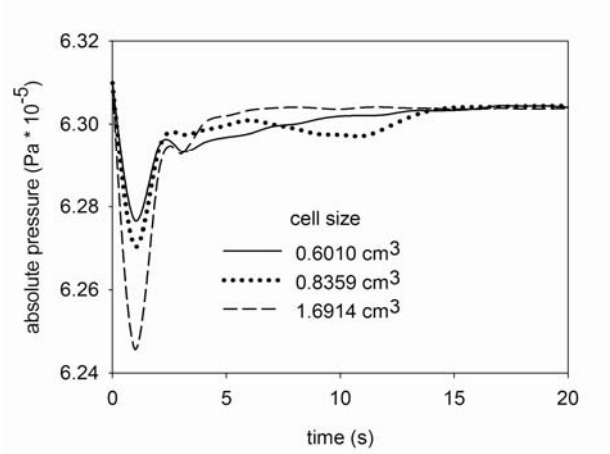

Figure 5.3: Effect of grid size (Catalyst flow rate = 0.19 kg/s, Primary gas = 5 m/s, Secondary gas velocity = 7 m/s).

Figure 5.4 shows snapshots of catalyst volume fraction contour and catalyst velocity vectors on axis plane, path lines of gas phase entering from primary and secondary gas inlets for the base case simulation. It was observed that the catalyst falls though the inlet with an increasing velocity and decreasing volume fraction under the effect of gravity and the convective effect of the secondary gas (Figure 5.4a and b). The secondary gas velocity reduces considerably after passing through the baffle region due to sudden increase in the cross sectional area (Figure 5.4c). It appeared that the recommended secondary gas velocity was not adequate to fully fluidize the catalyst, therefore, resulting in a very poor mixing. Similarly, the primary gas immediately changed its direction upwards after entering the vessel and thus lifting the catalyst in the lift line although without any interaction with the bulk of solids (Figure 5.4c).

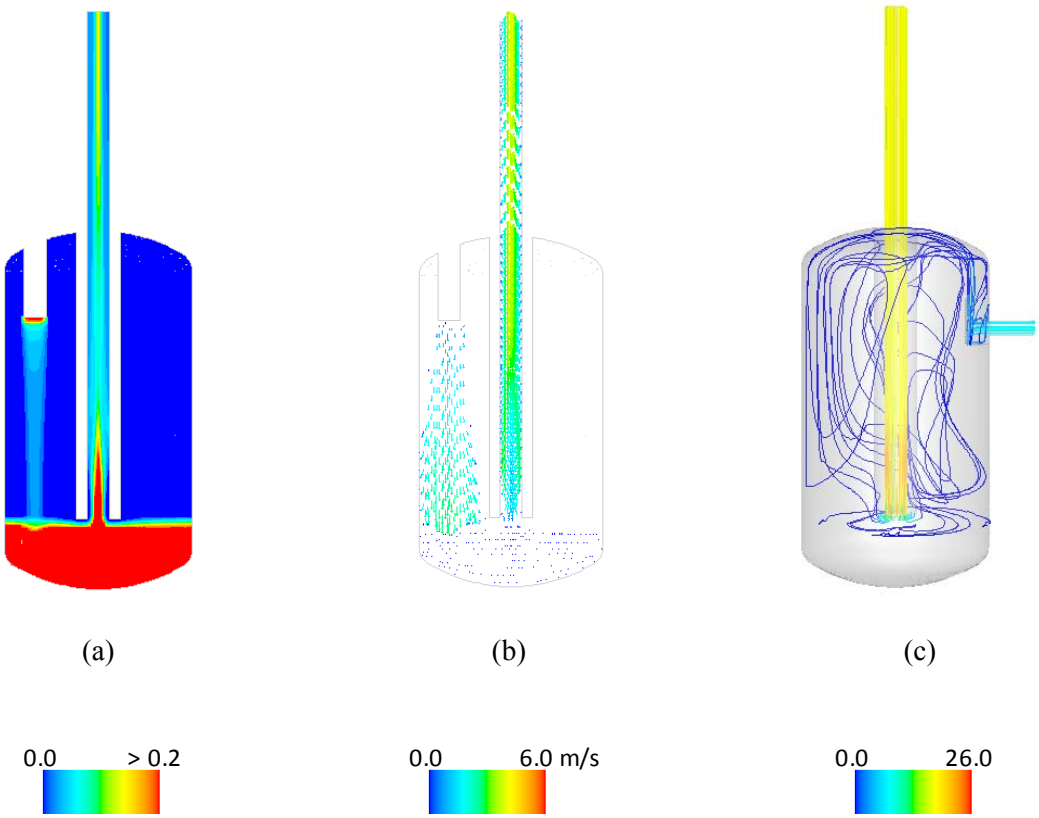

Figure 5.4: Snap shots: (a) Catalyst volume fraction contour, (b) Catalyst velocity vectors, and (c) Path lines of the lift gas entering from primary and secondary gas inlets (Catalyst flow rate = 0.19 kg/s, Primary gas = 5 m/s, Secondary gas velocity = 7 m/s).

5.3.1. Effect of drag models

Most gas-solid drag models are based on the empirical co-relations derived from physical or numerical experiments. Although, the drag models for the multiphase systems have been studied extensively, there are no clear guidelines for the selection of an appropriate drag model applicable specific to a particular system. This selection is primarily based on the granular flow regime and particles Reynolds numbers of the flow domain. However, the gas-solid flow in the lift engager can be characterized by existence of multiple granular flow regimes in different parts of the system with the bulk of the lift engager being in dense and the lift line exhibiting dilute gas-solid flow regime. Therefore, in this study, two drag models namely, Gidaspow (Gidaspow et al., 1991a) and Syamlal and O'Brien (Syamlal and O'Brien),

which are applicable for a wide range of particle Reynolds numbers and flow conditions were selected for a comparative analysis. It should be noted that reforming catalyst particle are larger in diameter and can be classified as group D of Geldart classification. These particles do not exhibit formation of clusters as discussed in the chapter 4. Therefore, the structured-based drag was not considered. Furthermore, the Syamlal-O'Brien drag model needs to be calibrated using particle terminal velocity and minimum fluidizing velocity. The method of calibration in the form of simple MS-Excel programme is specifically given in the MFIX user guide published by Syamalal et al. (1993) and was also summarised in Appendix II. Use of the model with the default values of constants as given in the commercial CFD code can give misleading results.

To study the effect of drag models on flow predictions for both dense and the dilute flows, the simulation results from three locations with two being in the lift line and one at the top of the catalyst bed were compared. The comparison of the time-averaged radial profiles of catalyst velocity and volume fraction at the selected locations is shown in Figure 5.5. The comparison revealed considerable differences in the values of catalyst velocity and volume fraction from two drag models. The Syamlal and O'Brien drag model (Syamlal and O'Brien, 1987) always predicted higher catalyst velocities than the Gidaspow drag model (Gidaspow et al., 1991b)(Figure 5.5a, c and e). The Gidaspow drag model calculated high volume fractions than the Syamlal and O'Brien drag model for the dilute flow in the lift line (Figure 5.5b and d). But in the dense catalyst bed, both drag models predicted same catalyst volume fraction (Figure 5.5f). It was also observed that both catalyst velocity and volume fraction profiles in the lift line are parabolic with lower values near the wall. The increasing catalyst velocity along the height of the lift line suggests that the flow is dominated by the drag force over the gravitational force in the lift line. However, in the catalyst bed region, there is no observable movement of the catalyst indicating the dominance of the frictional force over the interphase exchange drag force.

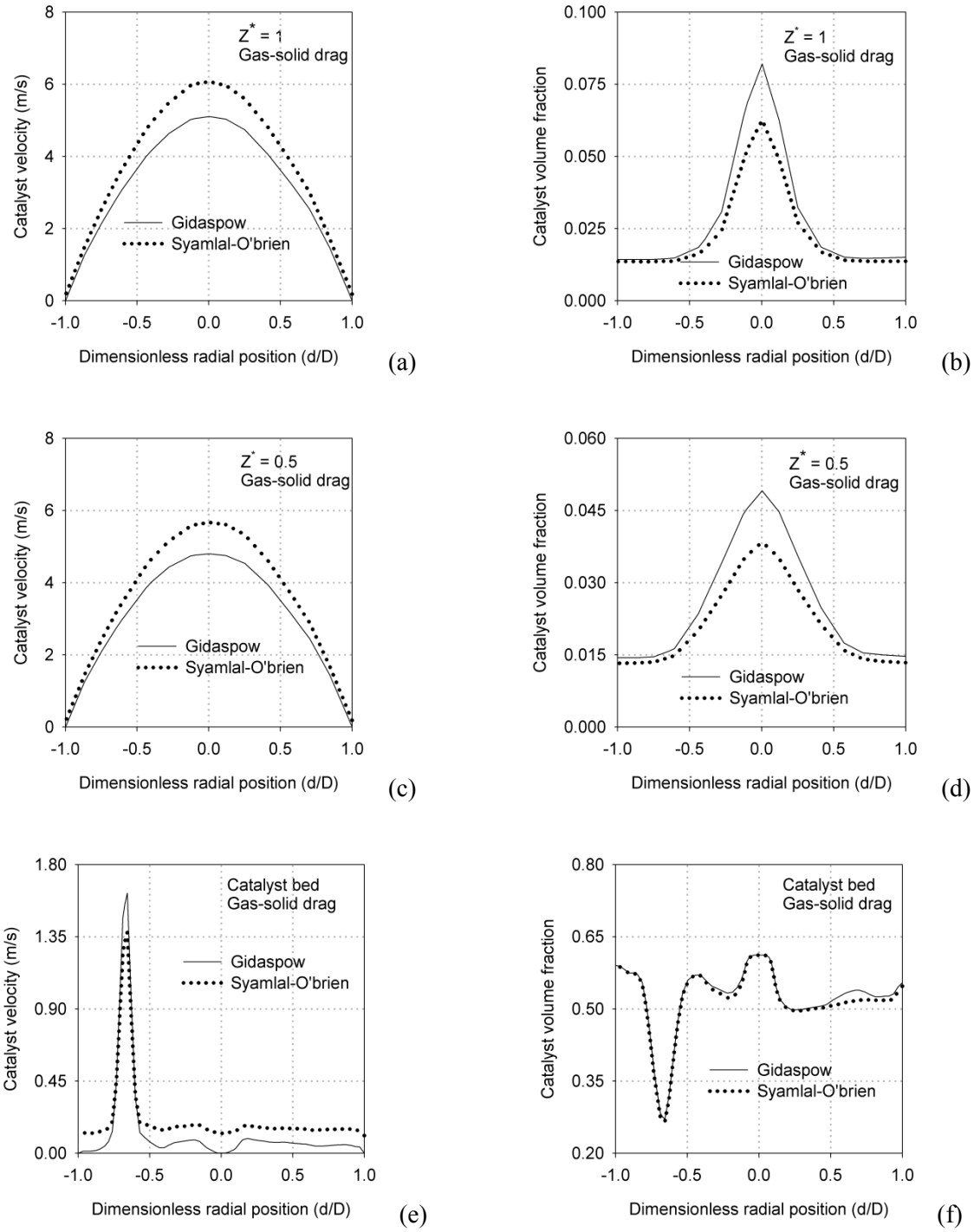

Figure 5.5: Time-averaged radial profiles: (a), (c) and (e) Catalyst velocity at top of the lift line, middle of the lift line and top of the catalyst bed respectively, and (b), (d) and (e) Catalyst volume fraction at top of the lift line, middle of the lift line and top of the catalyst bed respectively (Catalyst flow rate = 0.19 kg/s, Primary gas = 5 m/s, Secondary gas = 7 m/s))

Table 5.2: Selection of drag model for lift engager

	Author	Application	Model	Particle Diameter (mm)	Density (kg/m^3)	Drag Model
1	Sakai and Koshizuka (2009)	Pneumatic Conveying	DPM	1	1000	Ergun
2	Levy (2001)	Pneumatic Conveying	EE	3	880	Gidaspow
3	Duarte et al. (2009)	Spouted Bed	EE	6	1173	Gidaspow
4	Kawaguchi et al. (2000)	Spouted Bed	DPM	3	2500	Gidaspow
5	Gryczka et al. (2009)	Spouted Bed	EE	1.75	1040	Gidaspow
6	Du et al. (2006)	Spouted Bed	EE	1.41	2500	Gidaspow

From the above observations, it can be concluded that the selection of drag model can have significant effect on the simulation results. Hence, experimental observations should be considered to justify the choice of a drag model. However in absence of the relevant experimental data, the previously published literatures on gas-solid flow modelling of similar applications such as the spouted bed and pneumatic conveying with comparable solid phase properties can also provide useful ground for selection of the drag model. Table 5.2 lists the selection criteria for drag models from the applications similar to lift engager. Based on this criterion, the Gidaspow model, which had been applied in most of the previous studies with coarse particle, was selected for all successive simulations.

5.3.2. Effect of frictional pressure

The stress tensor that appears in the momentum balance equation for the granular phase includes a viscosity terms for kinetic/collision and frictional flow regimes. The frictional viscosity becomes dominant when the solid phase volume fraction nears the maximum packing limit. The effect of frictional viscosity is significant in applications such as fluidized and spouted beds. Whereas the frictional viscosity can be neglected for the dilute flows in the riser application. As shown in Figure 5.5e, the catalyst bed at the bottom of the lift engager

has volume fraction close to the maximum packing limit. Therefore, unlike the dilute flows in the riser, the frictional viscosity in the lift engager cannot be ignored. In this study, the frictional viscosity was accounted for using the Schaeffer model (Schaeffer, 1987). The Schaffer model also includes a frictional pressure term which can been modelled using (i) Johnson and Jackson (Johnson and Jackson, 1987), (ii) Syamlal (Syamlal et al., 1993) and (iii) the KTGF based models. According to van Wachem et al. (2001), the frictional stress calculated by Johnson and Jackson and Syamlal model can differ by orders of magnitude. In the KTGF based approach, the solid pressure is calculated using the granular kinetic theory (Fluent, 2006).

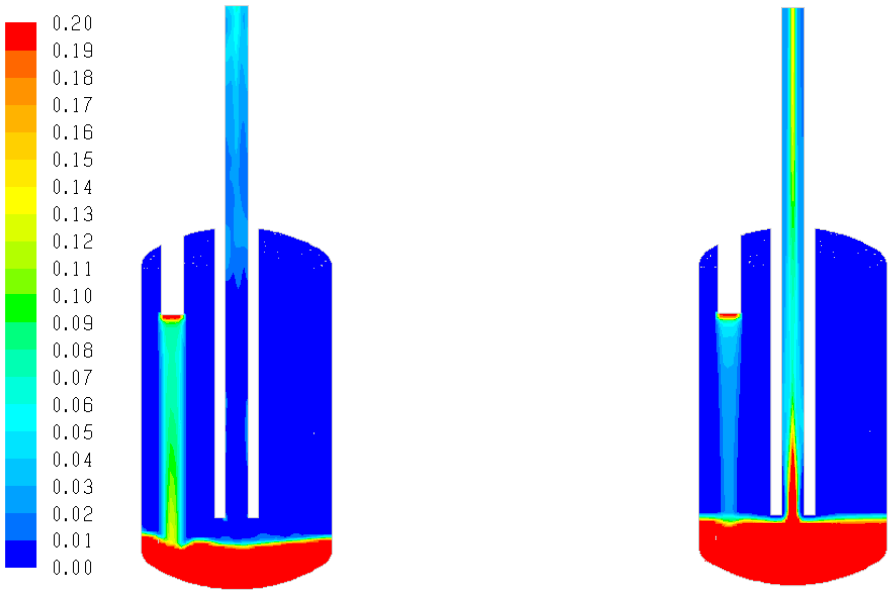

Figure 5.6: Effect of the frictional pressure model on contour of catalyst volume fraction: (a) KTGF based and (b) Johnson and Jackson approach respectively

A comparison between simulation results for the lift engager using Johnson and Jackson and KTGF-based models is shown in Figure 5.6. For the KTGF model, the catalyst volume fraction near the entrance of the lift line was observed to be almost zero and it increased along the height of the lift line (Figure 5.6a). Whereas, the Johnson and Jackson model predicted higher catalyst volume fractions near the entrance that reduced along the axial height of the

lift line (Figure 5.6b). The time averaged catalyst velocity and volume fraction profiles along the lift line were also compared and shown in Figures 5.7 and 5.8. It can be seen that for the KTGF model (Figure 5.7a and b), both catalyst velocity and volume fraction increased along the height of the lift line for a constant mass flow rate at the inlet. This prediction is illogical since it violates the fundamental principle of mass conservation. However, the profiles for Johnson and Jackson model overcame this drawback where the velocity increased and the volume fraction decreased along the axial height of the lift line. These results are consistent with the previously published data for vertical pneumatic conveying systems (Arastoopour and Gidaspow, 1979; Littman et al., 1993; Theologos and Markatos, 1994).

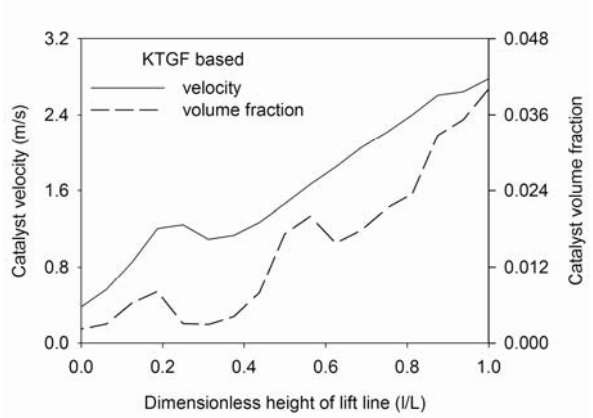

(a)

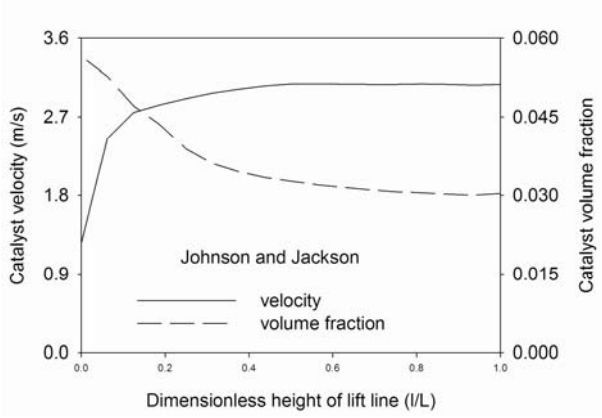

(b)

Figure 5.7: Effect of the frictional pressure model: (a) Catalyst velocity, and (b) volume fraction profiles for KTGF based and Johnson and Jackson approach respectively (Catalyst flow rate = 0.19 kg/s, Primary gas = 5 m/s, Secondary gas = 7 m/s).

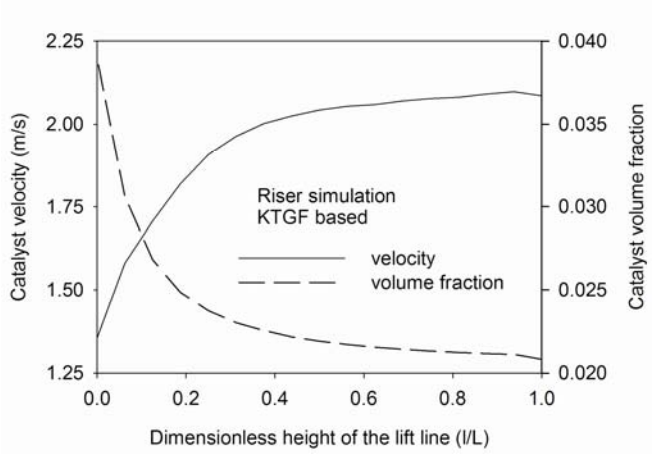

(a)

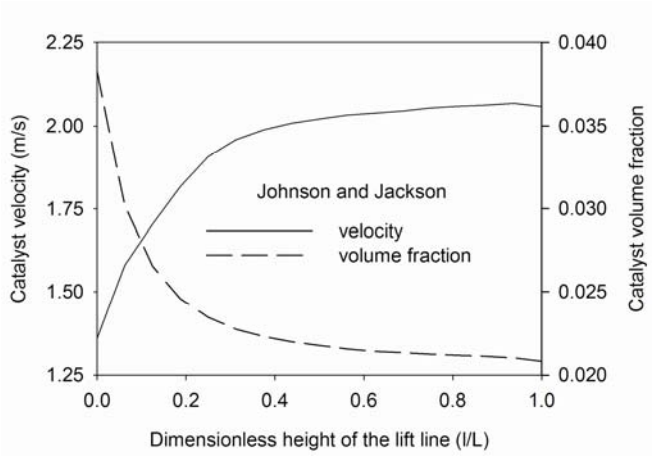

(b)

Figure 5.8: Effect of the frictional pressure model: (a) Catalyst velocity and volume fraction profiles for riser simulation with KTGF based model for riser simulation and (b) Catalyst velocity and volume fraction profiles for riser simulation with Johnson and Jackson model.

It is worth noting that the above drawback in the KTGF-based frictional pressure model has not been reported previously because most of the previously reported simulations are for a relatively simple geometry of risers. In order to evaluate the possible reasons for the discrepancy in Figure 5.7, simulations were conducted inside a simple riser (having the same diameter as the lift-line in Figure 5.8) with the same particle properties. As shown in Figure 5.8(a) and (b), both KTGF-based model and Johnson and Jackson model gave very similar results for the flow inside the riser. Hence, it can be concluded that the KTGF-based frictional pressure model can be useful for the flow inside simple geometries, but for the complex

granular flow systems such as that in the lift engager which involves a transition from the dense fluidization to dilute vertical pneumatic transport, the Johnson and Jackson model for the frictional pressure is more appropriate.

5.3.3. Effect of lift gas velocity

The primary and secondary lift gas velocities are very critical parameters which not only affect the catalyst lift rate but also associated disturbances therein. To study the effect of the lift gas flow rate on the catalyst transportation in the lift line, the simulations with various flow rates of primary and secondary gases were conducted. The simulated lift gas velocities, flow rate and the resulting superficial gas velocity in the lift line are shown in Figure 5.9. The mass flow rate at the outlet, the time-averaged catalyst velocity, volume fraction and slip velocity in lift line were calculated and compared.

Figure 5.10 shows the total mass flow rate at outlet as a function of time for a fixed secondary gas velocity (7 m/s) and three different primary gas velocities. It is clear that for approximately 15 seconds, depending upon the primary gas velocity, there were significant fluctuations in the outlet mass flow rate surging as high as 3 kg/s. After this period, the catalyst bed height and the catalyst accumulation reached to a dynamic steady-state where the mass flow rate fluctuated around an averaged-value equal to the inlet mass flow rate. Although similar trends were observed for all three primary gas velocities, there were considerable differences in the amplitude of fluctuations. For the primary gas velocity of 3 m/s, there existed both small and large-scale fluctuations before achieving the dynamic steady-state. For this primary gas velocity (3 m/s), as shown in the inset in Figure 5.10, even after achieving the dynamic steady-state, the small-scale fluctuations in the outlet mass flow rate persisted. However, for the higher value of primary gas velocity (e.g., 7 m/s), except for a couple of high amplitude oscillations in the first 2s, the predicted outlet mass flow rate was relatively free of small-scale fluctuations. For the primary gas velocity of 5 m/s, the fluctuations in the outlet mass flow rate could be characterized to be an average of those for 3 m/s and 7 m/s. Therefore, if smooth lifting is required, a higher flow rate of the primary lift gas is recommended. However, excessively high velocities may enhance the possibility of associated erosions, it is apparent that a primary gas velocity of 5 m/s will be optimal for the current system.

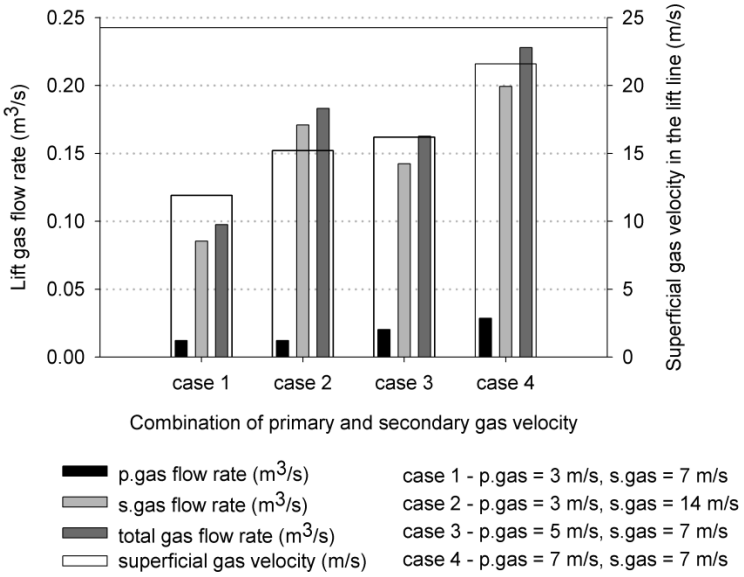

Figure 5.9: Simulated combinations of primary and secondary gas velocities.

As observed in Figure 5.10, the mass flow rate of solids going out of the lift engager fluctuates with time. These fluctuations in mass flow rate can be attributed to many sources including gas-solid interactions, solid accumulation and pressure balance inside lift engager. Identification and characterization of these sources is helpful in providing insight into the operation of the lift engager. Spectral analysis has been established as a useful tool for time series analysis. It has been used to provide valuable insight into the hydrodynamics of various gas-solid systems like circulating fluidizing bed (Sterneus et al., 1999), spouted-bed (Zhong and Zhang, 2005), fluidized bed (Sasic et al., 2005). The power spectra density (PSD) identifies dominant frequencies in a time series. These frequencies can then be mapped to the flow physics yielding useful information. The PSD for solid mass flow rate and solid accumulation time series are shown in Figure 5.11 for the lower primary lift gas velocity case. The power spectra were characterized by multiple dominant frequencies ranging from 0.1 to 10 Hz. For the signal from bed region i.e. the catalyst accumulation time series, only single dominant frequency in the range of 0.2 – 0.3 Hz was observed (Figure 5.11b). On the contrary to the signal from the bed region, the lift line signal showed presence of both low (< 1 Hz) and high (up to 10 Hz) dominant frequencies (Figure 5.11a). The dominant frequencies present in the bed signal were also reported in the lift line signal. This clearly indicates that

the low frequency oscillations in mass flow rate signals originated in the bed region. At lower primary gas velocity, the only predominant signals were in lower frequency range (< 1 Hz) as the primary gas velocity increase, higher frequency signals also become dominant. However, the physical processes corresponding to these dominant frequencies have not yet been fully understood.

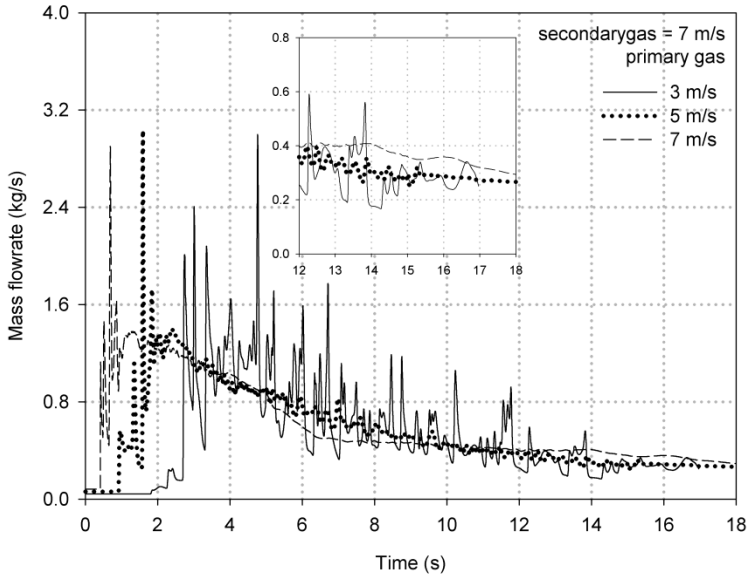

Figure 5.10: Mass flow rate at outlet as a function of time (Catalyst flow rate = 0.19 kg/s).

Figure 5.12 shows a comparison between the time-averaged catalyst velocities, catalyst volume fraction and slip velocity profiles along the height of the lift line for 4 different cases as described in Fig.5.8. Depending on the lift gas velocities, the catalyst velocity increased sharply for the initial 20 to 40% of the lift line. After this initial acceleration, the catalyst velocity became constant as it travelled upwards (Figure 5.12a). As expected, an increase in the primary gas velocity increased the catalyst velocity in the lift line (compare case 3 and case 4). A similar trend was observed for the increase in the secondary gas velocity (compare case 1 and case 2). Contrary to the catalyst velocity profiles, the catalyst volume fraction profile reduced initially and then became constant for the rest of the height of the lift line (Figure 5.12b). As shown in Figure 5.12(c), the slip velocity profiles were found to be constant for the most part of the lift line except near the entrance. For all simulated cases, the predicted slip velocities were greater than the terminal velocity of the catalyst particle (~ 6.87 m/s).

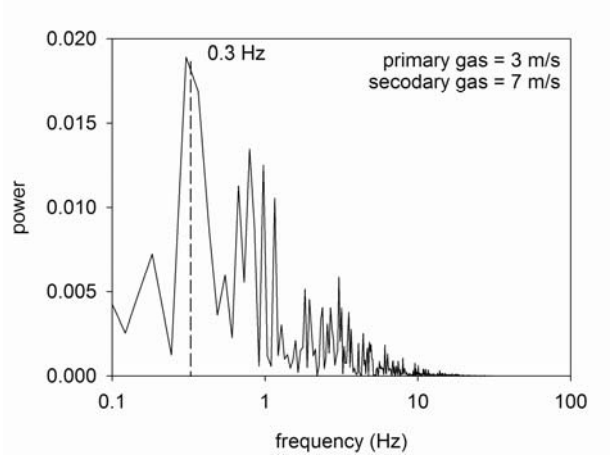

(a)

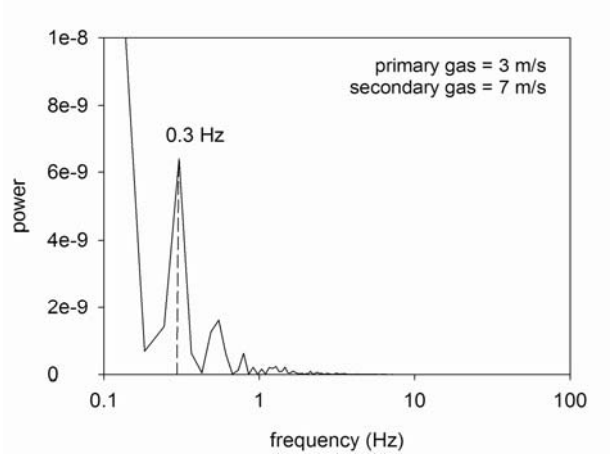

(b)

Figure 5.11: PSDs of solid (a) flow rate and (b) accumulation time series.

There is no reported study for the hydrodynamics of a lift engager, which not only has a dilute phase flow in the riser but also a dense phase flow below the lift line. With some caution, current simulations may be compared with previously reported studies on risers for which abundant data is available. In this study, we have compared the lift engager simulations with previously published studies on risers using Geldart D particles. Figure 5.12(d) compares the calculated solid velocity and previously published simulation results of (Theologos and Markatos, 1994) and it can be seen that our result are in good agreement with their predicted solid velocity profile.

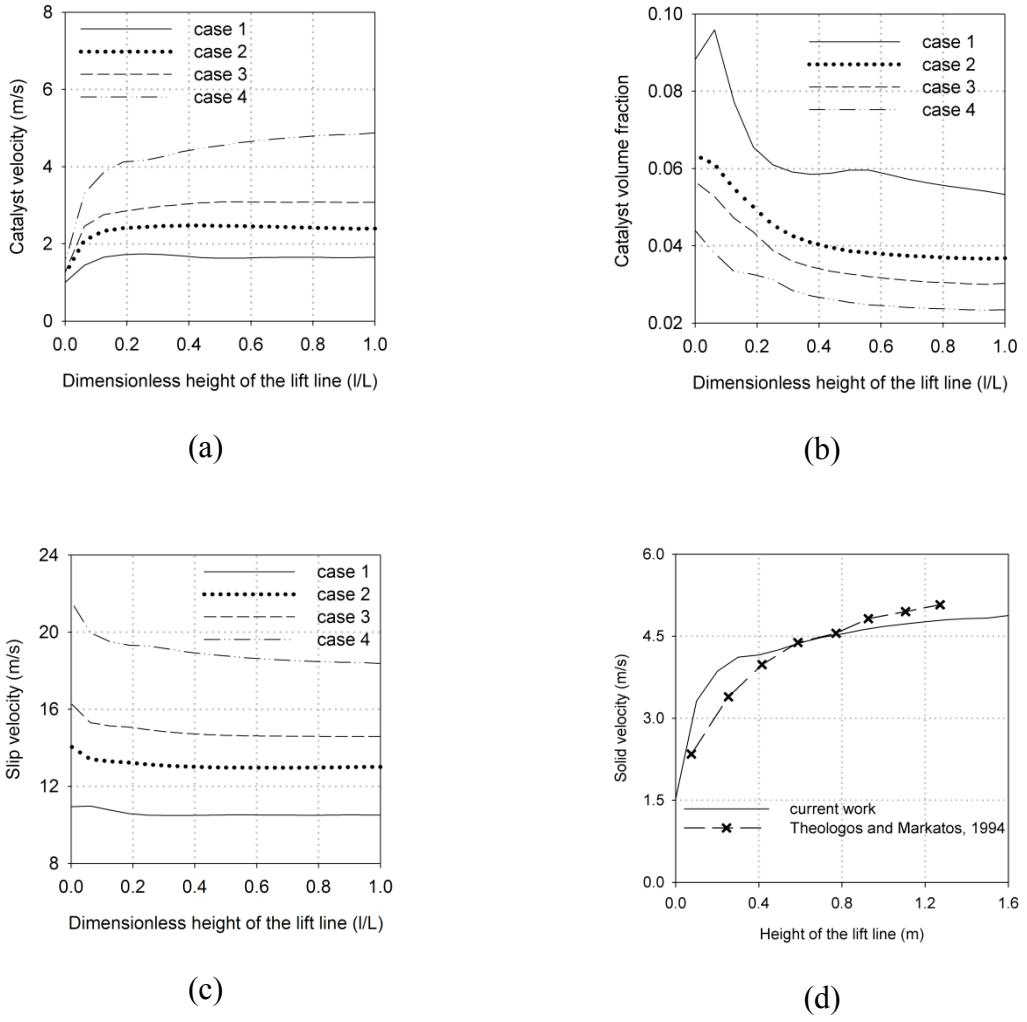

Figure 5.12: Time-averaged axial profiles along the height of the lift line: (a) Catalyst velocity, (b) Catalyst volume fraction (c) Slip velocity (catalyst flow rate = 0.19 kg/s) (d) Comparison between current simulation results with previously published simulation results (Theologos and Markatos, (1994), d_p = 0.503 mm, ρ_p = 2643 kg/m^3, D_t = 13.5 mm, H = 1.368 m, U_g = 12.3 m/s)

5.4. Conclusions

Hydrodynamics of a lift engager was investigated using the EE gas-solid flow model. Before studying the influence of operating parameters, the effect of several model parameters such as the drag model and frictional pressure on the predictions was also studied. Whilst the drag models investigated in this work (Gidaspow and Syamla-O'Brien models) gave qualitatively similar results, the choice of frictional pressure model affected the simulation results in a

rather astounding manner. Two approaches for the frictional pressure, namely the KTGF based and Johnson and Jackson (Johnson and Jackson, 1987) were simulated For the KTGF based approach, which has been found to give satisfactory results for fully developed risers, the catalyst velocity and volume fraction profile along the height of the lift line were not consistent and violated the basic principle of mass balance. However, using Johnson and Jackson(Johnson and Jackson, 1987) frictional pressure approach, this inconsistency in the simulations was removed. Therefore, it was concluded that for complex flow domains having both dilute and dense phase flows, the Johnson and Jackson model should be used. After optimizing the selection of model parameters, simulations were conducted to study the effect of lift gas velocity.

It was found that the secondary gas velocity decreased after passing through the baffle region due to a sudden increase in the cross sectional area. The “recommended secondary gas velocity” was not adequate to fluidize the catalyst inside the equipment. The primary gas caused lifting of the catalyst in the lift line without any interaction with the bulk of solids in the equipment. Thus, the current design and operation of the lift engager resulted in the poor mixing and fluidization in the equipment. A parametric study was also conducted by simulating four different cases having different combinations of the primary and secondary gas velocities. At the dynamic steady-state, the catalyst outlet mass flow rate was found to be fluctuating with the average value being around the inlet mass flow rate, with fluctuations dampening rapidly upon increasing the primary lift velocity. Therefore, a higher flow rate of the primary lift gas is recommended for smooth lifting of catalyst. Furthermore, the fluctuations in the mass flow rate was analysed using the power spectra density plots. The dominant frequency in the mass flow rate signal was mapped to that in the solid inventory signal from the bed. The time-averaged profiles of gas velocity showed that the catalyst accelerated along the height of the lift line with correspondingly decreasing volume fractions. The simulation results qualitatively compared well with the previously published simulation results for risers with a reasonable agreement.

6. Closure

6.1 Conclusions

In this study, the EE model was evaluated for predicting hydrodynamics of gas-solid flows in both 2D and 3D risers. Different model parameters such as boundary conditions and drag models were investigated for improving the performance of the EE model. In Chapter 3, the EE gas-solid model was briefly described. In addition, the effect of inlet and wall boundary conditions was investigated, and results from 2D and 3D simulations were compared. In Chapter 4, a structure-based drag model using the EMMS approach was evaluated for low and high flux flow conditions. Finally, in Chapter 5, the EE model was used to simulate an industrial scale lift engager to characterize its hydrodynamics. The study comprises of three parts which are summarised below:

Part 1: Effects of Boundary Conditions

A literature review on previous hydrodynamics studies clearly suggested that most of the simulations on riser flows have been conducted using a 2D geometry of riser instead of 3D cylindrical. These studies also showed that different types on inlet arrangements have been used, and they have been quite different from a 3D experimental set-up. Thus, in this part of the study, the effect of boundary conditions was investigated on 2D simulations by considering three types of inlet arrangements. The wall boundary condition was investigated by considering no-slip or partial-slip wall for the solid phase. Full-scale 3D simulations were also conducted implementing the boundary conditions similar to the experimental set-up. Simulation results were compared with the experimental data of Bhusarapu et al. (2005), who mapped the flow regimes inside the riser using non-invasive radioactive particle tracking (RPT) method.

The conclusions of this part of the study were:

- In 2D simulations, the inlet arrangements with different directions and positions for entry of each phase had dominant effects on the mixing of two phases at the entrance, and also on the radial profiles of solid velocity and volume fractions in so-called “fully developed zone”.

- The kinetic energies of both phases at the inlet were also compared with those of the experimental values. Interestingly, neither of these inlets gave agreements between the kinetic energies of phases and those of the experimental values. Thus, in 2D simulations, the energy balance did not reflect the actual 3D conditions.
- The wall boundary conditions such as partial-slip and no-slip were found to influence on the predictions using different inlet arrangements.
- The core-annulus type inlet and two-sided inlet with no-slip wall boundary conditions gave closer agreement with the experimental data.
- It was observed that the selection of boundary condition in 2D simulations was a challenging task, and previous studies using different boundary conditions could be misleading in judging validation of the EE model.
- Results from the 3D simulation were close to experimental values with some quantitative discrepancies.
- The time-averaged axial profiles of voidages from both 2D and 3D simulations were identical and showed uniform voidages along the height. This results disagreed with the experimental observations which have shown a dense bottom and dilute top section

Part 2: Using EMMS Drag Model

In the previous part of the study, both 2D and 3D simulations of the riser could not capture axial profiles of solid volume fraction even qualitative. Previous studies (Yang et al., 2004; Andrews Iv et al., 2005) using the multi-scale drag have been found to be effective in capturing the heterogeneous gas-solid flows in riser. Therefore, in this study, a structure-based drag from the EMMS model was evaluated over for both low and high flux flow conditions. The results using the EMMS drag and conventional Gidaspow drag models were compared. Furthermore, a sensitivity of the structure-based drag and its hydrodynamic predictions on cluster diameter correlations was also investigated using three different types of cluster diameter correlations i.e. those proposed by Chavan (1984), Harris et al. (2002) and Subbarao (2010).

The conclusions of this part of the study were:

- A significant drag reduction was achieved using the EMMS model compared to the Gidaspow drag model for both low and high solid flux flow conditions.
- The EMMS model was able to capture both axial and radial heterogeneity, but only qualitatively. Furthermore, the EMMS model successfully predicted the S-shape of the axial profiles with a lower voidages at the bottom and higher values at the top, whereas the Gidaspow model gave a uniform profile with lower values along the height of the riser. The radial profiles of voidages from both drag models (EMMS and Gidaspow models) gave only qualitative agreement with the experimental data.
- The cluster diameter correlations had considerable effect on the structure-based drag coefficients, and as a result, on the hydrodynamic predications. The correlation proposed by Harris et al. (2002) could capture qualitative profile of axial profile of voidage with reasonable quantitative agreement with the experimental data, particularly in the dense bottom. At dilute top section, the cluster diameter correlation of Chavan (1984) gave better agreement with the experimental data. Using the correlation of Harris et al. (2002), the axial profile showed lower values of voidages along the height of the riser.

Part 3: Hydrodynamics of an Industrial-Scale Lift Engager

After evaluating the effect of various model parameters on the performance of the EE model, it was then applied to simulate complex flows in an industrial-scale 3D lift engager. The objective was to conduct a parametric study for the effect of primary and secondary lift gas velocity on the state of fluidization inside the equipment. Before conducting this parametric study, the effects of drag models and frictional pressure models on the hydrodynamics predictions were also investigated.

The conclusions of this part of the study were:

- The hydrodynamics of both phases showed that the secondary gas velocity decreased after passing through the baffle region, and the “recommended secondary gas velocity” was not adequate to fluidize the catalyst.

- Furthermore, the primary gas caused lifting of the catalyst in the lift line without any interaction with the bulk of solids in the equipment. Thus, the current design and operation of the lift engager resulted in the poor mixing and fluidization.
- The catalyst outlet mass flow rate was found to be fluctuating with the average value being around the inlet mass flow rate, with fluctuations dampening rapidly upon increasing the primary lift velocity. Therefore, a higher mass flow rate of the primary gas was recommended for smooth lifting of the catalyst.
- Although the effect of drag models on the flows was minor, but that of frictional pressure model was rather surprising. For the KTGF based approach, which had been found to give satisfactory results for risers, the catalyst velocity and volume fraction profile along the height of the lift line were not consistent and violated the basic principle of mass balance. This could be attributed to the existence of both dense and dilute phases inside the lift engager. However, using Johnson and Jackson(Johnson and Jackson, 1987) frictional pressure approach, this inconsistency in the simulations was removed.

6.2. Recommendations for future work

In this research, CFD simulations were conducted for different flow conditions in the riser addressing the shortcomings of the previous simulation studies on selection of appropriate boundary conditions and gas-solid drag model. The structure-based drag from the EMMS model gave significantly improvements in hydrodynamics predictions by capturing the macro-scale heterogeneity of the flows in the riser. In addition, the use of different cluster diameter correlations with the EMMS framework gave further improvements in the hydrodynamics predictions. However, a key challenge of achieving quantitative agreement with the experimental data for both radial and axial variations in the voidages still remains. Wang et al. (2008) presented an advanced EMMS (EMMS-matrix) model, which calculated the EMMS drag coefficient for local flow conditions of mass flux and gas velocities in each computational cell. The simulations using this advance EMMS model is currently under investigations.

This study evaluated the current framework of the EMMS without questioning the fundamental essence of the model. Despite of its success, the author feels that the EMMS

model and its assumptions still need to be evaluated more fundamentally. For example, the principle of energy minimization, which has generally been applied to equilibrium conditions, still needs to be justified for the flows in riser. In the riser, the gas-solid flow is non-equilibrium in nature, and the clusters are also dynamic entities. Thus, the applying a stability condition of minimum energy to a highly non-equilibrium flow conditions in risers is questionable. However, the author agrees with the concept of decrease in the energy for suspension and transportation, but not with minima. The deviation from the energy minimization should be considered before applying the EMMS framework. The direct numerical simulations (DNS) or experimental studies can help to find out this deviation. One way to incorporate such modification is to formulate alternate cluster diameter correlations. Currently, the cluster diameter correlations are based on the indirect measurements reported in the experimental studies (Harris et al., 2002) and/or conceptual model (Subbarao, 2010) of the gas-solid flows. Furthermore, the EMMS model assumes constant voidage of the cluster to calculate the structure-based drag model. The high resolution simulations (Igci et al., 2008; Xiong et al., 2010) showed the clusters as a ribbon like irregular structures. Thus, a new approach is necessary to define the cluster and correlate its property with the flow conditions. This correlation of clusters with the EMMS can be useful to further enhance the accuracy.

Alternate to the EMMS approach, the SGS approach (Andrews Iv et al., 2005), has also been used to account for the effect cluster formations on the closure models. Recently, Igci et al. (2009) made further advancements in the SGS approach by studying the effect of filter size on derived correlations. Benyahia et al. (2009) evaluated both EMMS and SGS approaches for high solid flux flow conditions, and concluded that the SGS approach gave better agreements with the experimental data than the EMMS approach. Therefore, the SGS approach should also be evaluated before making decisive conclusion on the selection of the structure-based drag model. Finally, the real boundary conditions in riser simulations can only be applied by considering the simulation of the whole CFB loop. Mathiesen et al. (2000) and Zhang et al. (2008) simulated a whole CFB loop using 2D and 3D domains. Therefore, a 3D simulation of the CFB loop with the riser, solid disengage, downer, solid feeding system and gas inlet is recommended for future study.

Appendix I. Drag coefficient using EMMS model

In Chapter 4, the structured-based drag coefficient was calculated using the solution of the EMMS model. The calculation steps to solve the EMMS model and compute drag coefficient are briefly summarised in this section. Different methods have been proposed to solve the EMMS model. A simple solution method was proposed by Li et al. (1999) who avoided convergence problems and the calculation of intermediate terms involved in the previous solution methods (Li and Kwauk, 1994; Xu and Li, 1998). Yang et al. (2004) further modified the method by introducing an acceleration term in the momentum conservation equation. In this study, a method used Yang et al. (2004) was adopted to calculate the solution of the EMMS model.

In this method, the voidage of the dilute phase and the cluster were assumed to be unity and 0.69 respectively:

$$\varepsilon_f = 1 \qquad \text{eq. (A-1)}$$

$$\varepsilon_c = 0.69 \qquad \text{eq. (A-2)}$$

It should be noted that the voidage of the cluster phase was assumed to be the minimum fluidizing voidage in the previous solutions of the EMMS model. However in this study, the cluster voidage was assumed to be 0.69 as considered by Yang et al. (2004). The above assumption ($\varepsilon_f = 1$) implies that the dilute phase does not have particles, thus, the velocity of particle in the dilute phase can be equated to zero. The velocity of particle in the cluster phase was calculated using the superficial velocity of the solid phase. Similarly, the velocities of gas in both the cluster and dilute phases were derived from the superficial velocity of gas phase:

$$U_{pf} = 0 \qquad \text{eq. (A-3)}$$

$$U_{pc} = \frac{U_p}{f} \qquad \text{eq. (A-4)}$$

$$U_f = \frac{U_g - \frac{\varepsilon_c U_p}{(1-\varepsilon_c)}}{1-f} - \frac{f}{1-f} U_{sc} \qquad \text{eq. (A-5)}$$

$$U_c = \frac{\varepsilon_c}{1-\varepsilon_c} U_{pc} + U_{sc} \qquad \text{eq. (A-6)}$$

By substituting above correlations into mass, momentum and pressured balance equations; two non-linear equations can be derived:

$$0.15\left(\frac{\rho_f d_{cl}}{\mu_f}\right)^{0.687}\left[\left(U_f-\frac{\varepsilon_f}{1-\varepsilon_c}U_{pc}\right)(1-f)\right]^{1.687}+\left(U_f-\frac{\varepsilon_f}{1-\varepsilon_c}U_{pc}\right)(1-f)-$$
$$(1-f)^{5.7}\left(\varepsilon_f-\varepsilon_c\right)\frac{(\rho_p-\rho_f)(g+a)d_{cl}^2}{18\mu_f}=0 \qquad \text{eq. (A-7)}$$

$$0.15\left(\frac{\rho_f d_{cl}}{\mu_f}\right)^{0.687}U_{sc}^{1.687}+U_{sc}-\frac{\left[(1-\varepsilon_f)+(\varepsilon_f-\varepsilon_c)f\right]\varepsilon_c^{4.7}}{1-\varepsilon_c}\frac{(\rho_p-\rho_f)(g+a)d_p^2}{18\mu_f}=0 \qquad \text{eq. (A-8)}$$

The cluster diameter is assumed to be inversely proportional to the energy used for the suspension and transportation (Chavan and Mashelkar, 1980). The equation for the cluster diameters is derived by imposing constraints i.e. (i) its value approaches to infinity at the minimum fluidization and (ii) to particle diameter at the maximum voidage:

$$d_{cl}=\frac{d_p\left(\frac{U_p g}{(1-\varepsilon max)}-\left(U_{mf}+\frac{U_p\varepsilon_{mf}}{(1-\varepsilon_{mf})}\right)g\right)}{N_{st}\frac{\rho_p}{\rho_p-\rho_f}-\left(U_{mf}+\frac{U_p\varepsilon_{mf}}{(1-\varepsilon_{mf})}\right)g} \qquad \text{eq. (A-9)}$$

The energy required for the suspension and transportation of solids is calculated using the pressure drops in both cluster and dilute phases:

$$N_{st}=\left[U_g-\frac{\varepsilon_f-\varepsilon}{1-\varepsilon}f(1-f)U_f\right](g+a)\,\frac{\rho_p-\rho_f}{\rho_p} \qquad \text{eq. (A-10)}$$

On substituting the equations for U_f, U_{pc} and d_{cl} into the equations (A-7) and (A-8), these two non-linear equations can be solved for two unknowns such as *a* and U_{sc} for a given set of flow conditions (G_s and U_g) and voidge (ε). The calculations are summarised in the algorithm shown in Figure A-1. For a given set of G_s, U_g and ε, the solution of the EMMS model yields the flow structure parameters such as U_f, U_{pf}, U_c, U_{pc}, ε_c, ε_f, *f*, *a*, d_{cl} and N_{st}; which are then used to calculate the structured-based drag coefficient as mentioned in the last two steps of the algorithm. This solution scheme was evaluated by comparing its results for two different previous studies (Xu

and Li, 1998 and Yang et al., 2003) before applying it to calculate drag coefficient for the system considered in this study.

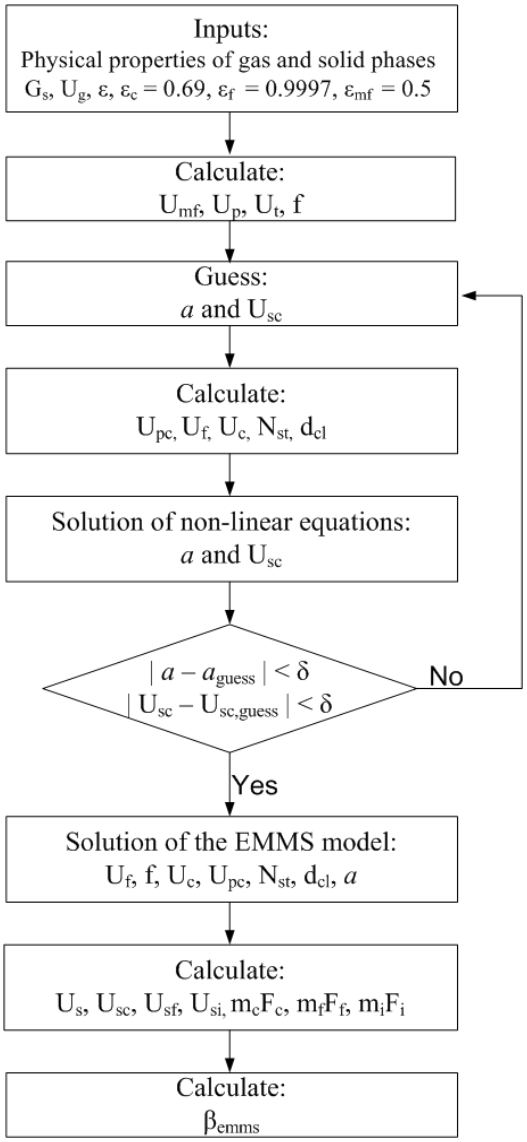

Figure A.1: Algorithm to calculate EMMS drag coefficients.

Before using above solution scheme, it was used to solve the EMMS model for a FCC/air system (G_s = 50 kg/m^{2}s, U_g = 0.5-3.3 m/s, ρ = 930 kg/m^3). As considered by Xu and Li, (1998), the cluster voidage was assumed to be constant at minimum fluidizing voidage (ε_{mf} = 0.5), and the acceleration term in momentum balance equation was neglected. The calculated parameters such as the cluster diameter, cluster fraction and superficial gas velocity were plotted, and compared against

published values in Xu and Li (1998) (Figure A-2). The solution scheme gave parameter values consistent with the published by Xu and Li, (1998).

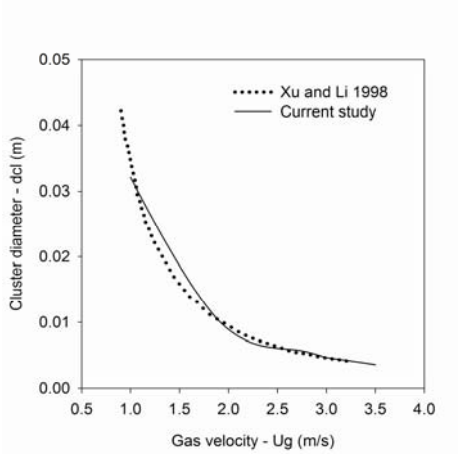

(a)

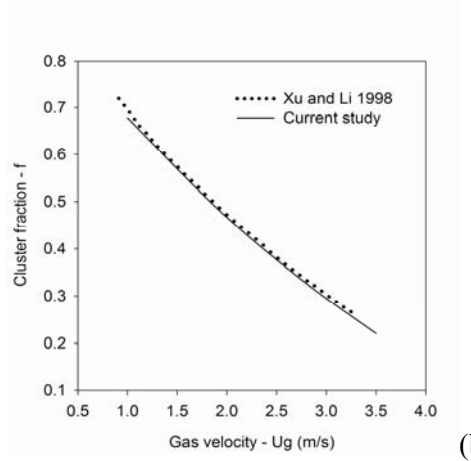

(b)

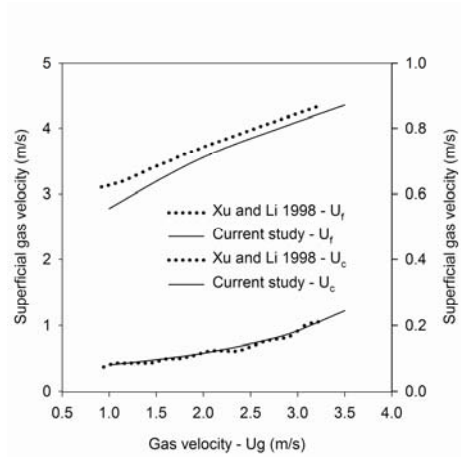

(c)

Figure A.2: Comparison between calculated values of (a) cluster diameter, (b) cluster fraction and (c) superficial gas velocities and those of Xu and Li, (1998)

Yang et al. (2003a) have reported different values of the structure parameter values for the FCC/air system (G_s = 14.3 kg/m^{2}s, U_g = 1.52 m/s, ρ = 930 kg/m^3) by modifying the EMMS model with an acceleration term in momentum balance equations and stability criteria to N_{st}/N_T = min. The calculated values of the cluster diameter, cluster fraction and superficial gas velocity were compared with the published data (Figure A-3). The comparison showed a good agreement between the solution calculated by the scheme considered in this work and that published in the literature. As reported in previous study (Yang et al., 2003), the deflection point was found at a voidage of 0.64, where the cluster voidage (ε_c) reached to the minimum fluidizing voidage (ε_{mf}). After this point, the cluster voidage was constrained to be constant at the minimum fluidizing voidage and the variation of other parameters were calculated by solving only one equation (eq. A-3) out of two non-linear equations mentioned in the solution scheme.

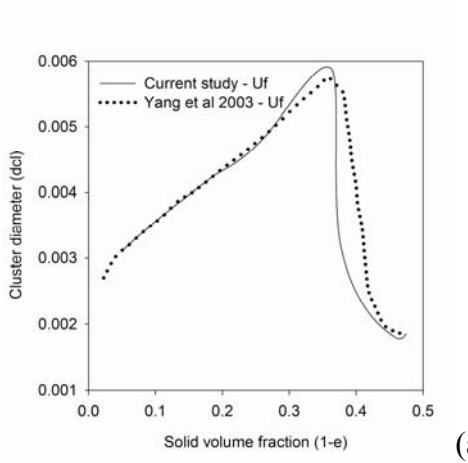

(a)

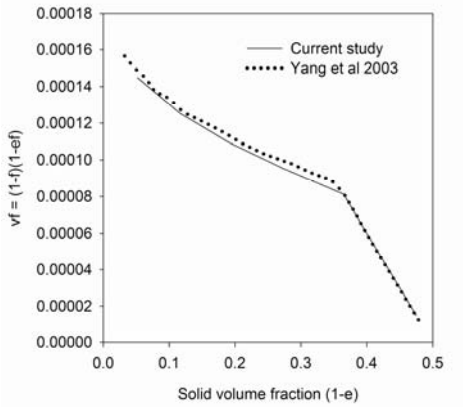

(b)

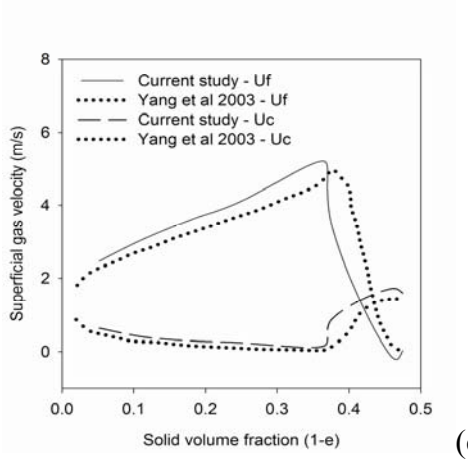

(c)

Figure A-3: Comparison between calculated values of (a) cluster diameter, (b) cluster fraction and (c) superficial gas velocities and those of Yang et al. 2003.

Appendix II. Calibaration of Syamlal-O'Brien model

The Syamlal and O'Brian drag model (Syamlal and O'Brien; Syamlal et al., 1993) (Equation B-1 to 4) is based on the velocity-voidage correlations derived using sedimentation and fluidization experiments of Richardson and Zaki (Richardson and Zaki, 1954) and Garside and Al-Dibouni (Garside and Al-Dibouni, 1977) respectively. The drag compares well with the Ergun equation in the void fraction range 0.5-0.6 and it correctly reduces to a single particle drag coefficient when the void fraction becomes one. The following are the equations describing this model:

$$\beta_{Syamlal-O'Brien} = \frac{3}{4}\frac{\varepsilon(1-\varepsilon)}{v_{r,s}^2 d_p}\left(\frac{Re_s}{v_{r,s}}\right)\rho_g\left|\vec{u}_g - \vec{u}_p\right|C_{D0} \qquad \text{eq.(B-1)}$$

$$C_{D0} = \left(0.63 + 4.8\sqrt{\frac{v_{r,s}}{Re_s}}\right)^2 \qquad \text{eq.(B-2)}$$

$$v_{r,s} = \frac{1}{2}\left[A - 0.06Re_s + \sqrt{(0.06Re_s)^2 + 0.12Re_s(2B - A) + A^2}\right] \qquad \text{eq.(B-3)}$$

$$A = \varepsilon^{4.14} \qquad \text{eq. (B-4)}$$

$B = a\varepsilon^{1.28}$ if $\varepsilon \leq 0.85$ default value of $a = 0.8$

$B = \varepsilon^{b}$ if $\varepsilon > 0.85$ default value of $b = 2.65$

The model provides for adjustable factors that can be tuned to match the minimum fluidization velocity for the solid particles in question. The method of calibration in the form of simple MS-Excel programme is specifically given in the MFIX user guide published by Syamalal et al. (1993) and summarised here in the form of simple algorithm (Figure B-1).

Despite of such clear guideline, many previous studies (REF) applied the model using the default values of constants as given in the commercial CFD code. The results of such studies can be misleading and needs to be re-examined before using them.

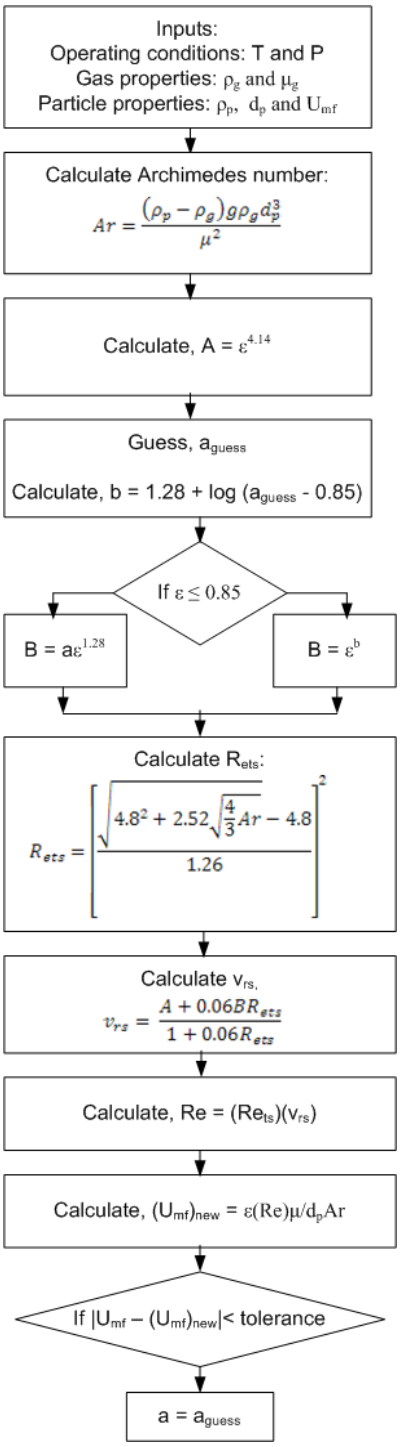

Figure B-1: Algorithm for calibration of Syamlal-O'Brien drag model

Agrawal, K., Loezos, P.N., Syamlal, M., Sundaresan, S., 2001. The role of meso-scale structures in rapid gas–solid flows. Journal of Fluid Mechanics, **445**, 151-185.

Ahuja, G.N., Patwardhan, A.W., 2008a. CFD and experimental studies of solids hold-up distribution and circulation patterns in gas-solid fluidized beds. Chemical Engineering Journal, **143**, 147-160.

Almuttahar, A., Taghipour, F., 2008. Computational fluid dynamics of high density circulating fluidized bed riser: Study of modeling parameters. Powder Technology, **185**, 11-23.

Anderson, T.B., Jackson, R., 1967. Fluid mechanical description of fluidized beds. Equations of motion. Industrial & Engineering Chemistry Fundamentals, **6**, 527-539.

Andrews Iv, A.T., Loezos, P.N., Sundaresan, S., 2005. Coarse-grid simulation of gas-particle flows in vertical risers. Industrial & Engineering. Chemistry Research, **44**, 6022-6037.

Arastoopour, H., Gidaspow, D., 1979. Vertical pneumatic conveying using four hydrodynamic models. Industrial & Engineering Chemistry Fundamentals, **18**, 123-130.

Arastoopour, H., Pakdel, P., Adewumi, M., 1990. Hydrodynamic analysis of dilute gas--solids flow in a vertical pipe. Powder Technology, **62**, 163-170.

Bader, R., Findiay, J., Knowlton, T.M., 1988. Gas/solids flow patterns in a 30.5-cm-diameter circulating fluidized bed. Elsevier Science, p. 123.

Bai, D., Issangya, A.S., Grace, J.R., 1999. Characteristics of gas-fluidized beds in different flow regimes. Industrial & Engineering Chemistry Research, **38**, 803-811.

Beetstra, R., Van der Hoef, M.A., Kuipers, J.A.M., 2006. A lattice-Boltzmann simulation study of the drag coefficient of clusters of spheres. Computers & Fluids, **35**, 966-970.

Beetstra, R., Van der Hoef, M.A., Kuipers, J.A.M., 2007. Drag force of intermediate Reynolds number flow past mono-and bidisperse arrays of spheres. AIChE Journal, **53**, 489-501.

Benyahia, S., 2009. On the Effect of Subgrid Drag Closures. Industrial & Engineering Chemistry Research, **49**, 5122-5131.

Benyahia, S., Arastoopour, H., Knowlton, T.M., Massah, H., 2001. Simulation of particles and gas flow behavior in the riser section of a circulating fluidized bed using the kinetic theory approach for the particulate phase. Powder Technology, **112**, 24-33.

Benyahia, S., Syamlal, M., O'Brien, T.J., 2005. Evaluation of boundary conditions used to model dilute, turbulent gas/solids flows in a pipe. Powder Technology, **156**, 62-72.

Benyahia, S., Syamlal, M., O'Brien, T.J., 2006. Extension of Hill-Koch-Ladd drag correlation over all ranges of Reynolds number and solids volume fraction. Powder Technology, **162**, 166-174.

Bhusarapu, S., Al-Dahhan, M., Dudukovic, M.P., 2004. Quantification of solids flow in a gas–solid riser: single radioactive particle tracking. Chemical Engineering Science, **59**, 5381-5386.

Bhusarapu, S., Al-Dahhan, M.H., Dudukovic, M.P., 2006b. Solids flow mapping in a gas-solid riser: Mean holdup and velocity fields. Powder Technology, **163**, 98-123.

Bhusarapu, S., Al-Dahhan, M.H., Dudukovic, M.P., Trujillo, S., O'Hern, T.J., 2005. Experimental study of the solids velocity field in gas- solid risers. Industrial & Engineering Chemistry Research, **44**, 9739-9749.

Bhusarapu, S.B., 2005b. Solids flow mapping in gas-solid risers, Department of chemical engineering. Washington University.

Bokkers, G.A., van Sint Annaland, M., Kuipers, J.A.M., 2004. Mixing and segregation in a bidisperse gas-solid fluidised bed: a numerical and experimental study. Powder Technology, **140**, 176-186.

Chalermsinsuwan, B., Piumsomboon, P., Gidaspow, D., 2009. Kinetic theory based computation of PSRI riser: Part I--Estimate of mass transfer coefficient. Chemical Engineering Science, **64**, 1195-1211.

Chapman, S., Cowling, T.G., 1991. The mathematical theory of non-uniform gases.

Chavan, V.V., 1984. Physical principles in suspension and emulsion processing. Advances in Transport Processes, **3**, 1-34.

Cheng, C.L., 1999. Research note. Institute of Chemical Metallurgy.

Chepurniy, N., 1984. Kinetic theories for granular flow: inelastic particles in couette flow and slightly inelastic particles in a general flow field. Journal of Fluid Mechanics, 223-256.

Das, M., Bandyopadhyay, A., Meikap, B.C., Saha, R.K., 2008. Axial voidage profiles and identification of flow regimes in the riser of a circulating fluidized bed. Chemical Engineering Journal, **145**, 249-258.

Deen, N.G., Van Sint Annaland, M., Van der Hoef, M.A., Kuipers, J.A.M., 2007. Review of discrete particle modeling of fluidized beds. Chemical Engineering Science, **62**, 28-44.

Ding, J., Gidaspow, D., 1990. A bubbling fluidization model using kinetic theory of granular flow. AIChE Journal, **36**, 523-538.

Du, W., Bao, X., Xu, J., Wei, W., 2006. Computational fluid dynamics (CFD) modeling of spouted bed: Assessment of drag coefficient correlations. Chemical Engineering Science, **61**, 1401-1420.

Duarte, C.R., Olazar, M., Murata, V.V., Barrozo, M.A.S., 2009. Numerical simulation and experimental study of fluid–particle flows in a spouted bed. Powder Technology, **188**, 195-205.

Dudukovic, M.P., 2009. Frontiers in Reactor Engineering. Science 325, 698.

Enwald, H., Peirano, E., Almstedt, A.E., 1996. Eulerian two-phase flow theory applied to fluidization. International Journal of Multiphase Flow, **22**, 21-66.

Ergun, S., 1952. Fluid flow through packed columns. Chemical Engineering Progress, **48**, 89-94.

Fluent, User Manual, 2006. Fluent Inc. Lebanon, NH.

Garside, J., Al-Dibouni, M.R., 1977. Velocity-voidage relationships for fluidization and sedimentation in solid-liquid systems. Industrial and Eng. Chemistry Process Design and Development, **16**, 206.

Ge, W., Li, J., 2002. Physical mapping of fluidization regimes--the EMMS approach. Chemical Engineering Science, **57**, 3993-4004.

Geldart, D., 1986. Gas fluidization technology. John Wiley & Sons New York.

Geldart, D., Rhodes, M.J., 1986. From minimum fluidization to pneumatic transport-a critical review of the hydrodynamics. Pergamon, p. 21.

Geng, F., Xu, D., Yuan, Z., Yan, Y., Luo, D., Wang, H., Li, B., Chyang, C., 2009. Numerical simulation on fluidization characteristics of tobacco particles in fluidized bed dryers. Chemical Engineering Journal, **150**, 581-592.

Gibilaro, L.G., Di Felice, R., Waldram, P.U., 1985. Generalized friction factor and drag coefficient correlations for fluid-particle interactions. Chemical Engineering Science, **40**, 1817-1823.

Gidaspow, D., 1994. Multiphase flow and fluidization: continuum and kinetic theory descriptions. Academic Press.

Gidaspow, D., Bezburuah, R., Ding, J., 1991a. Hydrodynamics of circulating fluidized beds: Kinetic theory approach, 7th Engineering Foundation Conference on Fluidization. CONF-920502-1, Illinois Inst. of Tech., Chicago, IL (United States). Dept. of Chemical Engineering.

Gluckman, M.J., Yerushalmi, J., Squires, A.M., 1976. Fluidization Technology. Hemisphere Publishing, NY.

Grace, J.R., 1982. Fluidized bed hydrodynamics. Handbook of Multiphase Systems.

Gryczka, O., Heinrich, S., Deen, N.G., Kuipers, J.A.M., Mörl, L., Verlag, U., 2009. Three-dimensional computational fluid dynamics modeling of a prismatic spouted bed. Chemical Engineering & Technology, **32**, 470-481.

Harris, A.T., Davidson, J.F., Thorpe, R.B., 2002. The prediction of particle cluster properties in the near wall region of a vertical riser. Powder Technology, **127**, 128–143.

He, Y., Deen, N.G., Annaland, M.S., Kuipers, J.A.M., 2009. Gas- Solid Turbulent Flow in a Circulating Fluidized Bed Riser: Experimental and Numerical Study of Monodisperse Particle Systems. Industrial & Engineering Chemistry Research, **48**, 8091-8097.

Hill, R.J., Koch, D.L., Ladd, A.J.C., 2001. The first effects of fluid inertia on flows in ordered and random arrays of spheres. Journal of Fluid Mechanics, **448**, 213-241.

Hoef, M., Beetstra, R., Kuipers, J.A.M., 2005. Lattice-Boltzmann simulations of low-Reynolds-number flow past mono-and bidisperse arrays of spheres: results for the permeability and drag force. Journal of Fluid Mechanics, **528**, 233-254.

Hoomans, B.P.B., Kuipers, J.A.M., Briels, W.J., Van Swaaij, W.P.M., 1996. Discrete particle simulation of bubble and slug formation in a two-dimensional gas-fluidised bed: a hard-sphere approach. Chemical Engineering Science, **51**, 99-118.

Horio, M., Kuroki, H., 1994. Three-dimensional flow visualization of dilutely dispersed solids in bubbling and circulating fluidized beds. Chemical Engineering Science, **49**, 2413-2421.

Huilin, L., Gidaspow, D., Bouillard, J., Wentie, L., 2003a. Hydrodynamic simulation of gas-solid flow in a riser using kinetic theory of granular flow. Chemical Engineering Journal, **95**, 1-13.

Huilin, L., Qiaoqun, S., Yurong, H., Yongli, S., Ding, J., Xiang, L., 2005. Numerical study of particle cluster flow in risers with cluster-based approach. Chemical Engineering Science, **60**, 6757-6767.

Huilin, L., Yurong, H., Gidaspow, D., 2003b. Hydrodynamic modelling of binary mixture in a gas bubbling fluidized bed using the kinetic theory of granular flow. Chemical Engineering Science, **58**, 1197-1205.

Ibsen, C.H., 2002. An experimental and computational study of gas-particle flow in circulating fluidised reactors. Citeseer.

Ibsen, C.H., Solberg, T., Hjertager, B.H., 2001. Evaluation of a three-dimensional numerical model of a scaled circulating fluidized bed. Industrial & Engineering Chemistry Research, **40**, 5081-5086.

Igci, Y., Andrews, Iv., Arthur, T., Sundaresan, S., Pannala, S., O'Brien, T., 2008. Filtered two fluid models for fluidized gas particle suspensions. AIChE Journal, **54**, 1431-1448.

Ishii, M., 1975. Thermo-fluid dynamic theory of two-phase flow. NASA STI/Recon Technical Report A 75, 29657.

Ishii, M., 1987. Two-fluid model for two-phase flow. Argonne National Laboratory, IL (USA).

Ishii, M., Mishima, K., 1984. Two-fluid model and hydrodynamic constitutive relations. Nuclear Engineering and Design, **82**, 107-126.

Jackson, R., 1963. The mechanics of fluidised beds: Part II The motion of fully developed bubbles. Chemical Engineering Research and Design, **41**, 22-28.

Jenkins, J.T., Savage, S.B., 1983. A theory for the rapid flow of identical, smooth, nearly elastic, spherical particles. Journal of Fluid Mechanics, **130**, 187-202.

Jiradilok, V., Gidaspow, D., Breault, R.W., 2007. Computation of gas and solid dispersion coefficients in turbulent risers and bubbling beds. Chemical Engineering Science, **62**, 3397-3409.

Jiradilok, V., Gidaspow, D., Damronglerd, S., Koves, W.J., Mostofi, R., 2006. Kinetic theory based CFD simulation of turbulent fluidization of FCC particles in a riser. Chemical Engineering Science, **61**, 5544-5559.

Johnson, P.C., Jackson, R., 1987b. Frictional-collisional constitutive relations for granular materials, with application to plane shearing. Journal of Fluid Mechanics, **176**, 67-93.

Jurascík, M., Blazej, M., Annus, J., Markos, J., 2006. Experimental measurements of volumetric mass transfer coefficient by the dynamic pressure-step method in internal loop airlift reactors of different scale. Chemical Engineering Journal, **125**, 81-87.

Kawaguchi, T., Sakamoto, M., Tanaka, T., Tsuji, Y., 2000. Quasi-three-dimensional numerical simulation of spouted beds in cylinder. Powder Technology, **109**, 3-12.

Kim, J.-S., Tachino, R., Tsutsumi, A., 2008. Effects of solids feeder and riser exit configuration on establishing high density circulating fluidized beds. Powder Technology, **187**, 37-45.

Knowlton, T., Geldart, D., Matsen, J., King, D., 1995b. Comparison of CFB hydrodynamic models. , PSRI challenge problem at the Eighth international fludization conference, France.

Kwauk, M., Ningde, W., Youchu, L., Bingyu, C., Zhiyuan, S., 1986. Fast fluidization at ICM. Pergamon, p. 33.

Lapple, C.E., Shepherd, C.B., 1940. Calculation of particle trajectories. Industrial & Engineering Chemistry Research, **32**, 605-617.

Levy, A., 2001. Two-fluid approach for plug flow simulations in horizontal pneumatic conveying. Powder Technology, **112**, 263-272.

Li, H., Xia, Y., Tung, Y., Kwauk, M., 1991. Micro-visualization of clusters in a fast fluidized bed. Powder Technology, **66**, 231-235.

Li, J., Cheng, C., Zhang, Z., Yuan, J., Nemet, A., Fett, F.N., 1999. The EMMS model--its application, development and updated concepts. Chemical Engineering Science, **54**, 5409-5425.

Li, J., Kawauk, M., 1994. Particle-fluid two-phase flow: The energy-minimization multi-scale method. Metallurgical Industry Press.

Li, J., Tung, Y., Kwauk, M., 1988a. Axial voidage profiles of fast fluidized beds in different operating regions. Pergamon, p. 193.

Li, J., Tung, Y., Kwauk, M., 1988b. Circulating Fluidized Bed Technology II. edited by Basu, P. and Large, JF, Pergamon Press, Toronto 75.

Littman, H., Morgan Iii, M.H., Paccione, J.D., Jovanovic, S.D., Grbavcic, Z.B., 1993. Modeling and measurement of the effective drag coefficient in decelerating and non-accelerating turbulent gas–solids dilute phase flow of large particles in a vertical transport pipe. Powder Technology, **77**, 267-283.

Liu, H., Lu, H., 2009. Numerical study on the cluster flow behavior in the riser of circulating fluidized beds. Chemical Engineering Journal, **150**, 374-384.

Liu, J., Grace, J.R., Bi, X., 2003. Novel multifunctional optical fiber probe: II. High density CFB measurements. AIChE Journal, **49**, 1421-1432.

Liu, S., Yang, W.Q., Wang, H., Jiang, F., Su, Y., 2001. Investigation of square fluidized beds using capacitance tomography: preliminary results. Measurement Science and Technology, **12**, 1120.

Lopes, R.J.G., Quinta-Ferreira, R.M., 2009. CFD modelling of multiphase flow distribution in trickle beds. Chemical Engineering Journal, **147**, 342-355.

Louge, M., Chang, H., 1990. Pressure and voidage gradients in vertical gas-solid risers. Powder Technology, **60**, 197-201.

Lun, C.K.K., Savage, S.B., Je rey DJ, and Chepurniy N., 1984. Kinetic theories for granular ow: Inelastic particles in couette flow and slightly inelastic particles in a general flow field. Journal of Fluid Mechanics, **140**, 223-256.

Mabrouk, R., Chaouki, J., Guy, C., 2007. Effective drag coefficient investigation in the acceleration zone of an upward gas–solid flow. Chemical Engineering Science, **62**, 318-327.

Makkawi, Y.T., Wright, P.C., 2002. Fluidization regimes in a conventional fluidized bed characterized by means of electrical capacitance tomography. Chemical Engineering Science, **57**, 2411-2437.

Makkawi, Y.T., Wright, P.C., 2003. The voidage function and effective drag force for fluidized beds. Chemical Engineering Science, **58**, 2035-2051.

Manyele, S.V., Pärssinen, J.H., Zhu, J.X., 2002. Characterizing particle aggregates in a high-density and high-flux CFB riser. Chemical Engineering Journal, **88**, 151-161.

Mathiesen, V., Solberg, T., Hjertager, B.H., 2000. An experimental and computational study of multiphase flow behavior in a circulating fluidized bed. International Journal of Multiphase Flow, **26**, 387-419.

Matsen, J.M., 1982b. Mechanisms of choking and entrainment. Powder Technology, **32**, 21-33.

Matsen, J.M., 1988. The rise and fall of recurrent particles: Hydrodynamics of circulation. Pergamon, p. 3.

Miller, A., Gidaspow, D., 1992. Dense, vertical gas-solid flow in a pipe. AIChE Journal, **38**, 1801-1815.

Mueller, P., Reh, L., 1993. Particle drag and pressure drop in accelerated gas-solid flow. Preprint Volume for Circulating Fluidized Beds IV, AIChE, Somerset, 193–198.

Naren, P.R., 2009. Modeling of high solid flux circulating fluidized bed reactors, Industrial flow modeling group. National chemical laboratories, Pune.

Naren, P.R., Lali, A.M., Ranade, V.V., 2007. Evaluating EMMS Model for Simulating High Solid Flux Risers. Chemical Engineering Research and Design, **85**, 1188-1202.

Neri, A., Gidaspow, D., 2000. Riser hydrodynamics: simulation using kinetic theory. AIChE Journal, **46**, 52-67.

Nieuwland, J.J., Annaland, S., Kuipers, J.A.M., Swaaij, W.P.M., 1996a. Hydrodynamic modelling of gas-particle flows in riser reactors. AIChE Journal, **42**, 1569-1582.

Nieuwland, J.J., Meijer, R., Kuipers, J.A.M., Van Swaaij, W.P.M., 1996b. Measurements of solids concentration and axial solids velocity in gas-solid two-phase flows. Powder Technology, **87**, 127-139.

Pandey, P., Turton, R., Yue, P., Shadle, L., 2004. Nonintrusive particle motion studies in the near-wall region of a pilot-scale circulating fluidized bed. Industrial & Engineering Chemistry Research, **43**, 5582-5592.

Pärssinen, J.H., Zhu, J.X., 2001. Particle velocity and flow development in a long and high-flux circulating fluidized bed riser. Chemical Engineering Science, **56**, 5295-5303.

Peirano, E., Delloume, V., Johnsson, F., Leckner, B., Simonin, O., 2002. Numerical simulation of the fluid dynamics of a freely bubbling fluidized bed: influence of the air supply system. Powder Technology, **122**, 69-82.

Pita, J.A., Sundaresan, S., 1993. Developing flow of a gas-particle mixture in a vertical riser. AIChE Journal, **39**, 541-552.

Qi, H., Li, F., Xi, B., You, C., 2007. Modeling of drag with the Eulerian approach and EMMS theory for heterogeneous dense gas-solid two-phase flow. Chemical Engineering Science, **62**, 1670-1681.

Ranade, V.V., 1999. Modeling of gas-solid flows in FCC riser reactors: fully developed flow, Second International Conference on CFD in Mineral and Process Industry, CSIRO, Melbourne, Australia.

Ranade, V.V., 2001. Computational flow modeling for chemical reactor engineering. Academic Press.

Rhodes, M.J., Geldart, D., 1986. The hydrodynamics of re-circulating fluidized beds. Circulating Fluidized Bed Technology, 193-200.

Rhodes, M.J., Geldart, D., 1989. The upward flow of gas/solid suspensions. I: A model for the circulating fluidized bed incorporating dual level gas entry into the riser. Chemical Engineering Research & Design, **67**, 20-29.

Richardson, J.F., Zaki, W.N., 1954. Sedimentation and fluidization. Transaction of Institute of Chemical Engineering, **32**, 1954.

Roy, S., Chen, J., Kumar, S.B., Al-Dahhan, M.H., Dudukovic, M.P., 1997. Tomographic and Particle Tracking Studies in a Liquid- Solid Riser. Industrial & Engineering Chemistry Research, **36**, 4666-4669.

Sakai, M., Koshizuka, S., 2009. Large-scale discrete element modeling in pneumatic conveying. Chemical Engineering Science, **64**, 533-539.

Sarkar, S., Mohanty, K., Meikap, B.C., 2008. Hydrodynamic modeling of a novel multi-stage gas-liquid external loop airlift reactor. Chemical Engineering Journal, **145**, 69-77.

Schaeffer, D.G., 1987. Instability in the evolution equations describing incompressible granular flow. Journal of differential equations, **66**, 19-50.

Shah, M.T., Mayne, J., Utikar, R.P., Tade, M.O., Pareek, V.K., 2010a. Gas-solid flow hydrodynamics of an industrial scale catalyst lift engager. Chemical Engineering Journal, **159**, 138-148.

Shah, M.T., Mayne, J., Utikar, R.P., Tade, M.O., Pareek, V.K., 2010b. Hydrodynamics of catalyst lift engager, CHEMECA, Perth, WA.

Shah, M.T., Utikar, R.P., Tade, M.O., Pareek, V.K., 2008. Hydrodynamics of solid lift engager using Eulerian granular model, CHEMCON, Chandigarh, India.

Shah, M.T., Utikar, R.P., Tade, M.O., Pareek, V.K., 2009. Effect of lift gas velocity on performance of catalyst lift engager, Conveying and Handling of Particulate Solids, Brisben, Australia.

Shah, M.T., Utikar, R.P., Tade, M.O., Pareek, V.K., 2011a. Hydrodynamics of low and high solid flux FCC risers using energy-minimization multi-scale drag model. Chemical Engineering Journal.

Shah, M.T., Utikar, R.P., Tade, M.O., Pareek, V.K., 2011b. Simulation of gas-solid flows in riser using energy minimization multiscale model: Effect of cluster diameter correlation. Chemical Engineering Science.

Shah, M.T., Utikar, R.P., Tade, M.O., Pareek, V.K., 2011c. Simulation of gas-solid flows in riser using energy minimization multiscale model: Effect of cluster diameter correlation, Gas Liquid Solids - 10, Portugal.

Sinclair, J.L., Jackson, R., 1989. Gas particle flow in a vertical pipe with particle particle interactions. AIChE Journal, **35**, 1473-1486.

Subbarao, D., 1986. Clusters and lean-phase behaviour. Powder Technology, **46**, 101-107.

Subbarao, D., 2010. A model for cluster size in risers. Powder Technology, **199**, 48-54.

Sun, G., Grace, J.R., 1990. The effect of particle size distribution on the performance of a catalytic fluidized bed reactor. Chemical Engineering Science, **45**, 2187-2194.

Sun, G., Grace, J.R., 1992. Effect of particle size distribution in different fluidization regimes. AIChE Journal, **38**, 716-722.

Sundaresan, S., 2000. Modeling the hydrodynamics of multiphase flow reactors: current status and challenges. AIChE Journal, **46**, 1102-1105.

Syamlal, M., O'Brien, T.J., 1994. The derivation of a drag coefficient formula from velocity-voidage correlations. US Department of Energy, Office of Fossil Energy. Technical Report.

Syamlal, M., Rogers, W., O'Brien, T.J., 1993. MFIX documentation: Theory guide. Technical Note, DOE/METC-95/1013.

Theologos, K.N., Markatos, N.C., 1994. Modelling of vertical pneumatic-conveying hydrodynamics. Applied Mathematical Modelling, **18**, 306-320.

Tsuji, Y., 2007. Multi-scale modeling of dense phase gas-particle flow. Chemical Engineering Science, **62**, 3410-3418.

Tsuji, Y., Kawaguchi, T., Tanaka, T., 1993. Discrete particle simulation of two-dimensional fluidized bed. Powder Technology, **77**, 79-87.

Utikar, R.P., Ranade, V.V., 2007. Single jet fluidized beds: Experiments and CFD simulations with glass and polypropylene particles. Chemical Engineering Science, **62**, 167-183.

Vaishali, S., Roy, S., Bhusarapu, S., Al-Dahhan, M.H., Dudukovic, M.P., 2007. Numerical simulation of gas-solid dynamics in a circulating fluidized-bed riser with geldart group B particles. Industrial and Engineering Chemistry Research, **46**, 8620-8628.

Vaishali, S., Roy, S., Mills, P.L., 2008. Hydrodynamic simulation of gas–solids downflow reactors. Chemical Engineering Science, **63**, 5107-5119.

Van de Velden, M., Baeyens, J., Smolders, K., 2007. Solids mixing in the riser of a circulating fluidized bed. Chemical Engineering Science, **62**, 2139-2153.

Van der Hoef, M.A., van Sint Annaland, M., Deen, N.G., Kuipers, J.A.M., 2008a. Numerical simulation of dense gas-solid fluidized beds: a multiscale modeling strategy.

Van der Hoef, M.A., van Sint Annaland, M., Deen, N.G., Kuipers, J.A.M., 2008b. Numerical simulation of dense gas-solid fluidized beds: a multiscale modeling strategy. Annual Review of Fluid Mechanics, **70**, 40-70.

Van der Hoef, M.A., van Sint Annaland, M., Kuipers, J.A.M., 2005. Computational fluid dynamics for dense gas-solid fluidized beds: a multi-scale modeling strategy. China Particuology, **3**, 69-77.

van Sint Annaland, M., Deen, N.G., Kuipers, J.A.M., 2005. Numerical simulation of gas-liquid-solid flows using a combined front tracking and discrete particle method. Chemical Engineering Science, **60**, 6188-6198.

van Wachem, B.G.M., Almstedt, A.E., 2003. Methods for multiphase computational fluid dynamics. Chemical Engineering Journal, **96**, 81-98.

Van Wachem, B.G.M., Schouten, J.C., Van den Bleek, C.M., Krishna, R., Sinclair, J.L., 2001. Comparative analysis of CFD models of dense gas–solid systems. AIChE Journal, **47**, 1035-1051.

W. Chan, C., Seville, J.P.K., Parker, D.J., Baeyens, J., 2010. Particle velocities and their residence time distribution in the riser of a CFB. Powder Technology, **203**, 187-197.

Wang, J., 2008. High-resolution Eulerian simulation of RMS of solid volume fraction fluctuation and particle clustering characteristics in a CFB riser. Chemical Engineering Science, **63**, 3341-3347.

Wang, J., Ge, W., Li, J., 2008. Eulerian simulation of heterogeneous gas-solid flows in CFB risers: EMMS-based sub-grid scale model with a revised cluster description. Chemical Engineering Science, **63**, 1553-1571.

Wei, F., Lin, H., Cheng, Y., Wang, Z., Jin, Y., 1998. Profiles of particle velocity and solids fraction in a high-density riser. Powder Technology, **100**, 183-189.

Weinstein, H., Shao, M., Schnitzlein, M., 1986. Radial variation in solid density in high velocity fluidization. Pergamon, p. 201.

Wen, C.Y., Yu, Y.H., 1966a. Mechanics of fluidization, pp. 100–111.

Wen, C.Y., Yu, Y.H., 1966b. Mechanics of fluidization, Chemical Engineering Progress Symposium Series, pp. 100–111.

Xiong, Q., Li, B., Chen, F., Ma, J., Ge, W., Li, J., Direct numerical simulation of sub-grid structures in gas-solid flow--GPU implementation of macro-scale pseudo-particle modeling. Chemical Engineering Science, **65**, 5356-5365.

Xu, G., Li, J., 1998. Analytical solution of the energy-minimization multi-scale model for gas-solid two-phase flow. Chemical Engineering Science, **53**, 1349-1366.

Yan, C., Fan, Y., Lu, C., Zhang, Y., Liu, Y., Cao, R., Gao, J., Xu, C., 2009. Solids mixing in a fluidized bed riser. Powder Technology, **193**, 110-119.

Yang, N., Wang, W., Ge, W., Li, J., 2003a. Analysis of flow structure and calculation of drag coefficient for concurrent-up gas-solid flow. Chinese Journal of Chemical Engineering, **11**, 79-84.

Yang, N., Wang, W., Ge, W., Li, J., 2003b. CFD simulation of concurrent-up gas-solid flow in circulating fluidized beds with structure-dependent drag coefficient. Chemical Engineering Journal, **96**, 71-80.

Yang, N., Wang, W., Ge, W., Wang, L., Li, J., 2004. Simulation of heterogeneous structure in a circulating fluidized-bed riser by combining the two-fluid model with the EMMS approach. Industrial and Engineering Chemistry Research, **43**, 5548-5561.

Yerushalmi, J., Cankurt, N.T., 1979. Further studies of the regimes of fluidization. Powder Technology, **24**, 187-205.

Yerushalmi, J., Cankurt, N.T., Geldart, D., Liss, B., 1976. Flow regimes in vertical gas-solid contact systems. City Coll., New York (USA); Bradford Univ.(UK); Coalcon, New York (USA).

Zhang, M., Qian, Z., Yu, H., Wei, F., 2003. The solid flow structure in a circulating fluidized bed riser/downer of 0.42-m diameter. Powder Technology, **129**, 46-52.

Zhang, N., Lu, B., Wang, W., Li, J., 2008. Virtual experimentation through 3D full-loop simulation of a circulating fluidized bed. Particuology, **6**, 529-539.

Zhang, Y., Reese, J.M., 2003. The drag force in two-fluid models of gas–solid flows. Chemical Engineering Science, **58**, 1641-1644.

Zhong, W., Zhang, M., Jin, B., Yuan, Z., 2006. Three-dimensional Simulation of Gas/Solid Flow in Spout-fluid Beds with Kinetic Theory of Granular Flow. Chinese Journal of Chemical Engineering, **14**, 611-617.